UNIVERSITY OF SOUTHAMPTON

THE USE OF TRANSIENT TRACERS TO STUDY UPPER OCEAN PROCESSES.

Thomas William Nicholas Haine

Submitted for the degree Doctor of Philosophy

Department of Oceanography

September 1992

UNIVERSITY OF SOUTHAMPTON

ABSTRACT

FACULTY OF SCIENCE

OCEANOGRAPHY

Doctor of Philosophy

THE USE OF TRANSIENT TRACERS TO STUDY UPPER OCEAN PROCESSES.

by Thomas William Nicholas Haine

An automated gas chromatographic technique to measure the concentrations of chlorofluorocarbon 113 (CFC-113 : CCl_2FCClF_2) dissolved in seawater has been developed. The method also quantifies chlorofluorocarbons 11 and 12 (CFC-11 : CCl_3F, CFC-12 : CCl_2F_2). Seawater collected from Niskin bottles in ground-glass syringes is stripped by a gas stream and concentrated on a cryogenic trap. By isolating and heating the trap the chlorofluorocarbon compounds are re-liberated and injected onto a high resolution, wide-bore capillary, gas chromatographic column, followed by electron-capture detection. The analysis time for each sample is less than fifteen minutes. Surface seawater precisions are 2.9%, 2.4% and 1.2% for CFC-113, CFC-11 and CFC-12, with detection limits of 0.003-0.004, 0.02 and 0.03-0.05pMol/l respectively. Estimates of the solubility ratios of CFC-113:CFC-11 and CFC-113:CFC-12 are 0.303 and 1.22 (disagreeing with previous work) and the optimum CFC-113 'ventilation age' resolution is +/- 0.9 years for both CFC-113/CFC-11 and CFC-113/CFC-12.

Results from field work in the North East Atlantic agree with previous studies in exhibiting non-equilibrium surface saturations. The variation of this saturation is significant because it is several times larger than the routine instrumental precision and characterises the fluid entering the permanent thermocline. By use of a Kraus-Turner mixed layer model the mechanisms producing this variability are investigated. The effect of uncertainty in air/sea transfer kinetics and maximum mixed layer depth is examined and the model results suggest that the CFC boundary condition for the main thermocline is sensitively dependent on the conditions prevailing at the time of entrainment, as well as the parameters used to model the tracer exchange. A mixed layer with an 800m depth of maximum seasonal mixing has an initial CFC-113/CFC-12 age of ~2.5 years. The model sensitivity to the initial state of the main thermocline fluid is also examined and the modelled mixed layer has a memory of this condition of 3-4 years.

The behaviour of CFC ratio age tracers is investigated by use of a generic expression for the evolution of ventilation age. Use of data from the North East Atlantic shows that non-linear and diapycnal contributions are small and the balance in steady state is given by,

$$\underline{v}_i . \nabla_i \tau \approx 1 + K_i \nabla_i^2 \tau$$

where $\underline{v}_i$ is velocity, τ is CFC-113/CFC-12 or CFC-113/CFC-11 age, K_i is a diffusion coefficient appropriate to scales of order 500km and each term is evaluated on an isopycnic horizon. Errors in the τ fields prohibit estimates of $\underline{v}_i$ for the data available, and always restrict the maximum observable velocity. The influence of isopycnic shear is discussed and shown to be an additional limit to the utility of ventilation age tracers as a means of diagnosing $\underline{v}_i$.

CFC-113 ventilation ages are used in combination with simultaneous dissolved oxygen observations to derive Oxygen Utilisation Rate estimates. Reasonable results are obtained for $27.1 \leq \sigma_\theta \leq 27.325$, but on deeper surfaces the consumption rates are too high. A simple box model suggests this may be due to unsteadiness or to a saturating value of the τ field.

To Stephen, Jennifer, Jonathan and Judy.

ACKNOWLEDGEMENTS.

This work would never have come to fruition without the enthusiasm and support of my supervisors, family and friends. I thank especially Drs. Andy Watson, Kelvin Richards and Prof. Steve Thorpe. Their exemplary professionalism and integrity steered my studentship and it was a privilege to work with them; I gratefully acknowledge their guidance and advice. I am also indebted to the staff of Plymouth Marine Laboratory (my formal CASE collaborator) and the James Rennell Centre for Ocean Circulation (where I was an informal visitor for my final year; thanks to Gwyn Griffiths and Raymond Pollard). The warm welcomes and generosity I received have contributed much. The skill and patience of Malcolm Liddicoat in the lab. and at sea inspired me, whilst Mikael Krysell, Jane Robertson, Rob Upstill-Goddard and Roger Ling were always willing to share their expertise and time too. At the Rennell centre George Nurser, Yanli Jia, Sheldon Bacon, Denise Smythe-Wright and Steve Boswell were keen to discuss my work, and in particular my contact with Stuart Cunningham and Mike Griffiths was productive and friendly. I would also like to acknowledge the assistance and co-operation of the officers and crews of RV ARANDA and RRS CHARLES DARWIN. Further acknowledgements of particular significance are made in the body of the text.

Thanks to my family, friends and various pubs and diving clubs for making my studentship more than tolerable. Foremost in my mind are Nana, Jackie, Alex, Sarah B, Nicola, Emily, Beccy, Ed, Sue, Bablu, Marcel, Gilly, Eva, Stef^2, Rita and, infrequently but never without passion, Ben. Finally, but most of all, thanks to Mark for his selfless friendship and amazing capacity, and to Sarah for her kind warmth, humour and understanding.

This research was supported by a CASE studentship award from the Natural Environment Research Council of the UK.

TABLE OF CONTENTS

CHAPTER 1

INTRODUCTION AND REVIEW.

1.1. Introduction to Thesis.

This dissertation is a report of work carried out in an attempt to understand more clearly the physical processes which influence chlorofluorocarbon (CFC) like tracers in the sea. The ultimate aim of this research is to be able to use dissolved CFC distributions to derive information about physical mechanisms in the ocean which is needed to understand earth's climate and the way in which it may respond to mankind's activities. At the outset the author concedes that the work reported here falls short of this goal; there are no new insights concerning oceanic regimes.

Of particular interest in this study is the volatile liquid trichlorotrifluoroethane (CFC-113; CCl_2FCF_2Cl), produced for use as a solvent since the early 1970s. Trichlorofluoromethane and dichlorodifluoromethane (CFCs 11 and 12; CCl_3F and CCl_2F_2 respectively) date back to the late 1930s, and are used in refrigerators, air conditioners and aerosols. It is believed on good evidence that there are no natural sources of these chemicals; they are entirely man-made. Furthermore, they are unreactive in the sea; simply following the path of the water inertly (CFCs are not passive in the atmosphere however, they contribute to the greenhouse effect and destroy stratospheric ozone). These features are reminiscent of a dye invading the ocean from the surface and oceanographers have used CFCs 11 and 12 as tracers for over a decade. CFC-113 has a special property, which CFCs 11 and 12 no longer possess, which motivates the interest in this compound; it can be used to tell how long water has been away from the sea surface. This so-called 'ventilation age' is a recurrent theme throughout the thesis. Although CFC-113 is the compound of interest for this work one hopes that the findings can be generalised. The concern over 'CFC replacements', which are less damaging to the environment, is clearly relevant here. Many of the ideas and arguments can be applied to other CFC-like chemicals which may well become more important as time goes by.

This work began in autumn 1989, at which time there was no reliable method to measure CFC-113 in seawater (dissolved CFC concentrations are extremely small). A J Watson had established that the technique described in a preliminary paper on CFC-113 was flawed in an unknown way. This was the starting point for this study, and two and a half chapters report the details of the analytical method developed. There was little published work on the systematics of CFC-113 ventilation age either. As a first attempt to understand these the way in which the CFCs penetrate into the open ocean interior, and their behaviour there, is investigated. An important thread running through this work is the use of real observations to compare and contrast with the theoretical suggestions. The difficulty of this task is one reason why there are no new results about oceanography.

Throughout this thesis a few abbreviations are used. These are;

CFC ⇔ chlorofluorocarbon, CFM ⇔ chlorofluoromethane (i.e. CFCs 11 and 12 only), PML ⇔ Plymouth Marine Laboratory, VIVALDI ⇔ VIVALDI '91 expedition to the North East Atlantic (see Section 4.1).

Unless specific reference is made to the research of others, this thesis is the work of the author, whilst in registered candidature at the University of Southampton. The author observed the preparation of standard ampoules described in Section 3.3.2, but neither designed nor used the apparatus personally. Although none of this material has been submitted for another degree, the contents of Chapter 2 and parts of Chapter 3 have been tendered as a manuscript for publication by the Journal of Geophysical Research (Haine *et al.*, Submitted).

1.2. Introduction to CFC Tracers.

Sections 1.2 to 1.5 are concerned with reviewing the literature on CFC tracers. In 1973 Lovelock and co-workers said that "interest lies in their potential usefulness as inert tracers for the study of mass transfer processes in the atmosphere and oceans". This was the first publication about halogenated tracers in the ocean, although Lovelock (1971) had already commented on using CFC-11 and SF_6 as tracers of air mass movements. It took nine years for this interest to really bear fruit (Gammon *et al.*, 1982), and several authors published work during the 1980s. Much of the intervening time was spent in developing the necessary apparatus for ship-board analyses. The technique used to measure CFC concentrations is electron capture gas chromatography (ECD-GC), a particularly sensitive method. The currently available measurements are able to resolve femto-molar concentrations (e.g. Bullister (1984) quotes a detection limit of 5×10^{-15}mol/kg). This work has been developmental and the style of many papers reflects this, with much detail of experimental technique and methodology, and less emphasis on theoretical considerations, or sophisticated mathematical and physical models.

All of the research carried out until 1988 involved the use of CFC-11 and CFC-12 only. However, Wisegarver & Gammon (1988; henceforth abbreviated WG in this chapter) point out the possibility of using CFC-113 too. Current gas chromatographs are at the point of being able to routinely measure this species, and very little work has been published on their distributions. WG explain that CFC-113 measurements allow a fluid 'ventilation age' to be derived by combination with either CFC-11 or CFC-12 fields, which makes CFC-113 observations particularly interesting. The concept of ventilation age is quintessential to this thesis and is introduced in Sections 1.3.1. and 4.3.2.

1.3. Systematics of Deriving CFC Concentrations.

This section discusses in detail the methods used to determine the atmospheric histories of CFCs and the corresponding surface ocean concentrations. This process is

essential to allow an accurate surface ocean boundary condition to be established. The procedure for CFC-11 and CFC-12 is reasonably straightforward and is explained first in each sub-section. The corresponding method for CFC-113 is more speculative and is dealt with subsequently. No specific details of instrumental design or calibration are included here; Chapters 2 and 3 discuss these issues respectively.

1.3.1. Defining Atmospheric Source Functions.

Increases in global atmospheric concentrations of CFC-11 and CFC-12 have been monitored since 1976 (Rasmussen *et al.* 1981, Cunnold *et al.* 1983a, 1983b, 1986), after it was recognised by Molina & Rowland (1974) that CFCs catalytically destroy stratospheric ozone. For the period prior to 1976 the concentrations are inferred by using data of the annual release of each CFC and the lifetime of each species. The production data are reported by the Chemical Manufacturer's Association (1983) for the period 1930-1982 with estimates of non-reporting sources included in these figures, whilst the lifetimes of CFC-11 and CFC-12 have been measured with reasonable accuracy as part of the Atmospheric Lifetime Experiment (ALE) reported by Cunnold *et al.* (1986). McCarthy *et al.* (1977) combine these data with factors to allow for delayed release of some CFC products into the atmosphere (for instance aerosols release CFC directly into the air, whilst sealed refrigerators delay the release for some time). These calculations give tables of estimated liberation of each species into the atmosphere for each year from which the atmospheric burden can be estimated. Smethie *et al.* (1988) describe the calculation explicitly. The atmospheric inventory in January of the ith year, I_i, is given by,

$$I_i = I_{i-1} - \frac{\lambda}{2}(I_i + I_{i-1}) + R_{i-1} \qquad 1.3.1$$

where R_i is the amount of chemical released in the ith year and λ is the reciprocal lifetime of the species. The lifetime is the effective half life of persistence (within a factor of ln2), the rate controlling sink being photodissociation in the stratosphere. Cunnold *et al.* (1986) estimate these times to be 74 years for CFC-11 and 111 years for CFC-12. The inventory calculation of Equation 1.3.1 is performed for each year and then matched with the measurements made by Rasmussen *et al.* (1981) in 1976, assuming the pre-industrial levels to be zero. The matching of the inventory history allows a scaling ratio of inventory : concentration to be calculated and in this way a complete history of atmospheric CFC concentration can be determined.

Although the main sources of CFCs polluting the atmosphere are in the Northern hemisphere (about 95%) the inter-hemispheric equilibration time is relatively short compared to the lifetimes of these gases and so the atmosphere is well mixed in CFCs. (Inter-hemispheric exchange times are estimated to be 1-2 years by Czeplak & Junge (1974) and Singh *et al.* (1979), whereas the lifetimes for CFC-11 and CFC-12 are two

orders of magnitude longer according to Cunnold *et al.* (1986).) Rasmussen & Khalil (1986) conclude from ten years of data that the rates of increase of CFC-11, CFC-12 and CFC-113 are the same in each hemisphere, but their measurements do show concentration differences of a few percent between hemispheres and these are borne out by Cunnold *et al.* (1986). In both of these studies the concentrations in the Northern hemisphere were higher than in the Southern hemisphere. Not only is the lifetime important in calculating inter-hemispheric differences, but the rate of increase of concentration is relevant too. With most CFC sources in the Northern hemisphere and an inter-hemispheric exchange time of 1-2 years one would expect the Southern hemisphere concentrations to lag by time scales of this order. Of course the Northern hemisphere 'leads' the globally averaged concentration values too, since recently released CFC in the Northern hemisphere will not have been diluted across the whole atmosphere.

Although no specific studies tracing the mixing behaviour of CFCs downwind of polluting regions has been attempted, Pack *et al.* (1977) report large variability in some remote locations of the North Atlantic over a few days, associated with air masses transported from polluting regions such as Western Europe. Nevertheless, Cunnold *et al.* (1986) show good evidence of average, even mixing within hemispheres (i.e. along lines of latitude). Their five year experiment involved regular daily measurements at coastal sites around the world; three in the Northern hemisphere and two in the Southern hemisphere. In this study the sampling stations were chosen so as to receive prevailing oceanic marine air and other work (e.g. Gammon *et al.* (1982)) also shows consistent concentrations of CFC in the marine troposphere. So, for most applications the CFC concentration at the ocean surface can be considered constant and the slight unevenness in global distribution can be ignored. The distributions of CFC-113 concentrations will be most out of synchronisation due to the fast rate of increase of CFC-113, as mentioned by WG. Similarly, the CFC-11 and CFC-12 atmospheric concentrations presumably became more evenly distributed after 1975 when legislation slowed their release.

The trends in CFC-11 and CFC-12 atmospheric concentration are shown in Figure 1.1 and the dependence of the CFC-11/CFC-12 ratio on time is shown in Figure 1.2. This data is taken from Warner (1988), and interpolated to the measurements made by the author in 1990 and 1991 (ARANDA and VIVALDI cruises; see Section 4.2.3). The error in the values of concentration is about 2%, since 1983, based on uncertainties in the field measurements and the reported error of Warner (1988).

The trend in atmospheric CFC-113 is shown in Figure 1.1; CFC-113/CFC-11 and CFC-113/CFC-12 are shown varying with time in Figure 1.2 (the inverse function, i.e. the year as a function of atmospheric ratio, r, is denoted by f(r) and is used repeatedly. See Sections 4.3.2 and 6.3, for example.). It is harder to calculate the variation of the atmospheric concentration of CFC-113 with time. This is because the data required to evaluate Equation 1.3.1, available for CFC-11 and CFC-12, are lacking for CFC-113.

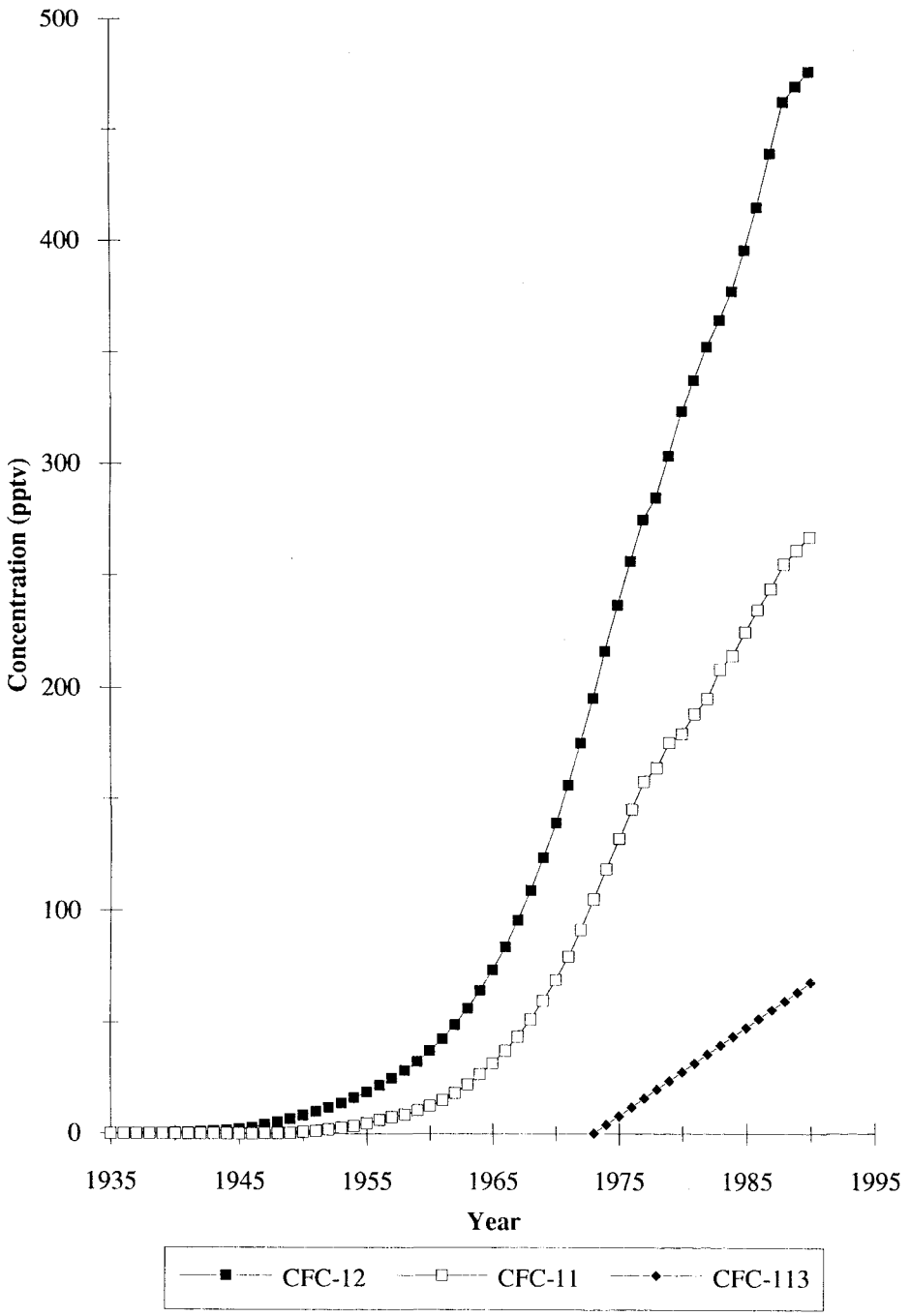

Figure 1.1. Northern hemisphere atmospheric concentrations of CFCs 12, 11 and 113 as functions of time (pptv $\Leftrightarrow$ parts per trillion (10^{12}) by volume). Data source is Warner (1988) to 1988, then extrapolated to the measurements made by the author in 1990 and 1991 for CFCs 11 and 12. CFC-113 data assumes linear increase since 1973, referenced to observations made in 1990 and 1991 (see Section 4.2.3).

(Annual release estimates are not available and no accurate lifetime measurements have been made.) However, limited direct measurements of CFC-113 concentrations in the atmosphere have been made since the late 1970s (e.g. Singh *et al.* 1977, 1983a). WG used these data in a linear least squares fit to calculate a mean annual rate of increase of 2.6pptv/year (pptv : parts per trillion by volume i.e. 10^{12}). In this thesis CFC-113 concentrations are referred to the PML standard scale; different to that used by WG. Assuming a linear increase since 1973 (following WG) and fitting to field data in 1990 and 1991, measured with respect to this standard, gives a rate of increase of 3.9pptv/year. WG report no error in their estimate of the source function, although ~5% is a suitable uncertainty based on the scatter of the data about the fitted function (their Figure 1.3). The influence of source function uncertainty on the calculations made in this work are discussed in Section 4.3.3.

Figure 1.2 shows that the CFC-113/CFC-12 ratio has rapidly changed over the last fifteen years compared to the CFC-11/CFC-12 ratio which has been almost constant since circa 1975. This stagnation is a direct result of restrictions on release in the USA since this time. It is the variability of the CFC-113/CFC-12 ratio which makes study of CFC-113 such an interesting matter. This is because a water parcel with a known CFC-113/CFC-12 ratio can be assigned a unique age over the last fifteen years. This is called the 'ventilation age' of the water packet, and contains information about the time elapsed since the water was last at the surface. Because the CFC-11/CFC-12 ratio has not altered since 1975 measurement of these two CFCs alone can reveal no new information on ventilation ages.

1.3.2. The Invasion of CFCs into the Ocean.

With the tropospheric CFC concentration derived, the next step is to examine how these gases penetrate the ocean. CFCs are chemically unreactive and sparingly soluble in seawater. For the aqueous and gaseous phases *in equilibrium* this type of behaviour is described by the relation,

$$C = F(\theta,S)\, C_{atm} \; ; \quad C_{atm} << 1 \qquad 1.3.2$$

where C is the equilibrium concentration of CFC in the aqueous phase, $F(\theta,S)$ is a solubility function of potential temperature θ and salinity S, and C_{atm} is the atmospheric partial pressure of CFC. $F(\theta,S)$ was measured for CFC-11 and CFC-12 over a range of (θ,S) values by Warner & Weiss (1985). Their paper includes and reviews previous work by Wisegarver & Cline (1985) and Hunter-Smith *et al.* (1983). Assuming equilibrium between phases, use of solubility data and atmospheric concentrations allows the concentration of CFC to be calculated for surface seawater at a known salinity, potential temperature, and time. Broecker & Peng (1982) estimate a period of about one month for atmospheric exchange with the ocean, assuming a mixed layer depth of order 50m and a piston velocity of order 2m/day (see below in this sub-section for explanation

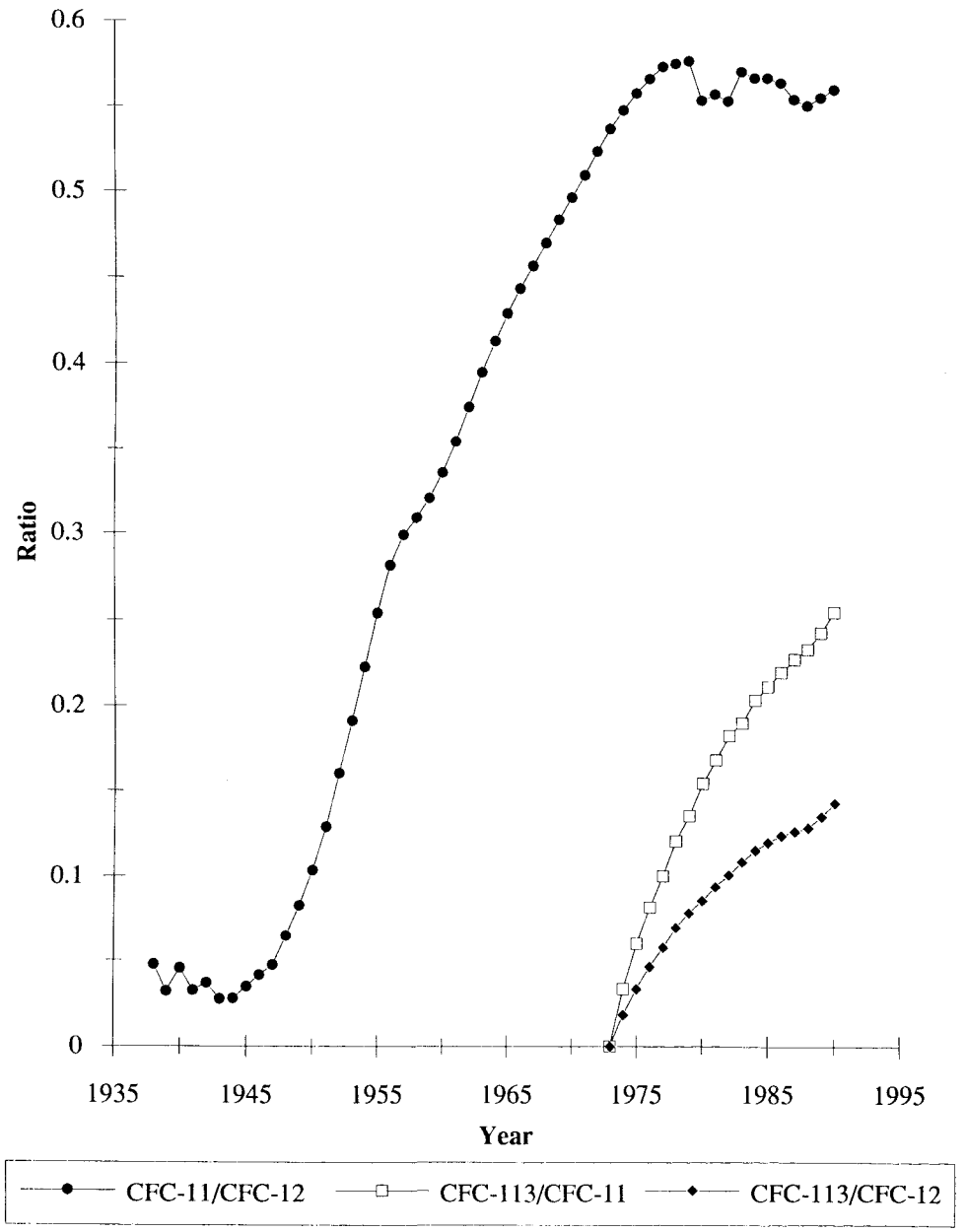

Figure 1.2. Northern hemisphere atmospheric ratios of CFC-11/CFC-12, CFC-113/CFC-11 and CFC-113/CFC-12. Data source as per Figure 1.1. The function f(r) used in Sections 4.3.2 and 6.3 corresponds to year(ratio) in this figure.

of piston velocities). This, then, is a timescale for the establishment of equilibrium and has been the starting point for many workers (see also the review of Section 5.1).

However, several authors have observed that this assumption between phases is manifestly not the case. Wallace & Lazier (1988) measured 60% saturations in Labrador Sea water for example, and Warner (1988) has observed both super- and under-saturations. Warner (1988) observes that areas with a deep mixed layer are often under-saturated and that thin mixed layers reveal super-saturations in warmer summer months. (Solubility sharply decreases with temperature increasing.) He also notes that generally CFC-12 is closer to equilibrium than CFC-11.

The dynamics of the air-sea interaction are reviewed by Liss & Merlivat (1986). The transport across an interface for a sparingly soluble gas is modelled by

$$j = k\,(C_{eq} - C) \qquad 1.3.3$$

where j is the gas flux into the sea, k is the piston velocity or transfer coefficient, C_{eq} the equilibrium concentration and C the current mixed layer concentration. It is because C_{eq} - C changes more rapidly than the timescale of the piston velocity that surface waters depart from equilibrium in their concentrations. The piston velocity varies with many things, including wind speed, wave size and distribution, and gas species. Liss & Merlivat (1986) discuss the variability of transfer coefficients in detail and these mechanisms are themselves a research topic of intense interest (see also Upstill-Goddard *et al.*, 1990 and Wanninkof, 1991). With specific reference to CFCs Warner (1988) reviews various theoretical parameterisations and attempted measurements of these piston velocities and concludes by saying there is a need for experimental measurements of these values for CFCs. A rigorous attempt to determine the surface water concentration of CFCs for a particular time, temperature and salinity requires a model of the history of the mixed layer in order to resolve this problem of non-equilibrium saturations. The general problem of the seasonal variation of mixed layer CFC characteristics is the subject of Chapter 5.

There are a few other potentially significant issues involved with defining surface ocean CFC boundary conditions. One possible problem is leaking refrigerators and air conditioning units on sunken ships. This is hard to quantify but should be a minor nuisance overall; samples with unrealistic concentrations or ratios are reasonably easy to identify. For high latitude regions ice melting during summer months can cause water to be released which is saturated with CFC from previous years. The extent to which this can bias the surface saturations depends on how rapidly the meltwater is subducted from the mixed layer, as is the case for polluted river runoff. Ice cover also isolates the surface ocean from the atmosphere during winter at high latitudes, and this complicates the exchange processes. Another mechanism important for some trace substances is loss to the deep ocean by absorption onto organic particles which then fall through the water

column. However, Krysell & Wallace (1988) show that for CFC-11, CFC-12, CCl_4, and CH_3CCl_3 this is not a significant sink; it is ignored for CFC-113 throughout this work.

The discussion on the ocean/atmosphere interaction presented above has involved CFCs 11 and 12. The same principles apply to CFC-113 but there have been no solubility measurements in the detail required for accurate analysis. WG have provided an initial estimate of the solubility function for CFC-113, based on the assumptions that CFC-113 is in the same state of saturation, and has the same temperature dependence of solubility as CFC-11. From this a simple ratio of solubilities can be determined. By applying the same method to CFC-12, whose solubility is known, an approximate error of 4% was calculated. WG comment that their CFC-113 data quality is limited by measurement techniques, rather than by the uncertainty in solubility. A similar method is used in the work reported here (Section 4.3.2), where the influence of the unknown CFC-113 solubility is also examined.

1.4. Survey of Uses, Techniques and Models for CFC Tracers.

The usefulness of CFC gases in tracing ocean mechanisms was enthusiastically suggested by Lovelock *et al.* (1973), although at that time the role of CFCs in ozone depletion or their contribution to global warming as greenhouse gases was not known. Measurements by two separate teams confirmed this potential (Hahne *et al.* 1978, Hammer *et al.* 1978), but their data quality was limited by sample contamination. Nevertheless, by refining the gas chromatography techniques Gammon *et al.* (1982) were able to publish reliable data of CFM concentration distributions with depth, from two locations in the eastern North Pacific. With this pioneering research confirming the utility of CFCs, several authors have published work using CFC tracers to characterise a variety of oceanic processes. It is the purpose of this section to review this work.

One of the simplest models used with CFC data sets is well-described by Gammon *et al.* (1982). This involves a one-dimensional advection/diffusion system to represent the invasion of an atmospheric trace gas into an infinitely deep (and horizontally homogeneous) ocean. This type of model predicts a rapid decrease of CFC concentration with depth below the mixed layer, and this has been observed in many locations. (See for example Bullister & Weiss (1983) (Arctic Ocean); WG (North Pacific); Warner (1988) (Subtropical Pacific and South Atlantic).) The concentration at depth z, C(z,t), is governed by the equation,

$$\frac{\partial C}{\partial t} = K \frac{\partial^2 C}{\partial z^2} - w \frac{\partial C}{\partial z} \qquad 1.4.1$$

where the vertical diffusivity, K, and upwelling velocity, w, completely describe the behaviour. The boundary conditions chosen to complete the problem are that the atmospheric concentration is rising exponentially, and a sufficiently well-mixed layer of this concentration communicates the tracer with the interior. The diffusion coefficient, K,

is considered constant in this analysis, there is no variability in the depth or temperature of the mixed layer and the ocean is assumed to be free of any tracer initially. Gammon *et al.* (1982) solve the problem analytically for the 'transient steady state' where the period since tracer turn on is several times longer than the atmospheric growth time scales. The solution is an exponential decrease of concentration with depth, which has a characteristic e-folding depth scale dependent on K and w. Using data collected from the North Pacific, Gammon and co-workers perform a least squares fit to obtain estimates of the diffusivity and upwelling velocity. In principle the contrasting behaviour of CFC-11 and CFC-12 should allow the simultaneous determination of both K and w. However, in practice the penetration depths for these two tracers are insufficiently dissimilar. Gammon *et al.* (1982) use temperature as an alternative tracer, with a different depth distribution, and calculate consistent values for K and w using both the CFC-11 and CFC-12 penetration depths. With these values they are able to describe the behaviour of anthropogenic CO_2 in terms of their simple model; they predict that the mean depth of penetration for perturbation CO_2 is about 300m.

Wallace & Moore (1985) solve Equation 1.4.1 numerically, using empirical source functions and compare their results with stations in the Arctic ocean. They derive values for K and w as did Gammon, but believe that a purely vertical model represented the ocean inadequately. They go on to use two simple horizontal box-models as upper and lower bounds on the true situation. One model simply advects shelf water into the deep Arctic Ocean, the other involves mixing within layers as water flows away from the shelf formation region. These are reasonably successful but the authors conclude that a more sophisticated approach is required.

Warner (1988) uses a slightly different approach to model Antarctic intermediate water flowing north along the West African rise. The governing equation is the same as Equation 1.4.1, but in this case the displacement co-ordinate is horizontal, and represents distance north from 53°S and the diffusivity is an isopycnic value. No account is made of diapycnal processes or advection components in the east/west direction. Warner derives values for K and w and then working from these, calculates an oxygen utilisation rate (OUR) using dissolved oxygen data collected with the CFC samples. He quotes a Peclet number of 5.6 for his section along the subtropical gyre of the South Atlantic ocean (the Peclet number is a ratio of advective to diffusive timescales), suggesting that it is the advective processes which dominate in distributing CFCs in this area. This model was successful in that the predicted variation of CFC concentration with latitude along the meridional track simulated the observed concentrations quite accurately.

Many authors have published reports of work collecting CFC data in the Arctic and North Atlantic oceans. Much of this research has been committed to determining the mechanisms of formation of deep, cold water in the Arctic ocean and the study of this water as it flows into the North Atlantic basins then southward towards the equator. CFC

data have been used in models of various sophistication, though simple box models are most common.

The work of Bullister & Weiss (1983) is a good example of this. Their model includes two reservoirs, of equal volume, representing the Greenland and Norwegian Seas below 1500m. The Greenland Sea basin can exchange water with the surface and the Norwegian Sea basin; the Norwegian Sea basin is otherwise isolated. Using CFC-11 and CFC-12 data from stations in this region they calculate times for deep convective mixing in the Greenland sea to be about 40 years, and the exchange between the two basins to be between 20 and 30 years. Bullister (1984) computes an OUR using this model in much the same way as does Warner (1988). He also uses the CFC-11/CFC-12 ratio as a mechanism to analyse the length of isolation of Greenland and Norwegian Sea deep water masses, but the results are inconsistent with the box model (e.g. 11 years for the age of Greenland Sea water).

In a more comprehensive study of this region (Smethie *et al.*, 1988) CFC-11 and CFC-12 are used to constrain conceptual models of circulation. CFC evidence for the existence of a deep cyclonic boundary current, transporting high salinity shelf water around the Eurasian basin is discussed. A box model of mixing between Eurasian basin bottom water and Eurasian basin deep water is calibrated with the CFC data. The overflow thus derived is used to drive another box model of water circulation in the Greenland and Norwegian seas. This second model is very similar to that of Bullister & Weiss (1983), except that the Norwegian Sea basin is fed by the Eurasian basin model. The flow of Eurasian basin deep water through Fram Strait was estimated to be between 0.80Sv and 0.93Sv (1Sv ('Sverdrup')= 10^6 m^3/s) using this method. The use of CFCs as tracers is particularly well highlighted in this paper since water masses in the Norwegian sea are indistinguishable in their θ-S characteristics, but are distinct in their CFC concentrations.

Rhein (1991) reports the distributions of CFCs 11 and 12 in the Greenland and Norwegian Seas observed in 1989. She finds that the CFC burden of the Greenland Sea Deep Water was unaltered since 1982 (comparing the data of Bullister & Weiss, 1983), whilst the Norwegian Sea Deep Water CFC concentrations increased during this period. CFC measurements are also reported from a deep convection event, showing homogenisation, but not atmospheric equilibrium. Using two box models Rhein (1991) investigates the ventilation rates of Greenland and Norwegian Sea Deep Waters consistent with the CFC observations. The Greenland Sea Deep Water ventilation times are much shorter (13-20 years) than previous estimates (e.g. Bullister & Weiss, 1983).

Pickart *et al.* (1989) use CFMs to analyse the strength of the deep western boundary current (DWBC). They investigate a simple process of overflow water formation and compare the predicted concentrations of CFMs with measurements made

downstream. With this source model they drive two sorts of DWBC; a uniform flow and a shear flow. In both models the mobile core of the DWBC is constantly being diluted with CFM free water. In this way a shoulder of intermediate concentration forms. In the uniform flow this shoulder is still; in the shear flow it moves with the core, but more slowly. Both of these are more sophisticated representations than previously published work. Pickart and co-workers use their models to constrain values for the speed and volume transport of the DWBC. This paper also shows how a more refined flow-analysis can alter the CFM ratio, which was previously considered a conservative quantity when mixing with CFM free water.

There has also been some work on the DWBC in sub-tropical and equatorial regions. (Weiss *et al.*, 1985, Fine & Molanari, 1988). This research uses CFM concentration measurements as constraints in entrainment/mixing calculations and as observables in characterising water masses. The CFC-11/CFC-12 ratio is considered to be a true ventilation age and the actual concentrations give the extent of dilution. Fine *et al.* (1988) and Warner (1988) have also published similar work analysing the Agulhas retroflection, whilst Gordon *et al.* (1992) report CFC-11 and CFC-12 sections to support other tracer data in diagnosing the Atlantic-Indian Ocean exchange of thermocline and intermediate water.

A study of the water formation processes in the Labrador sea was published by Wallace & Lazier (1988). They use CFC-11 and CFC-12 data to analyse a deep convection (>1000m) model of the region which is poorly successful. Their mixed layer model removes heat and water vapour daily, allowing the mixed layer to deepen as the water column loses buoyancy. However, the degree of undersaturation observed in the field is not duplicated in the numerical experiment. The nature of the interannual variability in the occurrence of deep water mixing is suggested as a reason for this. The authors conclude that long term monitoring of CFM tracers is essential in the Labrador sea to pin down the water formation processes and as constraints for ocean circulation models.

Published CFC measurements in other oceans of the world have been sparse. However, Trumbore *et al.* (1991) report CFC evidence to support rapid ventilation of the Ross Sea. They develop a time dependent box model which includes the effects of mixed layer entrainment, gas exchange through leads, and mixing with waters ventilated remotely. Their results show that the dominant process ventilating sub-surface shelf water in the eastern Ross Sea is entrainment, whilst air/sea exchange is also significant in the western shelf waters. Using reasonable OUR values the simple circulation model they propose can account for the dissolved oxygen and nutrient distributions if an undersaturation of 10% occurs at entrainment.

In a study of the eastern Mediterranean deep circulation Schlitzer *et al.* (1991) use CFC-12 data with oxygen measurements. They argue that the Adriatic is the only source of deep and bottom waters in the eastern Mediterranean, and that inflow of Aegean water occurs as isolated lenses. Continuing this work, Roether & Schlitzer (1991) use tritium observations to provide a dual tracer tool which constrains the convective deep water renewal.

Two recent studies based on modelling work are worthy of note. Musgrave (1990) analyses the invasion of transient tracer pairs into a wind driven geostrophic gyre to examine the effect of circulation and lateral mixing. Although the tracers used are tritium (^{3}H) and helium (^{3}He) the research is of direct relevance to CFC workers. Musgrave (1990) points out that the behaviour of transient tracers cannot be uniquely described by a single Peclet number. The distributions depend on both the diffusive and the advective timescales rather than simply of the ratio of these two parameters. (The Peclet number still characterises steady state flows.) He also shows that ^{3}He measurements cannot distinguish between direct ventilation (e.g. Ekman pumping) and diffusive ventilation at the northern boundary of the model.

Thiele & Sarmiento (1990) present work investigating generic tracer ventilation ages (including tritium/helium but not CFC-113/CFC-12). They form a steady state tracer age equation which has sources and sinks of age due to mixing and very simple boundary conditions (age = 0 at the surface). By assuming that a long term average circulation exists then a steady state ventilation age can be easily defined. Thiele & Sarmiento (1990) examine how successfully tracer ages can be used to test this assumption. Their model results suggest tritium/helium is more useful in this respect than the CFC-11/CFC-12 ratio, although they believe CFC-113 "offers considerable promise".

The work described above used CFC-11 and CFC-12 for calculations. Apart from the pioneering work of WG there have been no other published reports of work using CFC-113 as an ocean tracer, although Dickson *et al.* (1990) makes use of CFC-113 data in the Denmark Straits overflow region (A J Watson, Pers. Comms.). Indeed, as Chapter 2 explains, the analytical technique of WG is liable to contamination and is not trustworthy.

1.5. The Suitability of CFCs as Oceanic Tracers.

The aim of this section is to draw together elements introduced in Sections 1.3 and 1.4 to put CFCs in a context of other ocean tracers. CFCs are anthropogenic, conservative, transient tracers. To understand their usefulness each of these terms must be explained. For the purposes of this work a 'tracer' is defined as a quantity which has no influence on the property which it is tracing, or on the flow. Anthropogenic CO_2 certainly does influence marine chemistry for example, and potential vorticity is a dynamically active tracer, albeit conserved.

The term anthropogenic means man-made in origin. CFCs are anthropogenic because there are no (known) natural sources of the gases. Any error associated with a non-anthropogenic source of CFC species is certainly swamped by current errors in measuring their concentrations, as borne out by the study of deep, old water masses (the scatter in the data is centred about zero concentration). This is not the case for several other transient tracers, which have both anthropogenic and non-anthropogenic sources, and this introduces uncertainty in interpreting fields of their concentration. Carbon tetrachloride (CCl_4), for example, may well have a small natural background level (Krysell & Wallace, 1988) and radiocarbon (^{14}C) certainly does have a non-anthropogenic source, which is variable in its rate.

Conservative, in this context, means that there are no processes which are sinks for the species in the ocean. Salinity and temperature are also conservative in the (adiabatic) ocean, whereas radioactive tracers such as ^{228}Ra are not because they spontaneously decay into other isotopes. The ocean is not a promising sink for CFCs since their solubilities are too low (about 0.01% in the aqueous phase at 25°C); the small amounts which are slowly removed to the deep sea by thermohaline circulation are swamped by the photodissociative sink in the stratosphere.

'Transient tracer' means that the tracer concentrations are changing with time; it is the opposite of steady state. This is due to the time dependency of the CFC concentrations in the atmosphere.

These three properties all arise ultimately from the chemically inert nature of CFC species. This unreactivity offers CFCs an advantage over other tracers whose behaviours can be less well determined. CFCs are sparingly soluble in water with atmospheric rates of increase, and lifetimes, much larger than the characteristic period for atmospheric mixing. This means that, in general, atmospheric CFC is well mixed giving a uniform global concentration. Other transient tracers are not evenly distributed in this way and there are large regional variations in atmospheric burden. In the case of tritium, for instance, the atmospheric source was nuclear weapons tests, and the reactivity of tritium radicals ensured a significant rainout, local to the test site. Weiss & Roether (1980) estimate that by 1972 75% of the total oceanic input of tritium had been received by the northern ocean. Gammon *et al.* (1982) and Bullister (1984) point out that this makes CFCs useful as tracers in the southern ocean where the efficacy of tritium/helium tracers is compromised.

Another advantage of CFC tracers is that their source functions are reasonably well established. Although direct global measurements have only been made since 1976 (Rasmussen *et al.* 1981), use of release data allows an inventory technique to predict how atmospheric concentrations vary with time, and so the atmospheric concentration at the ocean surface in any particular year is known with some confidence (Section 1.3.1).

Finally, a particular feature of CFC systematics is the rapid analysis of samples (the method discussed in Chapters 2 and 3 takes about thirty minutes for each sample). The sample volume can also be taken from the same Niskin bottle used for salinity and oxygen determinations (compare this with the hundreds of litres required for ^{39}Ar or ^{85}Kr analyses, for example). These characteristics have benefits in the field and, for example, Wallace & Moore (1985) used CFCs in real time analysis to plan where to take larger samples of ^{90}Sr and ^{137}Cs for later analysis in the laboratory.

1.6. Explanation of Chapter Content.

This thesis is arranged in six main chapters, plus this chapter on Introduction and Review.

Chapter 2 deals with experimental method. Following introductory remarks there is a brief discussion of the background to the CFC-113 instrument used; some shortcomings of WG's system are mentioned and an alternative method is proposed. The remainder of the chapter deals with a description of the instrument, the analysis technique, and details of sampling methodology.

Chapter 3 is concerned with Data Processing and Calibration. Section 3.1 discusses the chromatogram processing tasks required, their impact is assessed and the method to calibrate the ECD is described in Section 3.2. The techniques used to prepare and calibrate standard gas mixtures are described in Section 3.3, whilst Section 3.4 reports the results of such a calibration experiment. Chapter 3 is concluded by a section concerning an inter-calibration exercise and statements about the instrumental accuracy.

The results of two field work campaigns are discussed in Chapter 4. After an introduction (Section 4.1) the instrumental performance is appraised in the light of the field data (Section 4.2). Minor technical problems are discussed and then a particular difficulty is identified, and the steps taken to correct the data described. The results of marine air observations, used in the atmospheric source functions of Section 1.3.1, are reported and Section 4.2 ends with conclusions concerning the instrumental detection limit, precision and dynamic range. Section 4.3 is concerned with CFC-113 ventilation ages and reports some results from the VIVALDI survey. A section on the hydrography of the north east Atlantic is followed by a discussion on the calculation of ventilation ages where the key parameterisation to deal with the (unknown) CFC-113 solubility is described and appraised. Finally, some typical CFC-113 ventilation age distributions from the VIVALDI survey are reported and briefly discussed. The reader who is less interested in analytical detail may proceed directly to Section 4.3, although Sections 4.2 and 4.3 are intimately linked.

Chapter 5 deals with the effect of the mixed layer dynamics on the CFC boundary condition for the main thermocline. Relevant literature is reviewed in Section 5.1 and

compared to VIVALDI data. A simple analytical model of tracer invasion into an homogeneous layer is developed in Section 5.2 which introduces important parameterisations and provides a comparison in special circumstances for the more general mixed layer model described in Section 5.3. The model sensitivity to parameterisations and initial conditions is discussed in Sections 5.4 and 5.5. Section 5.6 attempts to compare VIVALDI surface data with the model results and the chapter is concluded in Section 5.7.

Chapter 6 examines the influence of advection and mixing on ventilation age. A simple diffusive box model (Section 6.2) provides a special case of more general conditions developed in Section 6.3 in terms of a ventilation age evolution equation. Section 6.4 uses data from VIVALDI to analyse the balance in this expression. The influence of errors and the effect of isopycnic shear in the flow are discussed in Sections 6.5 and 6.6, with conclusions in Section 6.7.

Chapters 5 and 6 attempt to develop a basis for interpreting CFC-113 ventilation age fields by examining the effects of some physical processes on CFC distributions. In Chapter 7 the VIVALDI data presented in Section 4.3 are re-examined in the light of this work (Section 7.2). Section 7.3 continues this analysis by examining oxygen utilisation rates (OURs). Acceptable published values of OURs are used to imply features of the CFC-113 ventilation age behaviour which is comparable to the simple diffusive model of Section 6.2. The thesis is concluded in Section 7.4 and suggestions for future work appear in Section 7.5.

CHAPTER 2

EXPERIMENTAL METHOD.

2.1. Introduction to the CFC-113 Analysis Technique.

As explained in Chapter 1, existing research has been specifically applied to the two most abundant CFC gases in the atmosphere : CFC-11 and CFC-12. Established techniques render their determination dissolved in seawater routine (Gammon *et al.* 1982, Bullister & Weiss 1988). In addition, Wisegarver & Gammon (1988) demonstrate the promise of another CFC compound as an oceanographic tracer; namely CFC-113. The instrumental techniques described in the publications listed above involve use of a gas chromatograph (GC) with a packed column and an electron capture detector (ECD) to separate and quantify particular compounds. The ECD is well-suited to this application since it is simultaneously selective in its response and very sensitive. Seawater drawn from a Niskin bottle is used in the analysis technique. A seawater extraction system strips the dissolved gases from the seawater which are then dried before injection onto the chromatographic column. The ECD cell is calibrated regularly with samples from a cylinder of compressed standard gas which contains known concentrations of each compound of interest.

Research conducted by the PML tracer group established that the method described by Wisegarver & Gammon (1988) was inadequate in measuring CFC-113 (A J Watson Pers. Comms., Haine *et al.*, Submitted). In particular, there is at least one other compound, present in the ocean which elutes at similar times to CFC-113, causing severe problems with its quantification. Experiments performed by the author in the laboratory revealed this compound to be methyl bromide (CH_3Br), and Figures 2.1(a) and 2.1(c) show that CFC-113 and CH_3Br co-elute on a system built following the design of Gammon *et al.* (1982). This work also revealed that methyl chloride (CH_3Cl) can appear on the CFC-11 shoulder, giving less severe, though significant errors in the quantification of that species too (see Figure 2.1(b)). Singh *et al.* (1983b) found the average concentration of methyl bromide and methyl chloride in the eastern tropical Pacific to be 12 and 230 pMol/l respectively. Values for the western basin of the North Atlantic Ocean are similar; 10-20 pMol/l for methyl bromide, with increased values on the continental shelf, consistent with the postulated seaweed source for this species (R M Moore, Pers. Comms.). However, the author has also established that the GC column used by Wisegarver & Gammon (1988) can partially separate CFC-113 from methyl bromide under certain circumstances. These circumstances are difficult to specify, and the GC system never reliably distinguishes these two compounds. (These conditions may be associated with carrier gas impurities or the conditioning history of the GC column.) It appears as if the methyl bromide retention time may fluctuate somewhat. Other peaks on

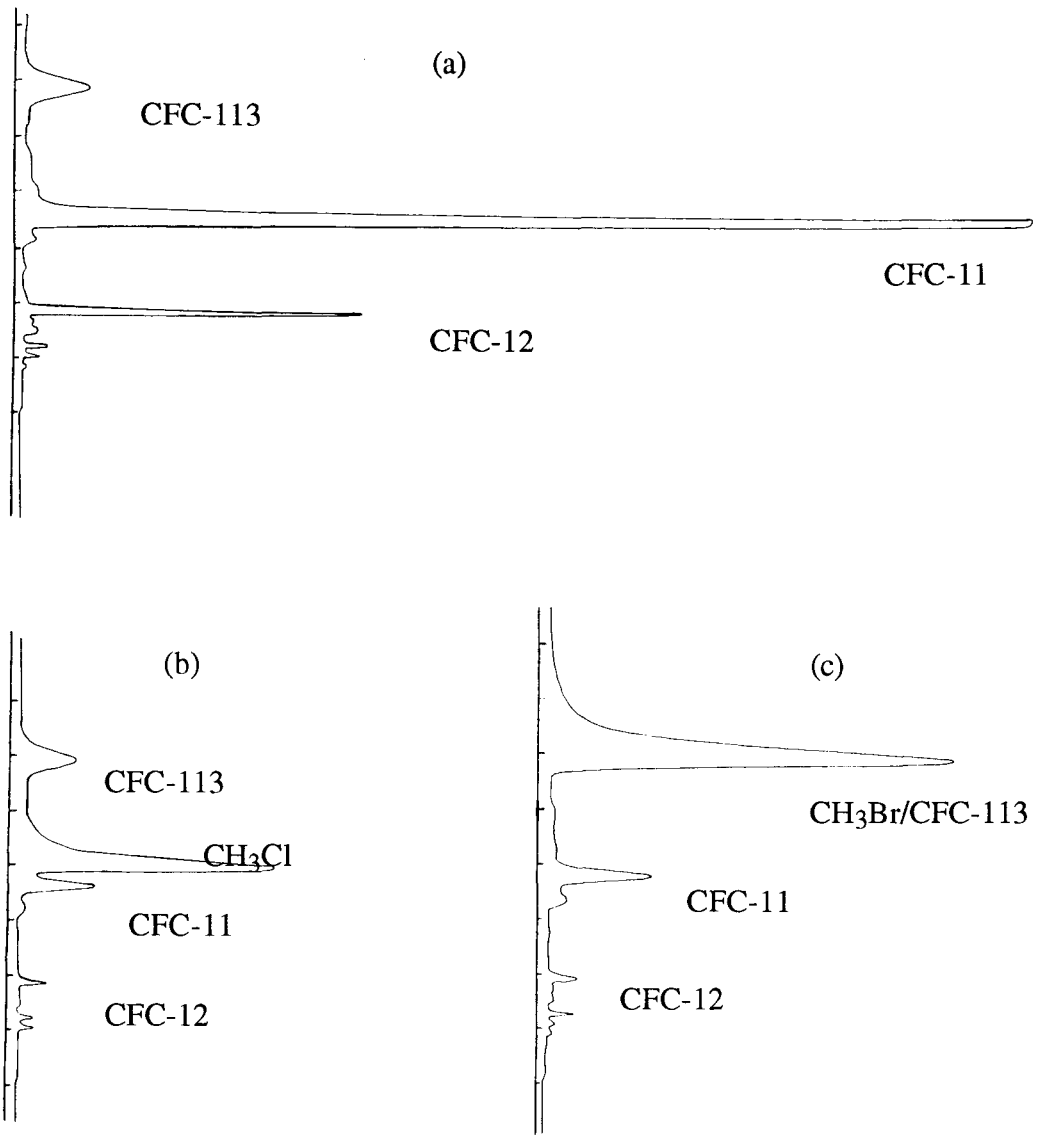

Figure 2.1. Chromatograms run using a manual system similar to Wisegarver & Gammon's (1988). Column 3m Porasil B, precolumn 15cm Porasil B (both at 100°C), Trap 5cm Porasil C. a) Injection of standard gas containing CFC-12, CFC-11 and CFC-113. b) Injection of outside air spiked with methyl chloride, c) Injection of outside air spiked with methyl bromide. In each chromatogram the axis is ticked with units of one minute, with the same attenuation throughout. Retention time increases up the page.

the chromatogram show this too (methyl chloroform, CH_3CCl_3 for example), but the CFC compounds are not subject to this variability.

Two approaches were tried initially in an attempt to resolve this problem. These were a) use of a catalytic technique to remove methyl bromide without affecting CFC-113, and b) use of two chromatographic packing materials in a single column in order to achieve improved CFC-113 resolution. Neither of these methods were successful, and a system with improved chromatography was sought in order to clearly separate CFC-113 from surrounding peaks.

A GC system incorporating a capillary column where the stationary phase is attached to the inside wall offers superior resolution to a packed column. One reason for this is that gas flow through a capillary column is laminar, whereas in the packed variety turbulent processes tend to smear out sharp concentration gradients thereby degrading peak resolution. The work presented in this chapter describes the technique for the simultaneous measurement of all three CFC compounds of interest using a wide bore capillary column (WBC, or MegaBore). Figure 2.2, a chromatogram from a simple GC system using such a WBC (DB-624), shows good resolution for the CFC compounds of interest (M Krysell recommended this column). With this performance established an instrument was designed and built which was capable of dealing with seawater samples on an oceanographic cruise. This system gives less precise replicate seawater concentrations and higher limits of detection for CFC-11 and CFC-12 than those quoted by Bullister & Weiss (1988) for example (see Section 4.2.4). However, it does allow CFC-113 analyses to be made with a precision and reproducibility not previously achieved.

The analytical system used to measure the concentrations of CFCs dissolved in seawater is shown in Figure 2.3. In essence it combines the seawater sampling method and valving scheme used by Gammon *et al.* (1982) with capillary GC techniques, and some different features which are explained below. The discussion is split into three pieces. Initially the system design is described in terms of its component parts, with mention of the reasons for the choice of these items (Section 2.2). Secondly the way in which the analysis proceeds is explained by following the progress of a seawater injection (Section 2.3). Finally Section 2.4 discusses procedures adopted at sea to minimise contamination problems.

2.2. Description of Constituent Components.

The basic design of the system including valves 1-4 of Figure 2.3, and their satellite apparatus is founded on the method of Gammon *et al.* (1982). The additions necessary to drive the capillary column modify that scheme and include the make-up gas cylinder and separate stripper and carrier gases. Specific idiosyncrasies of the PML system are the palladium catalyst, and needle valves mounted on valves 3 and 4.

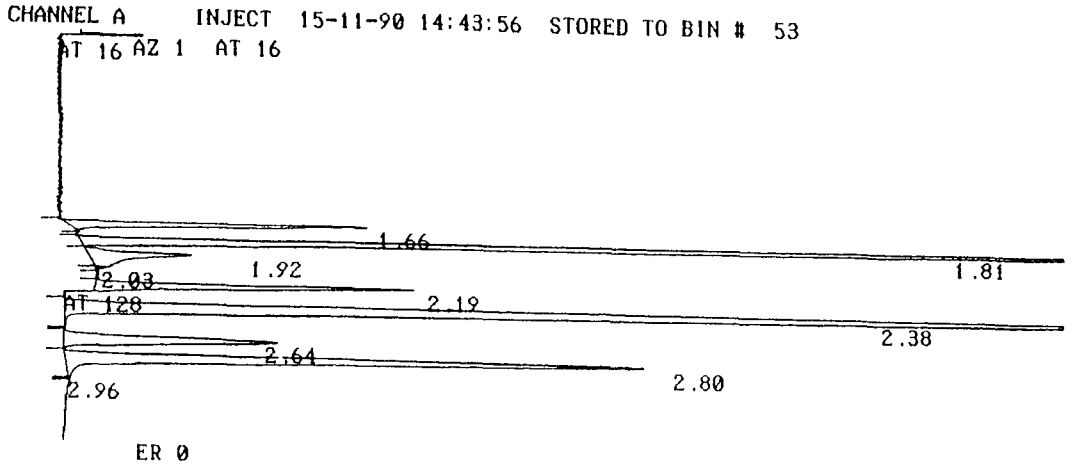

Figure 2.2. Chromatogram of standard gas mixture containing CFC-11, CFC-12, CFC-113, CH_3Cl, CH_3Br and CH_3I. Column is 27m DB-624 @ 70°C, Helium carrier flow = $4cm^3$/min, Oxygen-free Nitrogen make-up gas flow = $30cm^3$/min. Injection achieved directly into carrier stream using a Valco 6-port valve with a 190µl sample loop filled from the cylinder of standard gas. Retention times (RT, decimal minutes) below.

RT	1.66	1.81	1.92	2.03	2.19	2.38	2.64	2.80	2.96
Species	O_2?	CFC-12	CH_3Cl	?*	CH_3Br	CFC-11	CFC-113	CH_3I	†

* 2% of CH_3Cl peak, † Integrator Error.

Valve 1, the seawater sample volume, sparging tower and drying tube comprise the seawater sampling front end. The Hastelloy-C $\frac{1}{8}$" Valco valve has two positions; one to fill the sample volume by injection of the seawater in the syringe, and a second to route the stripper gas through the sample volume, transferring the sample into the sparging tower. The seawater sample volume is a specially blown glass bulb whose total volume (including connecting tubes and unions) is known to within 0.1% (38.800 cm^3). The sparging tower is a thick-walled glass column with epoxy-bonded stainless steel collets at each end. An air stone is silver soldered into the lower collet, and through this the seawater and subsequent stripper gas enters the sparging tower. The air stone provides a fine and even stream of bubbles with which the seawater sample is stripped. The water sample is drained from the sparging tower automatically via a valve pinching a length of silicone tubing. A 1m coil of stainless steel tube isolates the silicone from the sample. The drying tubes are blown from 6mm od thick-walled glass tubing of consistent cross section. They are loosely packed with anhydrous magnesium perchlorate which removes water vapour quantitatively from the stripper gas stream. These drying tubes tend to become exhausted after 30-40 hours use and are routinely replaced after each cast has been analysed. During construction all of the glassware items in the seawater extraction system were cleaned in laboratory detergent and then propan-2-ol so as to remove any greasy films.

Downstream of the seawater sampling system is valve 2 (Hastelloy-C $\frac{1}{8}$" Valco) and two sample loops which allow known volumes of gas to be introduced into the path of the stripper gas. (Volumes are 2.1232 and 0.3768 cm^3 with standard errors less than 0.03% for 10 determinations.) The ECD is routinely calibrated by injections of the small loop filled with standard gas (see Section 3.2), whilst the large loop is used for injection of air samples. When air samples are analysed the standard cylinder shown in Figure 2.3 is replaced with a Luer fitting which can mate directly with a ground glass syringe containing air.

Valves 3, 4, (Hastelloy-C $\frac{1}{16}$" Valco) the trap, precolumn and main column comprise a typical purge and trap arrangement with the facility to cut off the eluting sample from the main column at a convenient point. The system is, in essence identical to that used by Gammon *et al.* (1982). However, each of valves 3 and 4 also have a Nupro needle valve mounted between ports. They are used to control flow rates, and ameliorate pressure transients as valves 3 and 4 throw. This system is particularly sensitive to such pressure surges since the flow rate of carrier gas is an order of magnitude smaller than that of the stripper gas. The needle valve on valve 3 is used to reduce the flow of stripper gas to the flow meter when the carrier gas is routed to valve 4. This eliminates the danger of water sparging in the tower from blowing over onto the drying tube and potentially further into the system. The needle valve on valve 4 is adjusted to balance the trap impedance closely so that the carrier flow rate does not alter as valve 4 throws (hence

Figure 2.3. Diagram of CFC Analytical System.

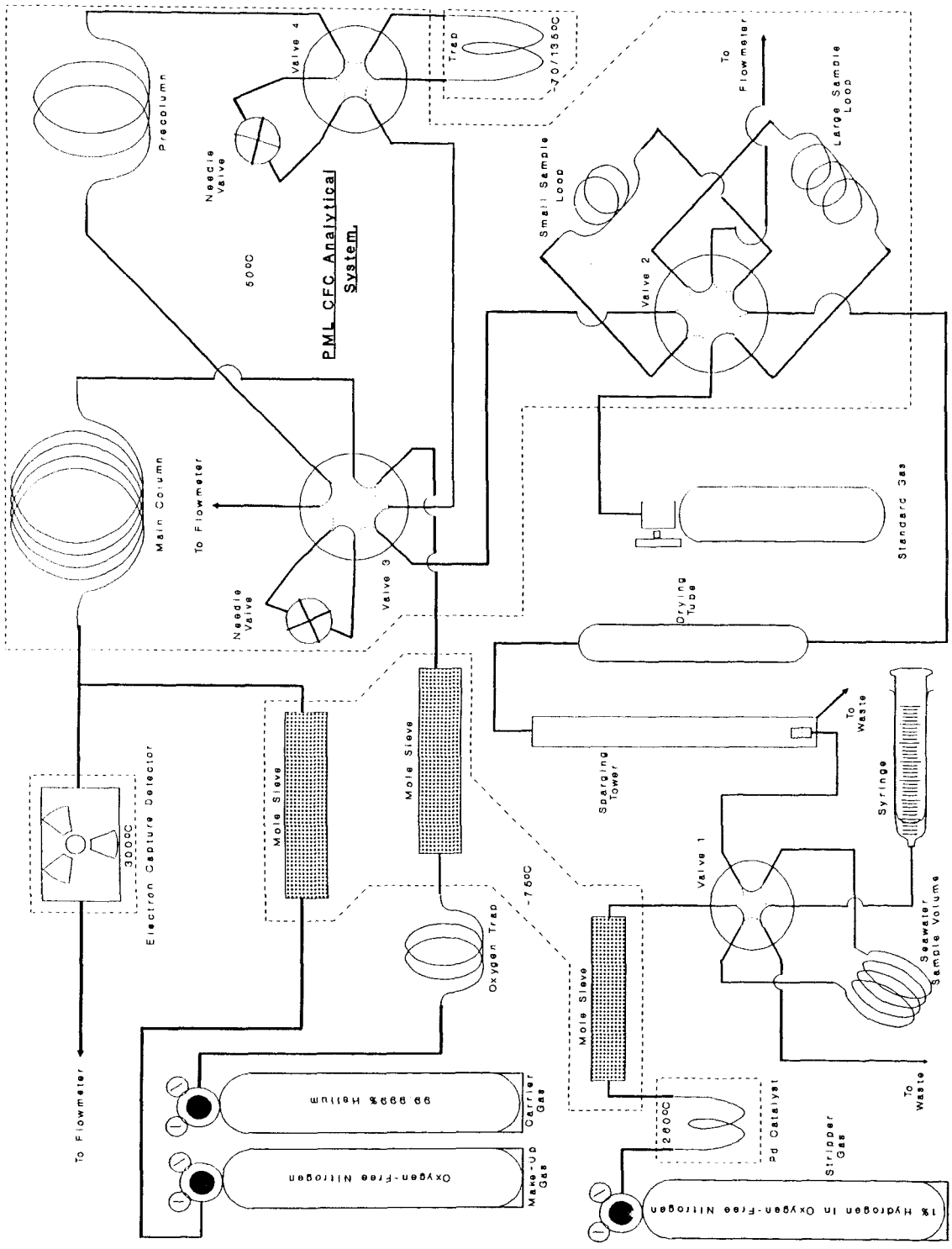
PML CFC Analytical System
Precolumn
Needle Valve
Valve 4
Trap
-70/135°C
60°C
Small Sample Loop
Large Sample Loop
To Flowmeter
Valve 2
Main Column
To Flowmeter
Needle Valve
Valve 3
Standard Gas
Drying Tube
Mole Sieve
Mole Sieve
Mole Sieve
Sparging Tower
To Waste
Syringe
Valve 1
Seawater Sample Volume
Electron Capture Detector
300°C
Oxygen Trap
-75°C
To Flowmeter
99.999% Helium
Carrier Gas
Oxygen-free Nitrogen
Make-Up Gas
200°C
Pd Catalyst
Stripper Gas
To Waste
1% Hydrogen in Oxygen-Free Nitrogen

reducing otherwise large baseline changes). The Gammon *et al.* (1982) valve arrangement was considered preferable to that used by Bullister & Weiss (1988) since the dead volume of the trap is more easily minimised. Although the Bullister & Weiss (1988) system has the advantage of back-flushing the trap, forward flushing was not considered a problem since the stripper gas is used to blow the trap clean, and this runs an order of magnitude faster than the carrier gas used to flow the sample onto the precolumn.

The trap itself consists of a short length (7cm) of $\frac{1}{8}$" stainless steel tube (id = 0.085") with 3cm lengths of $\frac{1}{16}$" stainless steel tube (id = 0.043") silver soldered into the ends of the larger diameter pipe. The trap is packed with Porasil 'C' and the packing retained with plugs of glass wool which penetrate no further than half way into the $\frac{1}{16}$" tubes. Zero dead volume unions connect the trap to $\frac{1}{16}$" stainless steel tubes (id=0.006") leading to valve 4. The integrity of the trap is absolutely critical to the success of the chromatographic separation. The qualities required of the trap conspire to be in opposition to each other; namely that the trap be sufficiently retentive to enable removal of each CFC compound from the stripper gas stream whilst being of low enough volume for these components to be adequately resolved by the column. With the configuration of trap used (the best of several tried of this type) the first requirement was not completely met. The stripper gas was carefully monitored and adjusted in order to guarantee full retention of the CFC-12 on the trap, with an accepted slight loss of sample due to incomplete sparging. This is of order 1-2%, and can be corrected for subsequent to the analyses (see also Section 4.2.1). Wisegarver & Gammon (1988) point out that CFC-11 is the most soluble of the three CFC species and this compound will be the least efficiently sparged. Indeed, comparison of standard and seawater replicates (Section 4.2.4) revealed that CFC-11 precisions were slightly lower for seawater samples, though CFC-12 and CFC-113 were not significantly affected (standards are injected onto the trap at the end of each stripping period). The trapping temperature is -70°C or lower, maintained by an immersion bath of propan-2-ol and dry ice. The burnoff temperature is 135°C, achieved by immersion in glycerol heated by a cartridge heater with a simple on/off controller.

The precolumn and main column are made by cutting a 30m Durabond-624 0.53mm id 'MegaBore' column into 3m and 27m lengths. The column has a surface bonded and crosslinked stationary phase on an inert silica substrate with a 3µm film thickness. The main column exhaust flows directly into the cell of the ^{63}Ni ECD and is mixed rapidly there with a faster flowing electron capturing make-up gas (oxygen-free nitrogen). The ECD working temperature is 300°C; that of the column and precolumn 50°C. Valves 2,3,4, the sample loops, plumbing and needle valves are also contained within the GC oven (a Shimadzu model GC-8A) This enables the valve rotors and needle seats to be conditioned with the columns between casts by raising the oven temperature to 130°C, whilst simultaneously providing an isothermal environment for the sample

volumes. All tubing connections downstream of valve 2 are made with $\frac{1}{16}$" stainless steel tube (id=0.006") to minimise dead volumes.

The gas cylinders used to run the system are shown on the left of Figure 2.3. Each of them has molecular sieve 13X tubes connected, held in a cooling bath of propan-2-ol at -75°C. In addition the carrier gas is treated by an O_2 trap upstream of the molecular sieve which removes any traces of O_2 from the helium. The most stringent requirement for low CFC content is of the stripper gas. This has a 20cm x $\frac{1}{8}$" stainless steel tube packed with pure palladium chips held in an oven at 260°C upstream of the molecular sieve. The stripper gas mixture of 1% hydrogen in oxygen-free nitrogen allows any trace halocarbon contaminants to be removed by hydrogenation on the hot catalyst The molecular sieve then serves to filter from the gas the catalysis end-products (halogen containing compounds, and fully saturated halocarbons). The flow rates are respectively : 35, 7 and 60 cm^3/min for make-up, carrier and stripper gas. The carrier flow must be deduced from the retention time of the column, since the ECD exhaust contains make-up and carrier gas. The ECD exhaust is however a good monitor of the make-up gas component, since the make-up flow is an order of magnitude larger than the carrier contribution. The stripper flow rate quoted is for a real water sample being bubbled in the sparging tower. At the end of each cast analysed valve 3 is left with carrier diverted to valve 4, and the GC oven temperature is raised in order to condition all the components it contains. Thus the needle valve on valve 3 helps to conserve the stripper gas (flow is typically halved at the flow meter) when the machine is idle. Once set up the gas conditioning apparatus need not be disturbed for long periods, and the lifetime of a typical 50l stripper gas cylinder (the most rapidly exhausted gas) is 3-4 months.

2.3. Description of Analysis Procedure.

The important steps necessary in running a seawater or standard sample analysis are explained below. The initial valve configuration is the same as that shown on Figure 2.3. The trap is immersed in the cold bath at this stage, and a thermocouple directly welded to the trap tubing is used to monitor its temperature; a useful aid in maintaining consistency between runs. For a seawater injection the syringe is attached to valve 1 via a length of stainless steel pipe and a Luer tap. Twenty cm^3 of the seawater sample are used to flush the tubes and valve before valve 1 is thrown to allow the sample volume to be flushed and filled. If standard gas is being analysed the standard cylinder is connected to valve 2 (in the 'load small loop' position) and a slow flow of gas is used to flush the loop. The standard cylinders used contain gas at 1000psi and although no regulator is fitted, the stop valve can be adjusted with care to maintain a flow of order 10cm^3/min.

At the start of the analysis valve 4 is thrown to open the trap (valves 3,4 and the pinch valve are controlled from the integrator). Seawater samples can be injected at this stage by throwing valve 1. With a stripper flow rate of 60cm^3/min the sample takes about

1.5mins to transfer to the sparging tower where it is stripped for a further four minutes, giving a stripping gas volume of 240cm^3 to be trapped (this volume strips more than 99% of the CFCs from the water sample). Alternatively, loops of standard may be injected towards the end of the run. This guarantees no loss of CFC-12 through the cold trap; the slow flow of standard gas is stopped, valve 2 is thrown after a 10 second pause, and a note made of the atmospheric pressure. Multiple injections are accomplished in a straight forward way by isolating the trap and refilling the sample loop. Marine air samples are injected onto the trap in the same manner as standards except that the large sample loop is used and a note of the relative humidity and air temperature is made. They are collected from exposed, upwind parts of the ship in dry ground glass syringes used for the seawater sampling.

At the end of the stripping period valve 3 is thrown. This allows carrier gas to flow over the trap for 18 seconds before it is isolated at 5.8 minutes. By doing this the nitrogen/hydrogen mix in the trap and pipes is flushed out at this stage and baseline fluctuations due to the stripper gas eluting near the CFC-12 peak are reduced. The trap pressure is also equalised with that of the carrier gas. Once the trap is isolated, the cold bath is replaced with a beaker of hot glycerol (135°C). During the period in which the trap is coming up to temperature the pinch valve attached to the sparging tower waste line is opened automatically to drain the stripped seawater. At 7.3 minutes into the run valve 4 is thrown in order to open the trap. By this stage the indicated trap temperature is within 1°C of the glycerol temperature (which is accurately thermostated). The precolumn is exposed to the carrier stream for 21 seconds before valve 3 diverts stripper gas towards valve 4 in order to flush the trap and precolumn. This allows the chromatogram emerging from the main column to be cut off after CFC-113 has eluted, and also improves resolution (see also the discussion in Section 4.2.2). After 100cm^3 of stripper gas has flushed the trap, it is isolated and the hot bath can be removed. The compounds of interest appear at 1.47, 2.26 and 2.68 minutes after the trap opens for CFC-12, CFC-11 and CFC-113 respectively (carrier flow rate of 7.2 cm^3/min). Methyl Iodide (CH_3I) is retained slightly longer than CFC-113 and once it has eluted the run can be terminated. When all data logging housekeeping has been finished the next run can commence.

2.4. Sample Handling Techniques at Sea.

The CFC analytical system described here was taken to sea for an extended trials period during the spring of 1991 (the VIVALDI expedition; see Section 4.1), and the following precautions were made for that cruise (also see Section 4.2).

The 20l General Oceanics Niskin bottles were hung outside and aired for three days in order to remove any volatile contaminants (methylethylketone can be smelt on new water bottles in particular, M I Liddicoat, Pers. Comms.). They were completely dismantled and the smaller component parts wiped free of grease and agitated with

propan-2-ol in an ultrasonic bath for twenty minutes. These were then soaked in strong detergent solution for three days, rinsed in distilled water and propan-2-ol, and baked at 80°C for twenty four hours (higher oven temperatures can damage the rubber in the 'O' rings). The bottle bodies themselves were washed with a commercial high pressure cleaner drawing detergent solution through a solvent feed. After hanging the bottles out to dry they were reassembled and left open, outside, to age for two weeks.

The Segma 100cm^3 ground glass syringes and Rocket Luer-lock taps were treated initially then every other cast as follows. Firstly they were rinsed well in fresh water with the syringe barrels and pistons separated. They were then left soaking in strong, warm detergent solution for eight hours whilst the taps were treated in the same solution ultrasonically. After copious fresh water rinses both syringe barrels and pistons and taps were washed in propan-2-ol and finally left to dry in an oven at 100°C. Note that fresh water was used at sea rather than the high purity de-ionised water available because it was found that the ion-exchange resins were a potent source of CFC-113. As parts of the sampling system become greasy contamination problems become more frequent (see Section 4.2.1). This is because the species of interest are significantly more soluble in non-aqueous solvents than they are in natural waters. When sampling in regions of high biological productivity the frequency with which the sampling apparatus was cleaned increased in an attempt to maintain the integrity of the syringes, taps and Niskins.

CHAPTER 3

DATA PROCESSING & CALIBRATION.

3.1. Baseline Fluctuation : Reprocessing Chromatograms.

One complicating factor in the analyses performed using the CFC analytical system described in Chapter 2 is that the baseline has a tendency to fluctuate. At least some of this variation is a result of the different gases used for carrier and stripper, and pressure transients, underlining an important point concerning the pragma used to design the instrument. As explained in Section 2.2, the trap must have a small enough volume to ensure a sharp injection, whilst being sufficiently retentive of CFC-12. In comparison to previous CFC systems these requirements demand a more tightly packed trap, and an increase in upstream stripper gas pressure if sufficient volumes are to be bubbled through the seawater sample in the sparger. The needle valve on Valve 4 (Figure 2.3) is adjusted to balance the trap impedance so that the flow of stripper gas does not surge when the valve throws, closing the trap. In addition, Valve 3 is thrown before the trap is isolated so as to flush the stripper gas from the trap and precolumn, in order to reduce baseline fluctuations. This is because carrier flow rates for WBC columns are of order a few cm^3/min (ten times less than those used for packed GC columns), presenting potential problems in transferring the trapped sample between stripper and carrier gas streams.

Despite these measures the baseline varies in such a way that the quantification of CFC-113 in particular is difficult. This perturbation is persistent and reproducible, although not present in the chromatograms from the packed column GC after Gammon *et al.* (1982) (Figure 2.1(a)). It has also been observed on a 75m DB-624 column using Ar/CH_4 carrier gas with a purge and trap injection system built in the way described by Bullister & Weiss (1988) (S M Boswell, Pers. Comms.). An example of this fluctuation is shown in the trapped stripper gas blank chromatogram of Figure 3.1(a), taken at sea using the instrument described in Chapter 2. This perturbation means the precision required of the technique demands that each chromatogram is replayed with the blank automatically subtracted before peaks can be quantified. The blank characteristics must be conscientiously monitored and in general blanks are routinely analysed every fifth or sixth sample, so that any particular run would have a blank taken away which was about 40 minutes distant. Figure 3.1(b) shows a raw chromatogram of a seawater sample, and Figure 3.1(c) the reprocessed version with the blank from Figure 3.1(a) subtracted (Figure 4.2 shows a reprocessed chromatogram of a marine air sample). This frequency of blank sampling is more than adequate, and, for example, the discrepancy between reprocessed peak heights for the same sample with two separate blank runs subtracted is about 0.002pMol/l for CFC-12 and CFC-11 and 0.004pMol/l for CFC-113 (Figure 3.2; blanks separated by 130 minutes). These uncertainties are of the same order as the

Figure 3.1. Chromatograms of water from bottle #72 (8dB), station 11004 (45B on Figure 4.1, 44 53.4'N 12 16.8'W) taken on 28/4/91. (a) Trapped stripper blank (225cm^3), (b) Raw chromatogram of water sample #72, (c) Reprocessed chromatogram of water sample #72, (bin #41 - bin #47). Attenuation change at 9.25 (increases 4x), and 9.7 (decreases to $\frac{1}{4}$ initial value) in (a) and (b). Time in decimal minutes of CFC peaks are listed below.

Time	8.65	8.77	8.92	9.00	9.26	9.39	9.51	9.91	10.05
Species	N_20	CFC-12	CH_3Cl	?	CH_3Br ?	?	CFC-11	CFC-113	CH_3I

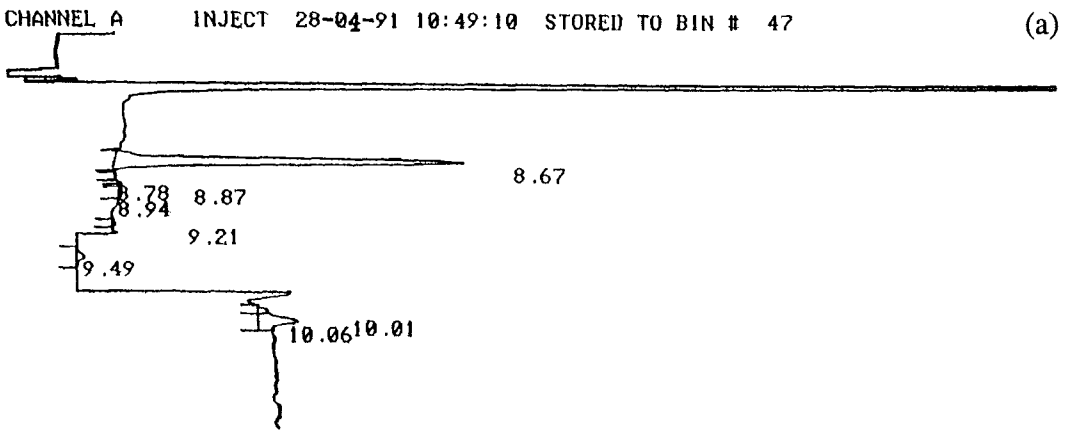
CHANNEL A INJECT 28-04-91 10:49:10 STORED TO BIN # 47
8.67
8.78
8.87
8.94
9.21
9.49
10.06
10.01

(a)

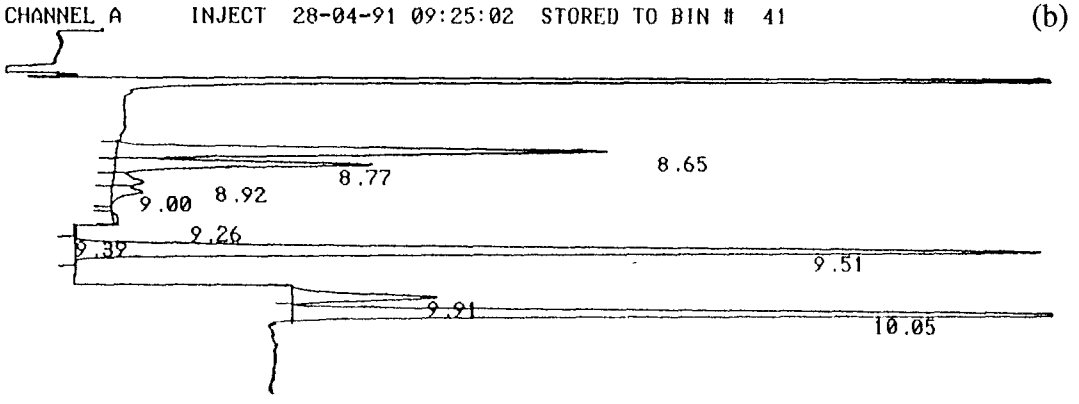
CHANNEL A INJECT 28-04-91 09:25:02 STORED TO BIN # 41
8.65
8.77
9.00
8.92
9.26
9.39
9.51
9.91
10.05

(b)

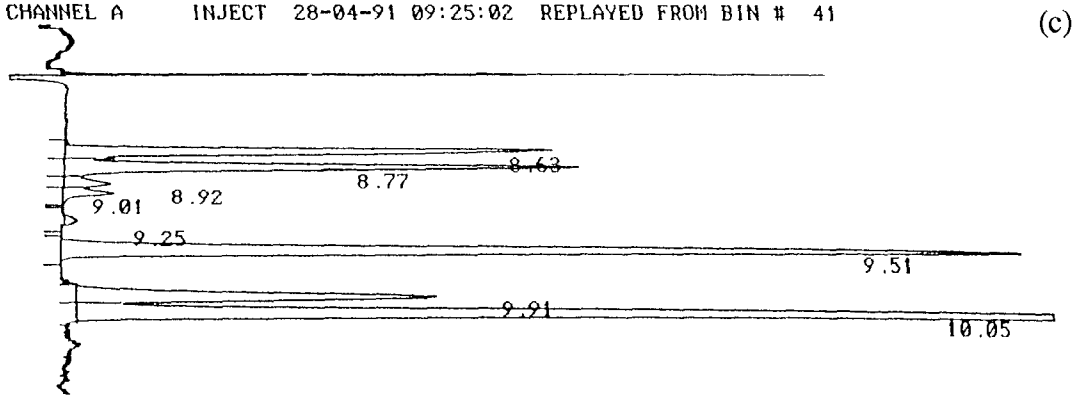
CHANNEL A INJECT 28-04-91 09:25:02 REPLAYED FROM BIN # 41
8.63
8.77
9.01
8.92
9.25
9.51
9.91
10.05

(c)

instrumental detection limit, and are negligible in comparison to the uncertainty due to the seawater sampling precision (see Section 4.2.4). Although reprocessing chromatograms with blanks subtracted is not, in general, a desirable technique, it was felt that the instrumental performance was enhanced, with insufficient compromise to prohibit its use.

3.2. ECD Response and Modelled Fit.

Electron-capture detectors are two electrode ion chambers with an internal beta particle supply; in the GC-8A machine used for this work a 370MBq ^{63}Ni source is doped on the internal wall of the detector chamber. Lovelock (1991) describes aspects of their research history and their theory (Lovelock 1974, Lovelock & Watson, 1978), although no model currently exists to adequately describe the behaviour of these detectors. ECDs offer great selectivity and sensitivity, whilst suffering from the disadvantage that their response tends to be non-linear (see, for example, Figure 3 from Gammon *et al.*, 1982).

The behaviour for compounds in the ECD of the system described in Chapter 2 is different to that in the detectors of the instruments designed by either Gammon *et al.* (1982) or Bullister & Weiss (1988) since the ECD contains both nitrogen make-up and helium carrier gas. The ratio of the carrier gas to the make-up gas in the ECD, as well as the combined flow rate, influences the way in which the detector responds to eluting compounds. Both the ratio and the flow rate are harder to control than in the traditional GC methods mentioned above. This is because there are two gases to regulate and the carrier is flowing slowly (7-8 cm^3/min). Nevertheless, the sensitivity to standard injections is reasonably stable over the time scales of a cast analysis, and if standards are run every 90 minutes or so, the ECD drift is within the noise limits of replicate samples.

All quantitative analyses using an ECD involve an empirical fit, and the fitting function used for this work is a quadratic (the primary standard preparation described in Section 3.4 used a spline fit). Bullister & Weiss (1988) employ a complicated approach using the ratios of polynomials specific to each CFC species, but this is considered unnecessary. The empirical calibrations described here must remain makeshift until an accurate theoretical description of the ECD is available. All analyses are bracketted in time by calibration runs of standard gas. An initial fitting function is derived from a set of standard injections at the beginning of each cast analysis and this function is linearly interpolated throughout the analysis session by regular injections of standard gas. The initial calibration normally comprises several repeat injections of a single small loop of standard gas in order to check the reproducibility, followed by two or three injections containing two small loops of standard. The size of the small sample loop is chosen so that two small loops of the working standard gas just bracket typical surface sea water responses (see Section 2.2 for the volumes of these loops). So, for each CFC species,

$$h = A(t)\, n^2 + B(t)\, n \qquad 3.2.1$$

Figure 3.2. Chromatograms of water from bottle #133 (1211dB), station 11007 (45A on Figure 4.1, 44 59.2'N 16 11.3'W) taken on 1/5/91. (a) Reprocessed chromatogram with blank run at 1354GMT subtracted, (b) Reprocessed chromatogram with blank run at 1604GMT subtracted. Seawater sample #133 was analysed at 1508GMT. Note how peak at 8.62mins (N_2O) has changed height between blanks, due to incomplete sparging of this compound from the water sample in the previous run. Apparent double peak, and reduced time for the CFC-113 peak in (b) is a result of integrator error ; time of CFC-113 peak in raw chromatogram is 9.92mins. Attenuation change at 9.25 (increases 4x), and 9.7 (decreases to $\frac{1}{4}$ initial value). Time in decimal minutes of CFC peaks are listed below.

Time	8.76	9.50	9.84,9.91	10.05
Species	CFC-12	CFC-11	CFC-113	CH_3I

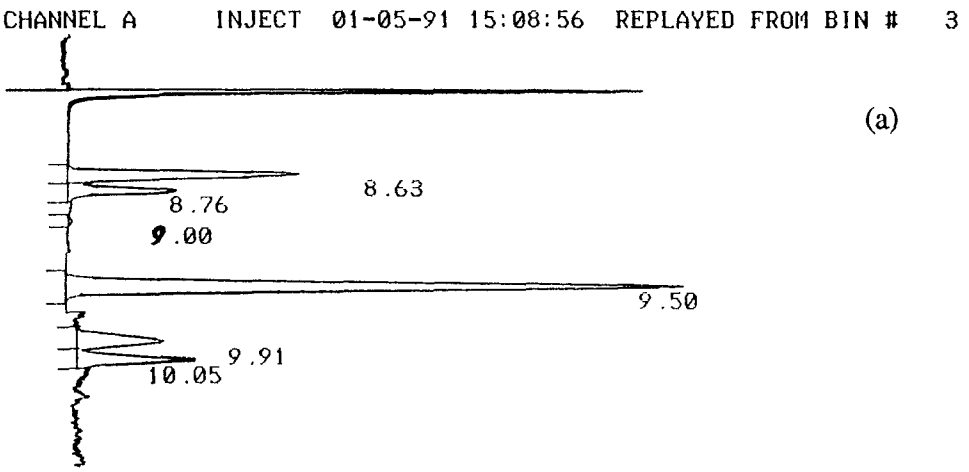
CHANNEL A INJECT 01-05-91 15:08:56 REPLAYED FROM BIN # 3
8.63
8.76
9.00
9.50
9.91
10.05

(a)

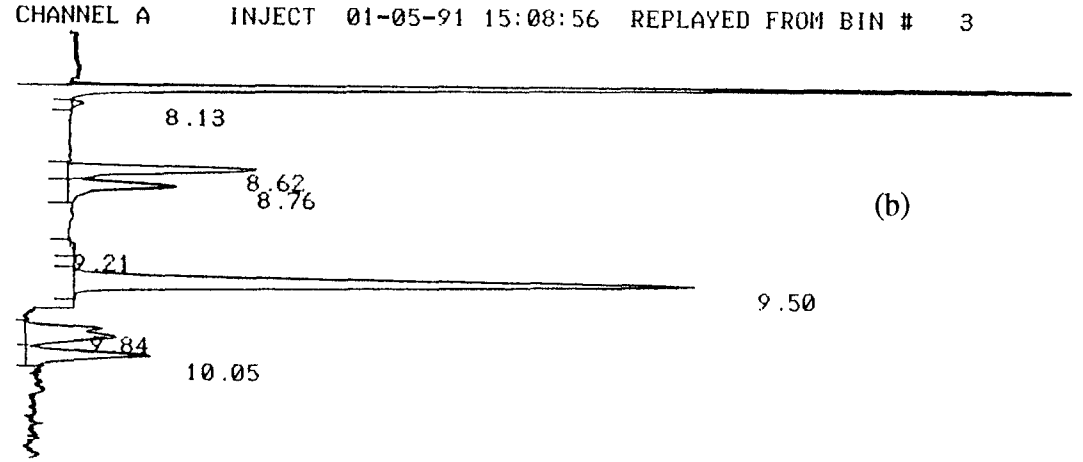
CHANNEL A INJECT 01-05-91 15:08:56 REPLAYED FROM BIN # 3
8.13
8.62
8.76
9.21
9.50
9.84
10.05

(b)

and $$A(t) = A_0 + at, \quad B(t) = B_0 + bt \qquad 3.2.2$$

where h is the peak height corresponding to the number of standard loops injected, n. Equation 3.2.2 applies for times, t, between bracketing standard injections. In addition,

$$aB_0 = bA_0 \qquad 3.2.3$$

is imposed. This is an additional assumption about the detector behaviour, which allows the standard curve to be re-normalised at any time by a single injection of standard gas. With h, A(t) and B(t) known, Equation 3.2.1 can be solved for n and thus related to the number of CFC molecules present in the detector. Table 3.1 shows statistical information regarding 34 calibrations made in this way. These data demonstrate the ECD response for CFC-12 and CFC-113 is not significantly non-linear, and is sub-linear for CFC-11, with the contribution of the squared term in Equation 3.2.1 19 ± 5% of that for the linear term, for this compound, in the range where saturated 1991 surface seawater concentrations lie.

Table 3.1. Statistics of calibration fitting parameters for 34 calibrations. A_0/B_0 is the ratio of non-linear coefficient to linear coefficient in the ECD fit. The Mean Non-linear/Linear row is the ratio of squared to linear terms in Equation 3.2.1 for typical surface seawater concentrations (n=2).

	CFC-12	CFC-11	CFC-113
Mean A_0/B_0. (Pk Ht units)	0.0017	-0.095	-0.047
A_0/B_0 Std. Error.	0.044	0.027	0.038
Mean Non-linear/Linear	0.0034	-0.19	-0.094

3.3. Preparation and Calibration of Standards.

Several methods for producing primary standards are established. Work by Rasmussen & Lovelock (1983) for the Atmospheric Lifetime Experiment showed that CFC-11 and CFC-12 standards could be made which showed negligible drift in concentration over the four year period of the experiment. However, interlaboratory calibration exercises have revealed large discrepancies amongst alleged values in test samples, demonstrating systematic errors between primary standards (Rasmussen 1978, Rasmussen & Khalil 1981). The method used to calibrate standards by the CFC tracer group at PML makes use of a large static dilution chamber. Small known quantities of

each species of interest are released into the cavity which is well mixed with ambient air. A sample of the CFC enriched atmosphere is drawn into a gas cylinder which is pressurised to approximately one bar above atmospheric pressure. Another sample of the dilution chamber air taken before the release is used in conjunction with the after-release sample to form what amounts to a primary standard. This primary standard is only available in small volumes however, since the metal bellows pump which draws air from the dilution chamber is incapable of producing large pressures. It is used to calibrate a secondary standard, which can be easily produced at high pressures although with poorly known mixing ratios. One advantage of using primary standards in this way is that several dilution chamber releases can be used to calibrate a single secondary standard allowing the precision of the technique to be estimated. Once the secondary standard has been calibrated the concentrations in tertiary standards can be determined straightforwardly with no danger of depleting the secondary standard. Tertiary standards are used routinely in laboratory and shipboard analyses.

3.3.1. Description of Static Dilution.

A diagram of the static dilution chamber is shown in Figure 3.3(a). The chamber is described by Lovelock and Watson (1978) and Upstill-Goddard *et al.* (1990). The research of Lovelock and Watson (1978) involved calculating initial release concentrations in the chamber by steadily diluting the air and sampling at regular intervals. By fitting data to an exponential relaxation in concentration they inferred the starting value of concentration for each species (this technique is referred to as exponential dilution). For this work their method is unnecessary since the chamber is sampled within five minutes of the release and there is no deliberate mechanism to introduce any fresh air. The chamber is located in rural south west England where ambient CFC concentrations are stable when the wind is westerly from the North Atlantic. Upwind outside air is drawn into the chamber by a pump capable of flushing the 50.6m^3 volume in about 20 minutes (pump 1 in Figure 3.3(a)). A large fan at the centre of the chamber circulates air rapidly in order to ensure even mixing and a small pump (pump 2 in Figure 3.3(a)), fitted with stainless steel bellows, draws air from the chamber down to the laboratory below at a rate of a few litres per minute. The mechanism for introducing known quantities of each CFC species is shown in Figure 3.3(b). At the given moment the weight is released crushing ampoules of each compound against a hot surface. Another fan blows chamber air onto the broken ampoules ensuring that the release is mixed around the chamber quickly. The method of preparation of ampoules is discussed in Section 3.3.2.

The procedure used to make a release is as follows. The concentrations in the chamber are monitored for several hours prior to release with the main fan circulating outside air. This ensures an homogeneous before-release environment and checks that the GC system is performing well. The hot plate is warmed up and both cylinders to be filled

Figure 3.3. (a) Diagram of the static dilution chamber. Pump 1 draws in outside air, pump 2 transfers chamber air to the laboratory below and the large fan circulates air in the chamber itself. The chamber is 2.4m high, with walls of polyethylene lined plaster board. (b) Release mechanism. The rope passes through eyes in the ceiling and down into the laboratory through an access hole.

(a)

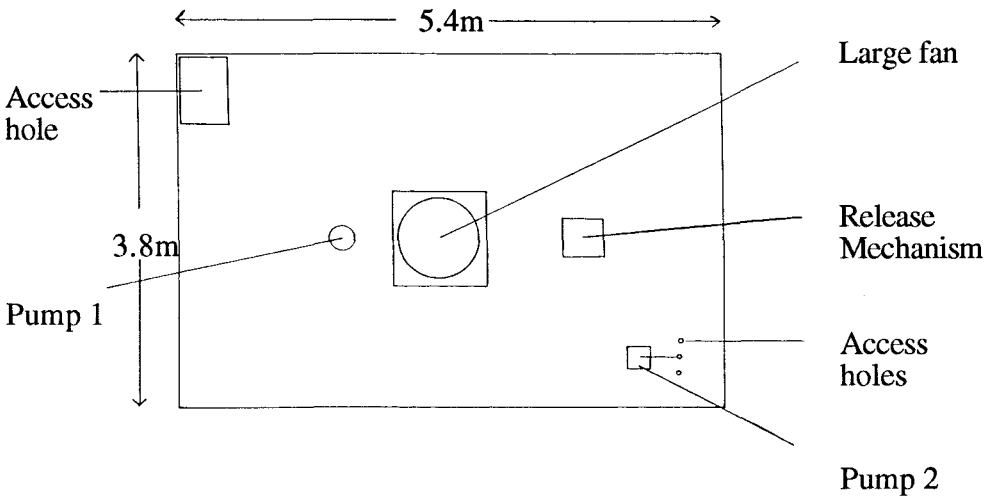
5.4m
Access hole
3.8m
Pump 1
Large fan
Release Mechanism
Access holes
Pump 2

(b)

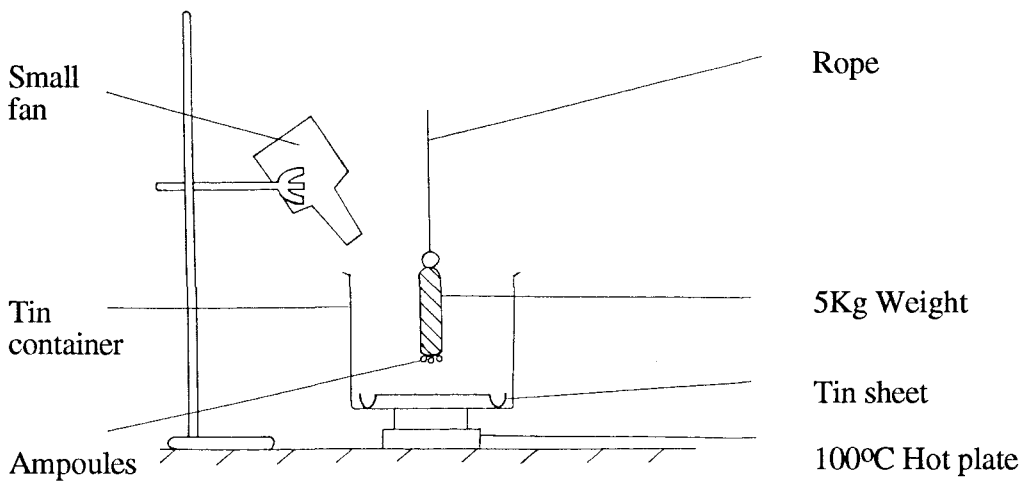
Small fan
Tin container
Ampoules
Rope
5Kg Weight
Tin sheet
100°C Hot plate

with before-release and after-release chamber air are purged for several minutes. (The cylinders are attached to pump 2 at the pillar valve and open at the bottom end.) With the before release cylinder attached to pump 2 a stop-watch is started. After two minutes (three e-folding scales for purging) the bottom end of the before-release cylinder is capped and once the cylinder has been brought to pressure (30 seconds or so) the cylinder pillar valve is closed. This cylinder is capped, the after-release cylinder connected to the outlet of pump 2 with its bottom end cap removed, and pump 2 switched off. The weight is allowed to fall and crush the ampoules and, after two minutes to allow mixing, pump 2 is switched back on. The after-release cylinder is purged for five minutes (7.5 e-folding time scales) before being capped at its bottom end, brought up to pressure and sealed. At this point measurements of the chamber air temperature and pressure are made. Finally pump 1 is switched on for several hours in order to thoroughly ventilate the chamber ready for the next release.

The cylinders used for all standards are Whitey 304 L stainless steel 1 gallon or 1 litre aliquots, fitted with Nupro type 'H' or 'HK' bellows type pillar valves which also have copper stems. The cylinders are electropolished and the pillar valves dismantled, wiped free of lubricant with a clean cloth, rinsed in propan-2-ol and baked in an oven. Pump 2, used to draw down chamber air into the laboratory, is fitted with stainless steel bellows and connected to the cylinders with a Teflon tube. In addition, all likely sources of electron capturing chemicals are removed from the laboratory before analyses were made. Comparison of measurements taken from before-release air and chamber syringe samples demonstrate that neither the cylinders, tubing nor pump are a source of CFC contamination to within the GC uncertainty limit.

3.3.2. Preparation of Primary Standard Ampoules.

A diagram showing how the ampoules are prepared is shown in Figure 3.4. A calibrated volume is filled with each CFC species at a low pressure and this gas is transferred into a glass ampoule which can be easily sealed. By measuring the temperature and pressure in the volume the number of moles of species in the ampoule is determined (perfect gas behaviour is assumed). The amount of CFC in the ampoules is calculated to be such that when the sample is diluted in the chamber the ECD responses are close to those observed when a sample of saturated surface sea water is analysed.

After fully evacuating the vacuum system, a small amount of the relevant CFC species is released to give a pressure of about 100mb. The apparatus is then fully re-evacuated with the valves at each end of the calibrated volume open. This flushing procedure is repeated twice more to ensure that the remnant background pressure is due to the CFC of interest. After preparing the apparatus in this way the ampoule valve is closed and enough CFC is released to pressurise the system to the desired level. The calibrated volume is then isolated from the main chamber and by placing the ampoule in a dewar of

liquid nitrogen and opening the ampoule valve the sample of gas can be quantitatively drawn into the ampoule. This is then sealed with a flame and checked for integrity by immersion first in boiling water, then in water at 20°C. Bubbles of escaping gas and evidence of water inside the ampoule are proof that the sealing was unsuccessful. The calibrated volume, V_0, was found to be $3.089 \pm 0.01 cm^3$. A Keithley Barocell pressure detector is used to measure the low pressures inside the apparatus, giving an uncertainty in p_0, the ampoule creation pressure, of 0.15% or $9Nm^{-2}$, whichever is larger. Table 3.2 shows values of p_0 for the ampoules used to make calibration releases (see Section 3.4).

3.3.3. Preparation of Secondary and Tertiary Standards.

Secondary and tertiary standards are produced by an *ad hoc* method that involves the release of CFC into a small room. The aim of the exercise is to produce a large quantity of inert gas which has consistently reproducible mixing ratios of each CFC species in trace amounts. The concentrations in the standard are not easily controlled, but the target levels are those that are present in a typical sample of saturated surface ocean water. This allows the calibration injections to be close to the levels that are measured in the environment.

Micromole quantities of each species are released into a small room by exposing bottles of CFC to the atmosphere and, after mixing the air evenly, a syringe sample is taken. This sample is diluted with outside air by a factor of order one hundred and analysed on the GC system. At the same time a partially evacuated cylinder, to be used for the secondary standard, is filled with an amount of the enriched atmosphere. If the GC analysis shows that the ratio of compounds is wrong the cylinder is purged with clean air and re-evacuated. Further small releases of the appropriate species are made in an attempt to set the CFC levels as desired and the process is repeated. When a good sample has been obtained, the standard cylinder is diluted with oxygen free nitrogen gas. The volume of gas used to do this is calculated in order to give standard mixing ratios as close to the desired levels as possible. In general the final pressure of the standard cylinder is between 67 and 133 bar (1000 and 2000 psi). With the 3.8l cylinders the PML group use for secondary and tertiary standards this gives enough standard for several thousand injections.

3.4. Results of 1990 Calibration Experiment.

Three release experiments were made in February 1990 in order to calibrate CFC standards (it is a pleasure to acknowledge J E Lovelock for granting access to his dilution chamber facility). Unfortunately, the results of the first release cannot be used since the standard with which they were compared was contaminated. Data from the two releases which were successfully used to calibrate a secondary standard are shown in Table 3.2. These data were derived using an instrument built following Gammon *et al.* (1982) and Wisegarver & Gammon (1988). The ambient atmospheric concentration of methyl

Figure 3.4. Vacuum apparatus for preparing ampoules. The round bottomed flask contains the CFC species of interest. The calibrated volume is $\frac{1}{4}$" od stainless steel tubing. Main chamber dimensions are 1m length, and 0.02m diameter. All valves shown are Nupro 'H' or 'HK' type.

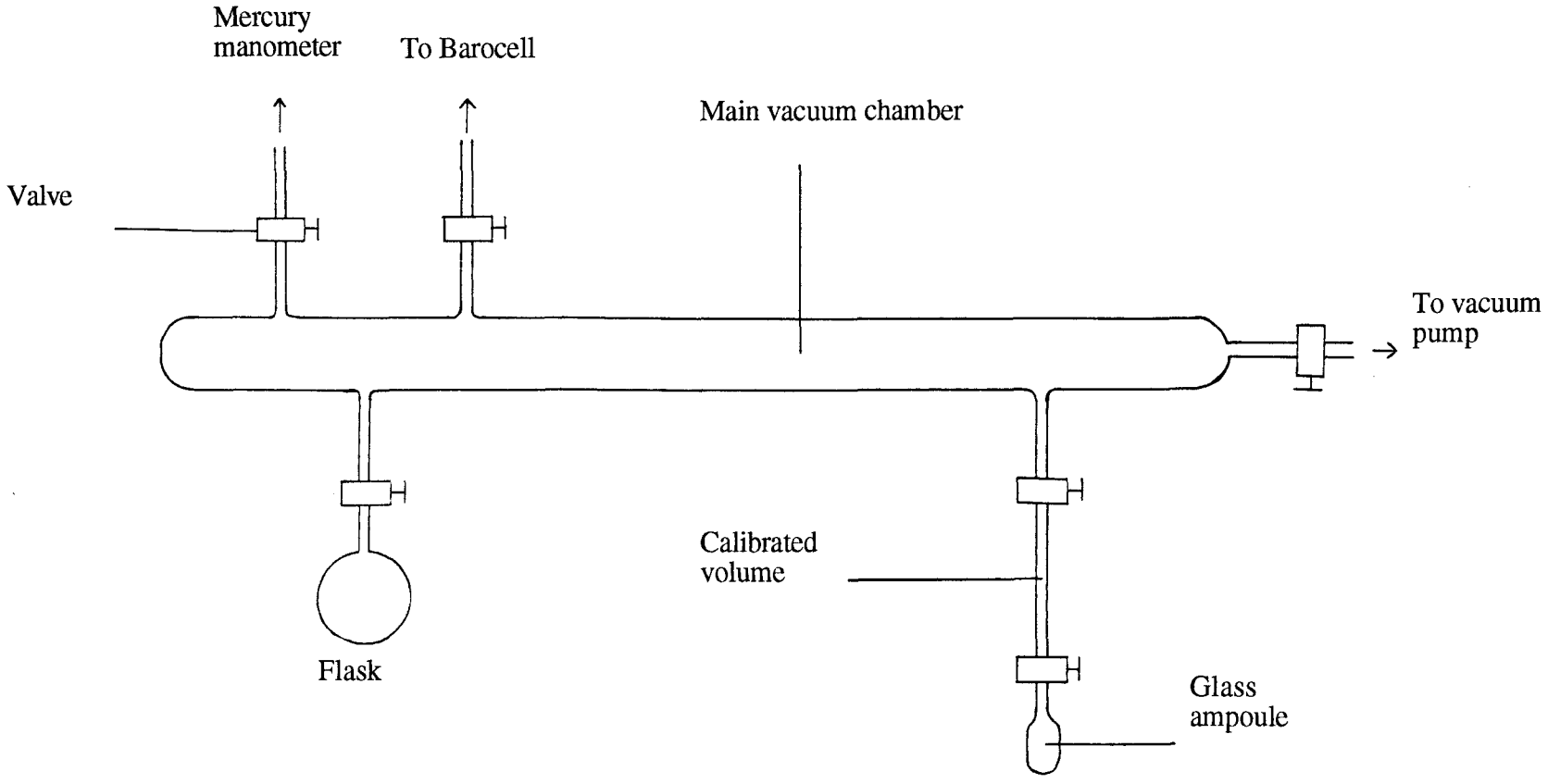
Mercury
manometer
To Barocell
Main vacuum chamber
Valve
To vacuum
pump
Calibrated
volume
Flask
Glass
ampoule

bromide, established as the interfering compound with CFC-113 on these systems, is low (see Section 2.1). Singh *et al.* (1983b) quote mixing ratios of 23pptv in Eastern Pacific marine air for this compound, and ocean surface mean supersaturations of 250%. However, even if there is a contribution to the CFC-113 peak from methyl bromide in the analyses performed during this calibration, this should not propagate to the final value for the standard concentration, since this is derived as the difference between CFC-113 peaks as a result of the known release (see discussion below).

If p, V and T generically denote pressure, volume and temperature and the subscripts 0, 1, 2 refer to the conditions at formation of the ampoule, release and sampling respectively, then the mixing ratio of the primary standard, R', for each species is given by

$$R' = \frac{p_0 V_0 T_1}{p_1 V_1 T_0} \qquad 3.4.1.$$

Table 3.2. Values of the ampoule pressure, p_0, and the derived mixing ratio for the PML secondary standard, R", for each species in each release. See Section 3.3.2 for discussion of uncertainties in the ampoule pressure, p_0. ppbv = parts per billion by volume (i.e 10^9)

Release Date	22/2/90			23/2/90		
Species	CFC-11	CFC-12	CFC-113	CFC-11	CFC-12	CFC-113
p_0 (Nm^{-2})	3345	4310	498.5	4910	2830	507.0
R" (ppbv)	2.088	1.943	0.362	2.035	1.929	0.333

V_0 is the calibrated volume in the vacuum apparatus, and V_1 the volume of the dilution chamber. The mixing ratio of the secondary standard, R", is

$$R'' = \frac{R' p_{2sample} T_{2std}}{m\, p_{2std} T_{2sample}} \qquad 3.4.2.$$

Equation 3.4.2 defines m. By calibrating the ECD with the secondary standard a response curve of peak height versus number of standard gas loops injected is obtained (see Section 3.2). Single loops of the primary standard are then analysed and by comparing these peak height values to the response curve an equivalent number of loops of the secondary standard is obtained. This number of loops is m. (Equation 3.4.2 shows how it is adjusted to account for differences in injection conditions between the analyses. Since the analysis runs are made consecutively, the pressures and temperatures for each injection are very similar and the adjustment to m is therefore slight.) R' is known, and so Equation 3.4.2 can be used directly to calculate R" for each species.

A more complicated method was used to fit the detector response for the primary standard calibration exercise than that described in Section 3.2. The fitting function used was a spline, rather than a quadratic, and a full calibration curve was established before and after the loops of primary standard had been analysed. This allowed values of m to be derived by each calibration fit, before and after the primary standard was analysed. These values were linearly interpolated in order to give a value of m at the time of detection for each species in each analysis run. (I.e. Equation 3.2.1 was a spline function, and the assumption of Equation 3.2.3 was not imposed.) Note that in Equations 3.4.1 and 3.4.2 above, the mixing ratio of the primary standard and the value of m refer to CFC molecules released into the barn by the breaking of ampoules, not due to any background level already present. Therefore in calculating this value there are two intermediate variables, one for before-release, and one for after release. These are subtracted to derive the true value of the variable m as defined by Equation 3.4.2.

3.5. Secondary Standard Intercalibration and Conclusions about Instrumental Accuracy.

Measurements of marine air on a cruise in July 1990 to the Denmark Straits revealed that the CFC-11 calibration, based on the 1990 barn release experiment (Section 3.4) was incorrect. These observations were made using the GC system described in Section 3.4, and are believed to be uncorrupted by methyl bromide co-elution since concurrent chromatograms from a DB-624 column instrument confirmed the absence of this contaminant. Re-examination of the calibration experiment suggested that the CFC-11 data was poor as a result of the pronounced non-linearity demonstrated by ECDs with pure nitrogen gas in the detector for this compound. Table 3.3 shows a predicted estimate of the accuracy of the secondary standard produced by the static dilution method. (In Tables 3.3, 3.4 and 3.5 wherever errors are combined they are assumed to be normally distributed and random. The + and - signs in the 'symbol' column have a special meaning as a result; it is the variances, not the standard deviations shown, which are combined by adding or subtracting.) The source of the calibration experiment curve fitting error is based on an estimate explained below. The precision of the secondary standard can also be evaluated by repeated releases, but with only two data points to calibrate the secondary standard a rigorous analysis of the standard's precision is impossible. However, Table 3.3 also shows reasonably good agreement between the predicted uncertainty and the precision obtained from the two successful releases. It is desirable that further releases in the dilution chamber be made so as to complete this calibration (and indeed the facility to do this is an advantage of the static dilution method).

Table 3.3. Estimated accuracy of static dilution standard preparation experiment. Note that in the experiment performed in February 1990 the calibration experiment curve fitting uncertainty for CFC-11 was much larger (see text). The quoted accuracy of the secondary standard is thus an estimate of the expected accuracy for this technique for CFC-11. The precision of the secondary standard is based on two barn releases. See text for explanation of SYMBOL column.

ESTIMATED UNCERTAINTY IN ...	SYMBOL	CFC-12	CFC-11	CFC-113
Ampoule Preparation	a	0.15%	0.15%	1.8%
Calibration experiment replicate precision	b	0.65%	0.45%	1%
Calibration experiment curve fitting	c	1%	1%	1%
Predicted accuracy of secondary standard	a + b + c	1.2%	1.1%	2.3%
Precision of secondary standard		0.7%	1.3%	4%

In a laboratory intercalibration of the PML secondary standard with two secondary standards from Scripps Institution of Oceanography (kindly supplied by D Smythe-Wright) the implied CFC-12 discrepancy was 3%. This value was encouraging; there is an expected uncertainty of about 1.8% with such an exercise and the residual error is presumably due to differences between the barn dilution method and SIO's technique (see Bullister (1984) for a description of this method). Table 3.4 shows the propagation of errors in this exercise. The SIO intercalibration replicate precision & curve fitting error was derived by using the quoted value of one SIO standard to calibrate the other SIO standard. The residual discrepancy in Table 3.4, between the estimated errors for the SIO standard preparation and the static dilution method, is based on a random distribution of the uncertainty in this quantity. If, however, this error is completely systematic, it can be found by simple subtraction of standard deviations, not variances, giving a value of 1.4%. Bullister (1984) estimates the absolute accuracy of the SIO scale to be about 0.5% for CFC-12.

Use of two SIO standards for the intercalibration has the advantage that an estimate of the error introduced by curve fitting the non-linear ECD can be made. This is done by comparing the ratio of species in each standard, without recourse to any absolute calibration scale. The SIO estimated ratios are 1.077 and 1.111 for CFC-12 and CFC-11 respectively, presumably using the ECD fit described by Bullister & Weiss (1988). The corresponding values as determined by the instrument described in Chapter 2, using quadratic curve fits explained in Section 3.2 are 1.069 and 1.106 (0.8% and 0.45%

different). The ECD was calibrated using the PML secondary standard for this exercise. The discrepancies in these values are a result of two replicate precision errors only, with no contribution from curve fitting uncertainty, which should not be manifested in the ratios. The observed SIO intercalibration replicate precision and curve fitting error (1.3%; see Table 3.4) however, has errors from analysis reproducibility and curve fitting (essentially the difference between the curve fits of SIO and PML). An estimate of the error due to curve fitting is therefore 0.7% at this point on the curve. A value of 1% was used in the estimates of Table 3.3 and Table 3.5, considered to be random and constant for the purposes of combination with other uncertainties.

Table 3.4. SIO/Static dilution intercalibration of standards. The estimated uncertainty in the CFC-12 secondary standard is from Table 3.3. See text for explanation of SYMBOL column.

ESTIMATED UNCERTAINTY IN ...	SYMBOL	CFC-12
PML secondary standard wrt static dilution technique	a	1.2%
SIO intercalibration replicate precision & curve fitting	b	1.3%
SIO standard wrt SIO scale	c	0.18%
Expected SIO intercalibration uncertainty	a + b + c	1.8%
Actual SIO intercalibration uncertainty	d	3%
Residual discrepancy in SIO/Static dilution methods	d - (a+b+c)	2.4%

The marine air mixing ratios and seawater concentrations presented in this thesis are given relative to the SIO scales for CFC-12 and CFC-11. There was barely measurable, uncalibrated, CFC-113 in the SIO standard so no comparison could be made for that species. The scale adopted for CFC-113 is therefore based on the static dilution chamber standard preparation described in this chapter. Table 3.5 shows the estimated absolute accuracy for the tertiary standard used to calibrate the ECD routinely. There is an extra 0.6% imprecision expected for CFC-113 compared with CFC-12, but no systematic deviation is anticipated for CFC-113 in the same way that the CFC-11 data was corrupted. The extra uncertainty introduced by using a tertiary standard is considered to be out weighed by the benefits won. These are security of the standard against accident in the field and increased lifetime of the secondary standard.

Routine analysis of marine air at sea is a useful method of monitoring the quality of ECD calibrations; the atmosphere provides an effective implied standard. Section 4.2.3 discusses results from marine air analyses.

Table 3.5. Estimated accuracy of tertiary standard used for routine analyses, relative to the SIO scale for CFC-11 & CFC-12 and the PML (static dilution) scale for CFC-113. Source of uncertainty for CFC-113 secondary standard from Table 3.3. Source of SIO intercalibration uncertainty for CFC-11 & CFC-12 is explained in text. See Table 3.4 for an estimate of the uncertainty due to the SIO & static dilution techniques themselves. See text for explanation of SYMBOL column.

ESTIMATED UNCERTAINTY IN ...	SYMBOL	CFC-12	CFC-11	CFC-113
SIO intercalibration of secondary standard; replicate precision & curve fitting	a	1.3%	0.7%	-
Static dilution calibration of secondary standard	a	-	-	2.1%
Secondary → Tertiary standard intercalibration replicate precision	b	1%	0.3%	1%
Secondary → Tertiary standard intercalibration curve fitting	c	1%	1%	1%
Accuracy of Tertiary standard	a + b + c	1.9%	1.3%	2.5%

CHAPTER 4

RESULTS.

4.1. Introduction.

This Chapter deals with the results from two field expeditions in July 1990 and April-June 1991 (ARANDA and VIVALDI cruises respectively, introduced in this section below). Section 4.2 assesses the analytical system described in chapters 2 and 3. The instrument suffered from a number of problems (Section 4.2.1) one of which required investigation with a simple model so that corrections could be applied (Section 4.2.2). The results of marine air observations are reported in Section 4.2.3, which are needed to establish a source function for CFC-113, and can be used to check the quality of CFC-11 and CFC-12 observations. In Section 4.2.3 conclusions about the instrumental detection limit, precision and dynamic range are stated. Section 4.3 reviews the hydrography of the north east Atlantic (Section 4.3.1) and discusses the concept of CFC-113 ventilation age, explaining the important parameterisation used to deal with the solubility of CFC-113 (Section 4.3.2). In Section 4.3.3 fields of CFC-113 concentration and ventilation age are reported and briefly discussed, although interpretation of these results is postponed until Chapter 7.

Some of the data discussed in this Chapter and elsewhere in this thesis is from the ARANDA cruise to the Denmark Straits in July 1990 aboard RV ARANDA. This expedition was part of a three year study of the Deep Western Boundary Current which overflows into the Atlantic across the sill between Greenland and Iceland (Dickson *et al.*, 1990). A test-bed version of the WBC instrument described in Chapter 2 was used on the ARANDA cruise, although the surface water values and marine air observations reported here are derived from a packed column instrument similar to Wisegarver & Gammon's (1988), and described in Section 3.4. This system cannot resolve CFC-113 and methyl bromide successfully, as Section 2.1 explains, however, use of the WBC instrument confirmed that there was negligible methyl bromide present in the surface waters, and so no contamination of the CFC-113 measurements is expected.

The VIVALDI '91 expedition was a trials cruise for a planned series of surveys to be repeated seasonally (Pollard *et al.*, 1991; throughout this thesis VIVALDI refers to VIVALDI '91). Two legs aboard RRS CHARLES DARWIN were completed in April, May and June of 1991 (Figure 4.1). The VIVALDI scientific plan involves a 300km spaced grid of full depth CTD casts with chemical tracer measurements (dissolved oxygen, nutrients, CFCs) and Acoustic Doppler Current Profiler (ADCP). These stations are separated by SeaSoar sections (towed, undulating CTD to 500db depth), shown in Figure 4.1 as full lines connecting the CTD casts. In addition, underway measurements of fluorescence, upper ocean zooplankton tows, surface meteorology and carbon chemistry

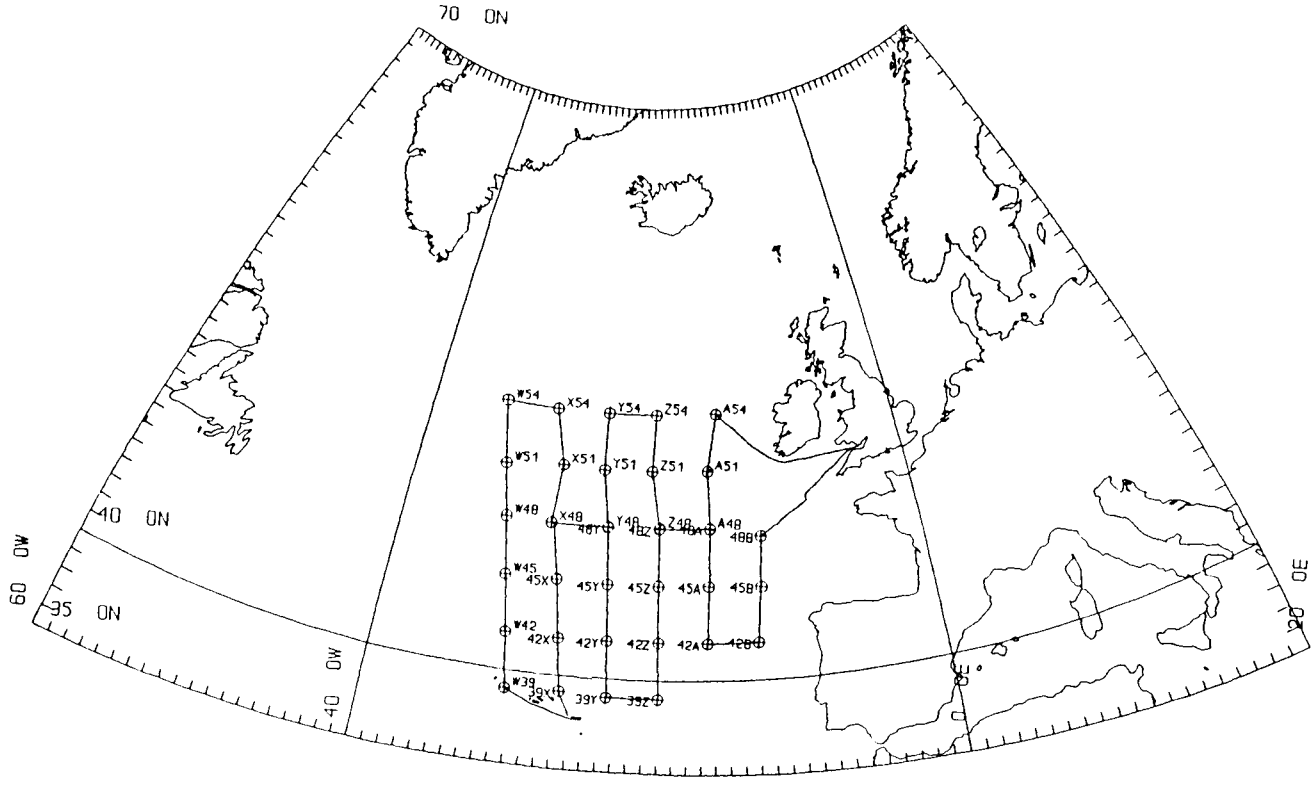

Figure 4.1. VIVALDI '91 cruise track. Leg 1 was ex Barry, South Wales to Ponta Delgada, Azores 25/4/91 - 16/5/91 (southern stations in grid). Leg 2 was ex Ponta Delgada to Barry 18/5/91 - 10/6/91. Annotated symbols are full depth CTD casts with water bottle analysis of dissolved oxygen, nutrient and CFC concentration. Connecting lines between stations are SeaSoar sections to 500db depth. The mid-Atlantic ridge axis roughly follows section X north until it turns to the north west passing between stations W54 and W51. The number in the annotation for each station refers to its latitude.

(leg 1 of VIVALDI '91 only) were made during the cruise. VIVALDI '91 was a trial for the instrument described in Chapter 2, and the author conducted CFC analyses on both legs of the cruise.

4.2. Appraisal of Instrumental Performance.

This section is concerned with assessing the instrumental performance during this period in the field, in order to focus on the the lessons to be learnt. To pre-empt the conclusions somewhat, the analytical system worked well for Leg 1 of the cruise, with an accumulation of problems during Leg 2 whose combined effect significantly reduced the number of good data values. Section 4.2.1 deals with problems which occurred, and recommendations for their avoidance. Section 4.2.2 discusses a specific problem of the analysis technique. Next is Section 4.2.3 which describes the results of the marine air observations, then Section 4.2.4 which reports statistical results of the limits of certainty of the instrument from the VIVALDI cruises, and assesses the criteria used for checking the data.

4.2.1. Problems Encountered.

One of the most serious problems encountered during the trials was of contamination of parts of the sampling system. In particular, throughout most of Leg 1 the CFC-11 analyses were corrupted. It is fortunate that contamination of a sample is easily recognised by elevated peaks, often several times above any conceivable seawater concentration and the number of samples which were discarded as a result of this corruption was about 25%. The problem could be reduced, although not convincingly eliminated, by scrupulous cleaning of the sample syringes, taps and Niskin bottles, as discussed in Section 2.4. This observation tends to suggest that the contaminating CFC-11 is absorbed onto layers of grease, consistent with the non-polar nature of this species (DuPont, Product Information). Biologically active waters contain lipids which can accumulate on the surfaces of the sampling apparatus, and contribute to this process. However, when the source of CFC-11 was located (air-conditioning plant room on RRS CHARLES DARWIN. DARWIN has a CFC-22 ($CHClF_2$) air-con.) it was thought likely that the direction, strength and variability of the wind could account for at least some of the intermittency in the contamination problem.

The build-up of biological material was a source of another problem, namely that the air stone of the stripping tower had a tendency to block, reducing the flow of stripper gas through the seawater sample (see Figure 2.3). Although in principle this can be corrected for by a simple model of exponential release of the dissolved gas into the stripper as mentioned in Section 2.2, it is obviously undesirable and the accumulation must not be allowed to continue. The measures taken at sea to remove the biological matter included use of ultrasonic immersion, acid and alkali washes, which were largely effective, although time consuming. This part of the analytical system probably needs

redesigning, and workers in the PML tracer group are pursuing this (C S Law, A J Watson, Pers. Comms.).

The seawater injection system was problematic in another respect. Namely valve 1 (Figure 2.3) had a short lifetime of about 200 injections. This was a result of scoring of the mirrored valve face by salt crystals formed as the stripper gas evaporated traces of seawater left in the valve ports after an injection of seawater. The tendency is rapidly increased by leaving the valve for long periods without a flushing injection of fresh water (the high quality de-ionised water available on board was a potent source of CFC-113). A suitable solution to this is to wet the stripper gas stream by bubbling it through a volume of fresh water upstream of valve 1.

The integrator caused a recurrent problem too, and Figure 4.2 shows an example of this. The baseline in this chromatogram was not drawn properly under the CFC-12 peak (due to an integrator error), and so an incorrect peak height estimate was derived. All integrations are examined manually and where necessary corrected by direct measurement. This introduces an additional error of no larger than about 0.01, 0.06 and 0.002pMol/l for CFC-12, CFC-11 and CFC-113 respectively, smaller than the appropriate seawater sampling precisions (Section 4.2.4 discusses sampling uncertainties). The proportions of each species adjusted in this way were approximately 19, 7 and 10% for CFC-12, CFC-11 and CFC-113, and although peak height corrections of this sort are undesirable, they do not significantly limit the dataset.

4.2.2. Methyl Iodide Contamination.

In Section 2.1 the suitability of the DB-624 column for a CFC-113 analysis system was discussed. Figure 2.2 shows that this column is capable of cleanly separating the compounds which are electron-capturing and volatile enough to co-elute with CFCs 11, 12 and 113. Although the chromatograms in Figures 3.1 (b) and (c) of a seawater sample show similar resolution this is not always the case. Figure 4.3 shows raw and reprocessed chromatograms of another seawater sample in which the resolution is not as good. In particular, the separation of CFC-113 from methyl iodide (MeI) is poor, and there may well be a contribution from the latter in evaluating the peak height of the former; this problem is discussed here. Although the technique is not rigorous, only slightly contaminated CFC-113 samples are corrected, those severely affected are discarded (~15% corrected; ~33% discarded).

In an attempt to gauge the severity of methyl iodide contamination use is made of factor-X variability as a function of chromatogram parameters (Section 4.3.2 discusses factor-X values). These quantities are expected to be constant, the argument below *assumes* this to be the case, and then, by use of a plausible model for MeI and CFC-113 interaction, shows that a large portion of the variability in the observed factor-X values is correlated with the magnitude of the modelled interaction mechanism. Because the

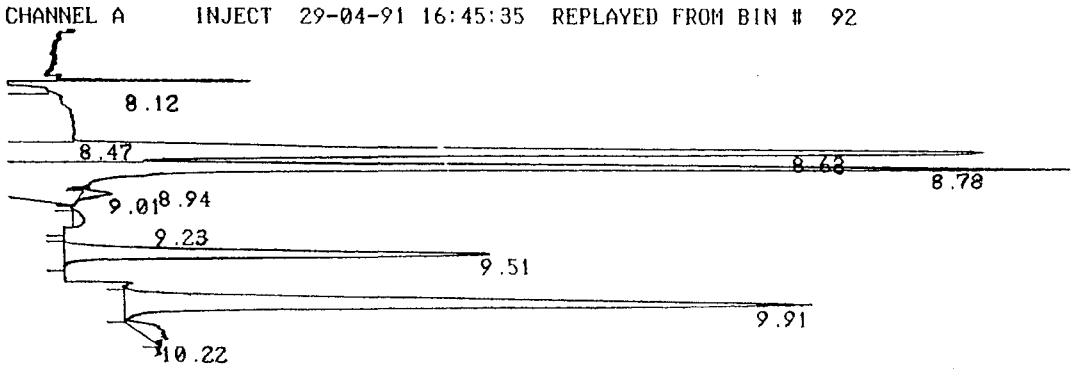

Figure 4.2. Reprocessed chromatogram of marine air from 42 00.0'N 13 56.6'W at 1645 GMT on 29/4/91. Peaks at 8.63, 8.78 and 8.94 minutes have not been integrated correctly. The baseline used in the evaluation of peak height is off scale, whereas for peaks at 9.51 and 9.91 the baseline has been drawn in the correct place.

Time	8.12	8.47	8.63	8.78	8.94	9.01	9.23	9.51	9.91	10.22
Species	*	*	O_2	CFC-12	CH_3Cl ?	?	†	CFC-11	CFC-113	†

* Integrator error (did not appear in raw chromatogram), † baseline wobble.

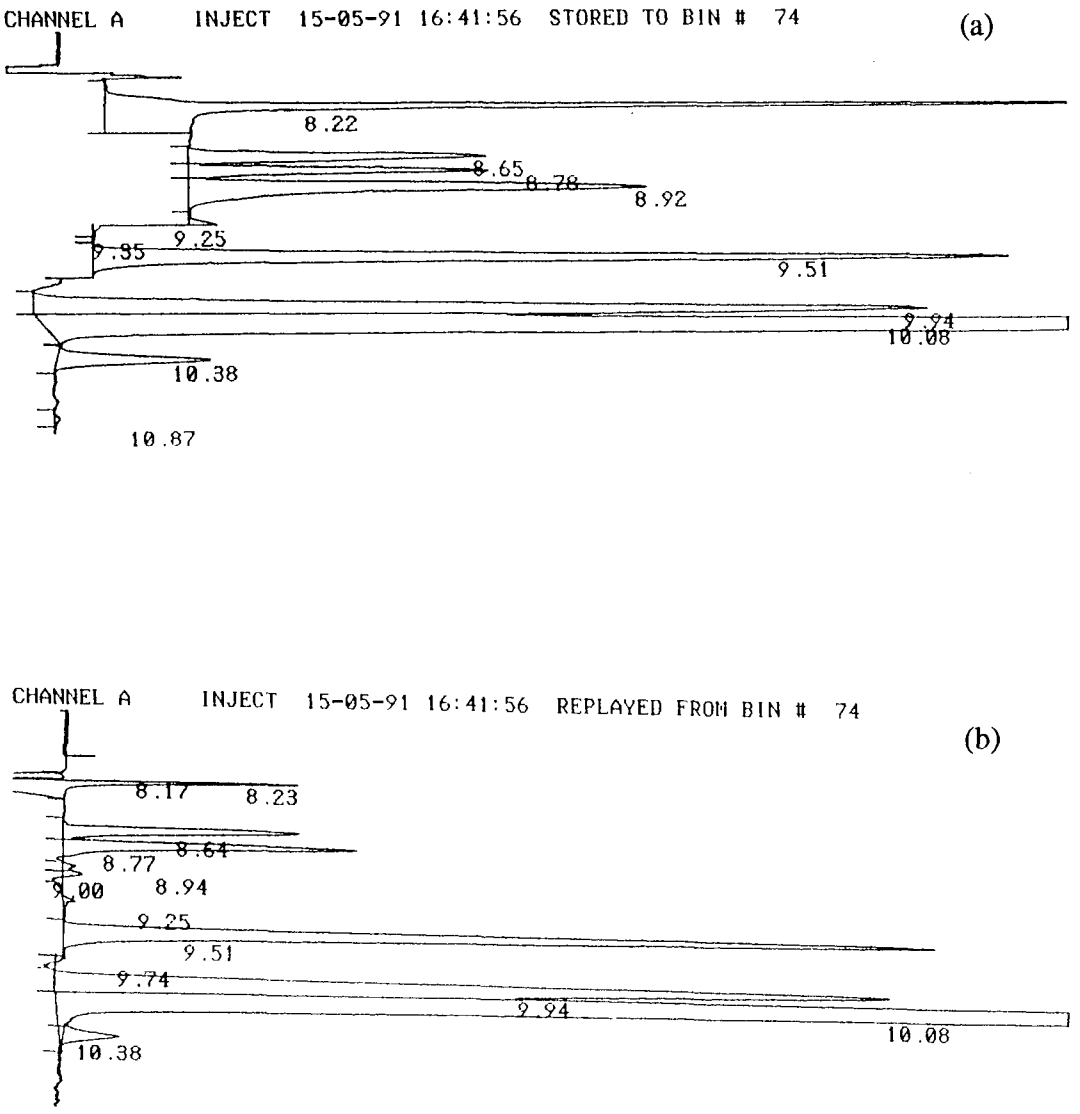

Figure 4.3. (a) Raw, and (b) reprocessed chromatograms of a seawater sample at 2db depth from bottle #432, station 11019 (39X on Figure 4.1, 39 10.2'N 26 43.4'W) taken on 15/5/91. Compared to other seawater chromatograms (e.g Figure 3.1 (b), (c)) the CFC-113/methyl iodide resolution is inferior.

Time	8.22	8.63	8.78	8.94	9.23	9.51	9.94	10.08	10.38
Species	*	O_2	CFC-12	CH_3Cl ?	†	CFC-11	CFC-113	CH_3I	CH_2Cl_2

* Injection transient, † baseline wobble. Only those peaks present in both chromatograms are listed.

correlations are so good, the hypothesis that MeI is actually contributing to the CFC-113 peak is accepted as credible, and so, by use of the modelled interaction, CFC-113 peaks can be corrected. No conclusion about the mechanism of interaction is made, although a possible process is mentioned. The assumption of constant factor-X values is examined in Section 4.3.2, but for the purposes of the present context it is obvious that any inherent variability in factor-X is unlikely to be correlated with a MeI contribution to the CFC-113 peak, and so should not systematically bias the correlation technique.

Let us assume that a measured mixed layer CFC-113 peak actually consists of two parts, due to the CFC-113 peak $\left([113]^{true}_{surf}\right)$ and also due to a contamination from methyl iodide h(MeI), i.e.

$$[113]_{surf} = [113]^{true}_{surf} + h(MeI) \qquad 4.2.1.$$

From the definition of factor-X given in Section 4.3.2 (Equation 4.3.3), one obtains,

$$_{113}X_a = \frac{\left\{ [113]^{true}_{surf} + h(MeI) \right\} [a]_{atm}}{[113]_{atm}\,[a]_{surf}} \qquad 4.2.2$$

where a can correspond to either CFC-11 or CFC-12.

Since $[113]_{surf}$ and $[a]_{surf}$ are surface values (or at least those samples from within an appropriately defined well mixed layer) one expects $\frac{[113]_{surf}}{[a]_{surf}}$ to be a constant (if h(MeI) = 0) for every station sampled; $\frac{[113]_{surf}}{[a]_{surf}}$ should merely reflect the atmospheric ratio $\frac{[113]_{atm}}{[a]_{atm}}$ scaled by the ratio of solubilities (this amounts to the premise of mixed layer age = 0 throughout the VIVALDI survey). Chapter 5 looks in detail at this assertion, and Section 5.1 deals with it specifically (see also Section 4.3.2). The value of $\frac{[113]_{atm}}{[a]_{atm}}$ is also a constant for these purposes; although in fact it is a slowly varying function of time as described in Section 1.3.1.

A valid test of Equation 4.2.1, therefore, is to see how $_{113}X_a$ varies as a function of h(MeI). The fact that $[a]_{surf}$ can vary slightly from station to station as a result of different surface conditions can also cause $[113]_{surf}$ to vary, even with constant h(MeI). However, this is statistically insignificant; the standard deviation in surface temperature for the VIVALDI cruises gives rise to an expected variation of about 18% in the value of $[11]_{surf}$, to be compared to a range of nearly six orders of magnitude in the variation of h(MeI) (Figure 4.5). The form of h(MeI) is crucial, and h is assumed to be due to a simple interaction of impinging Gaussian peaks, explained in Figure 4.4. What is actually used in the correlation analysis is the variable defined by

$$h(MeI) = H_{MeI} \exp\left\{\frac{(t_1 - t_0)^2}{\sigma^2}\right\} \qquad 4.2.3a$$

with t_1, t_0, σ and H_{MeI} defined in Figure 4.4. This form of peak shape and interaction is very simple, and is probably the least certain assumption in the whole exercise. For this reason the corrections for variation in $[a]_{surf}$ and the contribution to H_{MeI} from CFC-113 (explained in the caption of Figure 4.4) are inappropriate.

Figure 4.5(a) shows a plot of $_{113}X_{11}$ and $_{113}X_{12}$ versus h(MeI) for every VIVALDI station with surface data. It is evident that the hypotheses of Equations 4.2.1 and 4.2.3a, with the assumptions outlined above and on Figure 4.4, can account for a substantial part of the variation noticed in $_{113}X_{11}$ and $_{113}X_{12}$. With this confirmed CFC-113 peaks can be corrected due to the contribution from MeI. CFC-113 results for which $1 < h(MeI) \leq 10$ are considered to be slightly contaminated, and the surface values are corrected by the fitted functions drawn in Figure 4.5(a). Those samples for which $h(MeI) < 1$ are considered uncontaminated, whilst samples with $h(MeI) > 10$ are discarded. Data for which $h(MeI) < 10$ are used for the factor-X calculations of Section 4.3.2.

The fitting functions derived from surface data are also used to correct deeper samples where the CFC-113 age, and hence $[a]_{atm}$ and $[113]_{atm}$ of Equation 4.2.2, are unknown (the correction depends on the chromatogram parameters only). In total, CFC-113 values from twenty bottles and eight stations, for which $1 < h(MeI) \leq 10$, are corrected in this way. The maximum correction applied is 20%, and two thirds of the data are adjusted by less than 3%. Figures 4.8(c) and (d) and the discussion in Section 4.2.4 show examples of this. Apart from these corrections, no other adjustments based on the model of impinging peaks are made; Figure 4.7 is a map of the VIVALDI region with those stations sampled whose CFC-113 data is considered to be acceptable based on these criteria. The total number of CFC-113 datapoints eliminated as a result of MeI contamination is about 33%.

Figure 4.5(b) shows the absolute residuals for $_{113}X_{11}$ and $_{113}X_{12}$ calculated from the difference between the observed values and the fitted functions drawn in Figure 4.5(a). The residuals for $_{113}X_{12}$ show an increase at high values of the modelled contribution demonstrating that it is this area where the fit is poorest. Since the residuals in $_{113}X_{11}$ show no such variation, no firm conclusions can be reached about the shortcomings of the modelled interaction. Nevertheless, it is possible that these observations can be explained by an increasing contamination of the CFC-12 peaks, whereas the CFC-11 peak is always distinct enough to be independent of adjacent peaks. i.e. for those peaks where CFC-113 and MeI are poorly separated so too is CFC-12 from its neighbours.

Figure 4.4. Diagram explaining the simple model of impinging peaks used to estimate the contribution of MeI to the peak height of CFC-113. The x-axis is time, the first peak represents CFC-113, the second MeI. Theoretical Gaussian peak shapes are assumed for the two peaks and the solid line represents the sum of the curves; the modelled ECD response on the chromatogram itself. Each peak has the same characterisic width, σ, with displacement in time of $t_1 - t_0$. H_{MeI} and the peak height, H_{113}, corresponding to $[113]_{surf}$ in Equation 4.2.1 are as shown. Although, undoubtedly CFC-113 contributes to the MeI peak, and strictly speaking H_{MeI} in Equation 4.2.3a should have this contribution removed, the influence on the value of h(MeI) is slight. Figure 4.5 shows how h(MeI) varies over several orders of magnitude, and so it is the measurement of σ and $t_0 - t_1$ which are crucial in this calculation. The value of σ was measured from the MeI peak on each chromatogram using Vernier calipers, whilst t_0, t_1 and H_{MeI} were taken from the integrator report.

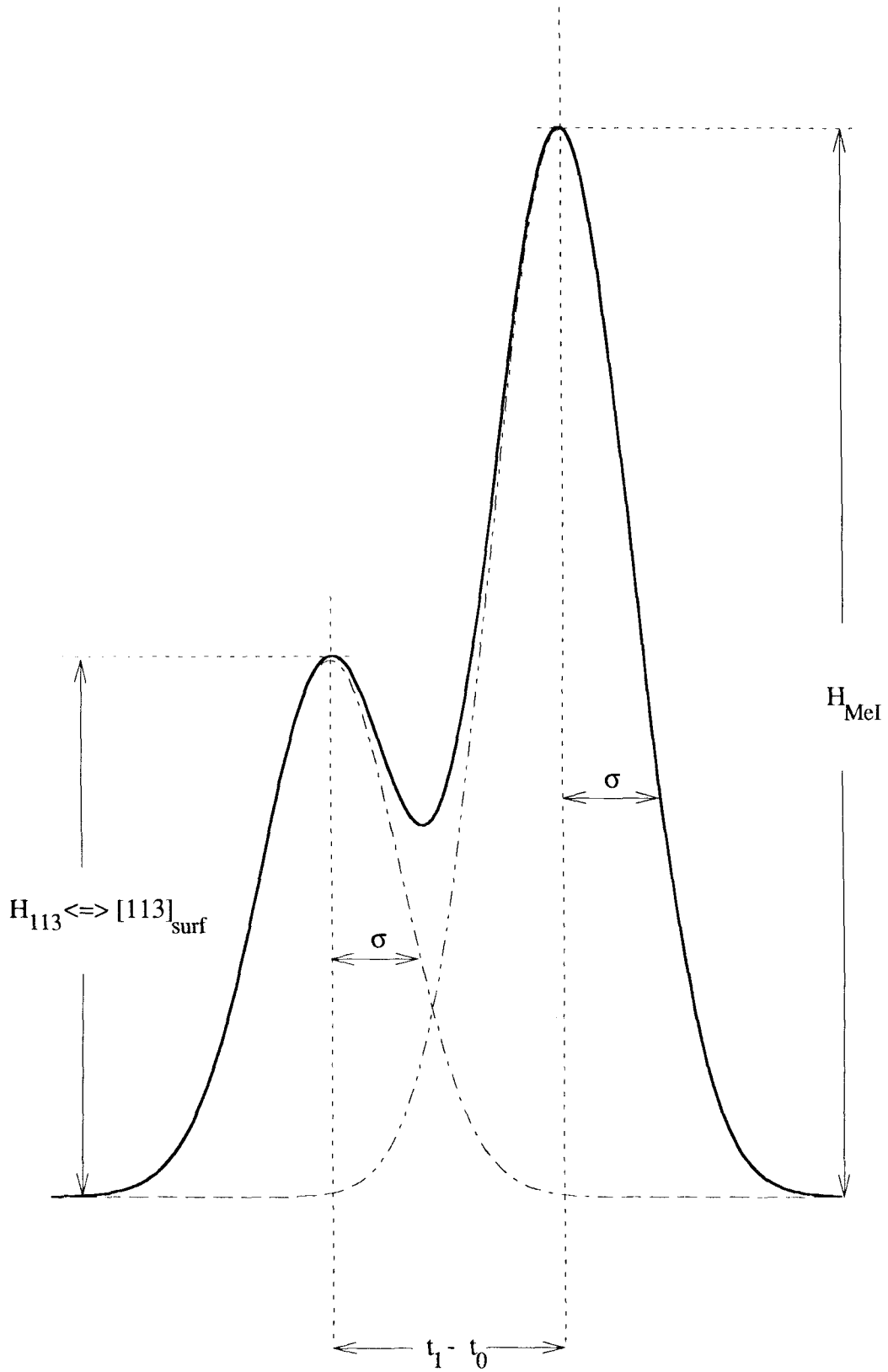
H_{MeI}
σ
H_{113}<=> $[113]_{surf}$
σ
t_1 - t_0

Figure 4.5. (a) Scatter plots of $_{113}X_{12}$, and $_{113}X_{11}$ against modelled contribution of MeI peak to CFC-113, h(MeI) in peak height units, as defined by Equation 4.2.3a. Fitted curves are fourth order polynomials with values of r of 0.941 and 0.927 for $_{113}X_{12}$, and $_{113}X_{11}$ respectively. (b) Absolute values of residuals of observations from fitted curves in (a).

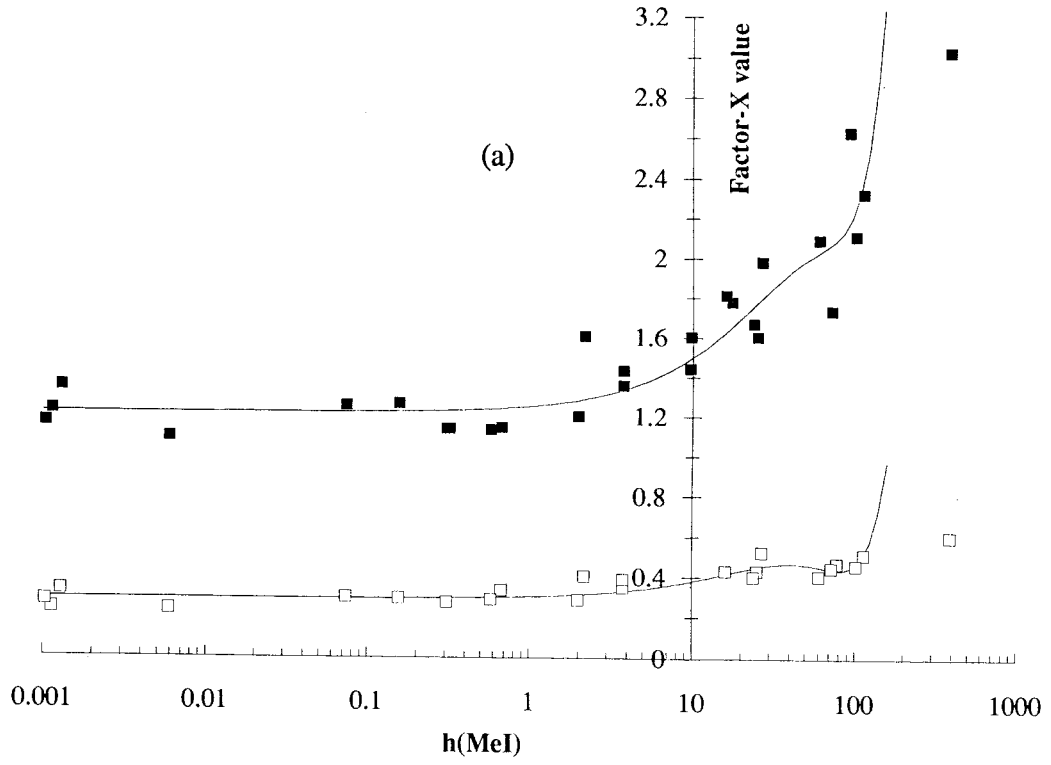

■ CFC-113/CFC-12 □ CFC-113/CFC-11

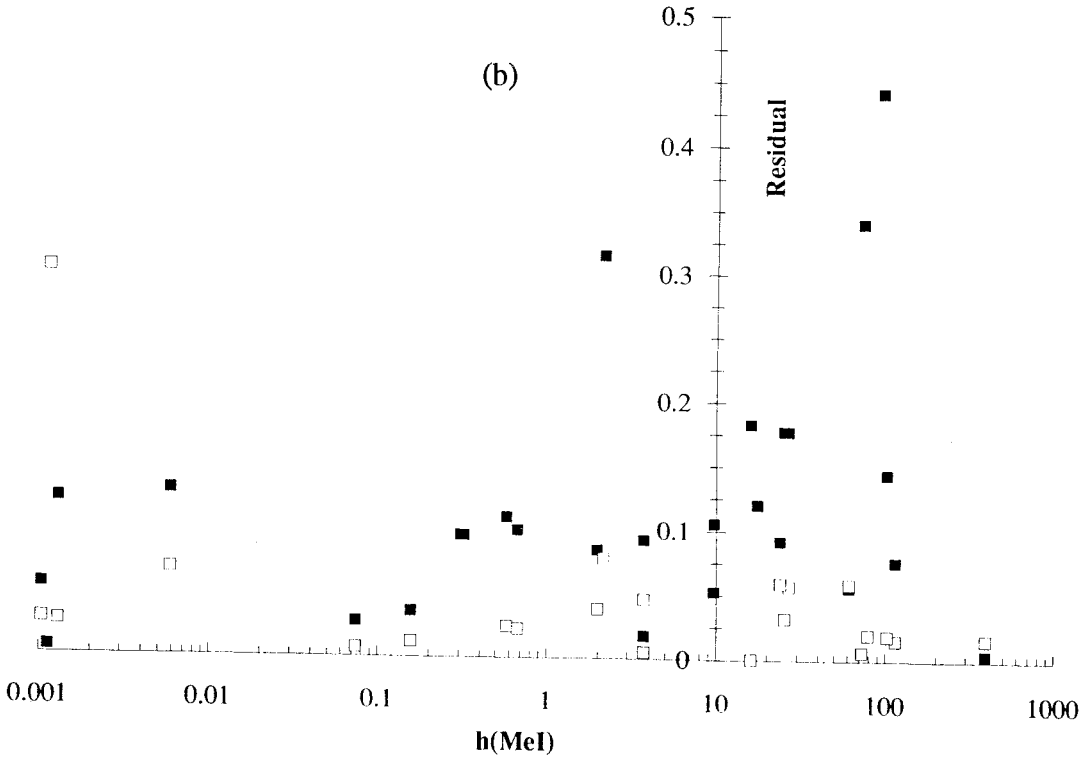

The resolution of CFC-113 and MeI was found to dramatically improve by prompt switching of valve 3 (Figure 2.3) once CFC-113 had eluted through the precolumn. The chromatogram in Figure 4.3 shows poor resolution, and in addition a CH_2Cl_2 peak 25 seconds after CFC-113 has appeared, whereas Figures 3.1(b),(c) and 3.2(a),(b) show no such peak and demonstrate good resolution. One reasonable argument for explaining the improvement in separation is to assert that cutting off the precolumn effluent just after CFC-113 has eluted actually cuts the MeI peak considerably. This will certainly cut some of the CFC-113 peak too since a 30m column barely separates the two. However, the evidence in Figure 4.5(a) shows that merely reducing H_{MeI} has very little effect on the contribution to CFC-113; it is the resolution of the column which reduces this, i.e. the exponential part of Equation 4.2.3a. Indeed, Figure 4.6 shows a plot of $_{113}X_{11}$ and $_{113}X_{12}$ versus h(MeI) which is alternatively defined by

$$h(MeI) = H_{MeI} \qquad 4.2.3b.$$

The correlations for these scatter plots are now very poor in comparison with Figure 4.5(a) where Equation 4.2.3a holds, suggesting that the variation in uncorrected factor-X values cannot be explained by simply cutting off the CFC-113 peak too quickly. A more likely possible mechanism that explains the MeI contamination is this; altering the valve timing for switching out the precolumn sensitively effects the column resolution, not only the mixture of compounds sufficiently volatile to reach the main column in time.

4.2.3. Marine air measurements.

Figure 1.1 shows a plot of the atmospheric source functions for CFCs 11, 12 and 113. The values in this Figure for 1990 and 1991 are based on observations made by the author in the Denmark Straits (1990, using a packed column GC system described in Section 3.4) and the eastern North Atlantic (1991, VIVALDI cruises; using the instrument described in Chapter 2). CFC-11 and CFC-12 are linearly interpolated since 1988 from the measurements reported by Smethie *et al.* (1988) and Warner (1988). The CFC-113 results assume a linear increase from zero concentration in 1973 as do Wisegarver & Gammon (1988). Table 4.1 shows the values of the field observations in comparison to the most recently available alternative source.

The standard deviations of atmospheric measurements as a result of the instrumental uncertainty during the VIVALDI expedition are 8.9, 3.2 and 5.6% for CFCs 12, 11 and 113 respectively. These compare poorly with observations made by other investigators. The corresponding statistics from the ARANDA cruise to the Denmark Straits in July 1990 are 2.2, 12 and 2.6%. The CFC-11 data from this cruise are inadequately calibrated and have been abandoned, although they are included here for comparison. Both these cruises used similar techniques; four large loops of marine air collected in a ground glass syringe are injected towards the end of the trapping period. There is no obvious explanation for these discrepancies in performance. Although it is plausible that CFC-12

from marine air on VIVALDI may have been eluting through the trap before it was isolated, seawater precisions show no such variability (Section 4.2.4) and the marine air CFC-113 precision is also degraded. It is more likely that the VIVALDI data are inferior because the large loop on the WBC instrument is considerably larger than on the packed system; 2.12cm^3 compared to 0.53cm^3. Fortunately, there are enough atmospheric observations on the VIVALDI cruises for the atmospheric mixing ratios to be quite well established (Table 4.1). A premise of this argument is that ambient atmospheric fluctuations are negligible.

Table 4.1. Atmospheric mixing ratios and instrumental precisions for 2 cruises (pptv). Included for reference are the IPCC Report (1990) values for 1990 based on extrapolations from measurements in 1988 and 1989. See text for details of absolute accuracy.

		ARANDA (7/90)	VIVALDI (5/91)	IPCC (90)
Atmospheric Mixing Ratio	CFC-12	476 ± 3.9	486 ± 7.5	484
	CFC-11	(259 ± 12.1)	273 ± 1.5	280
	CFC-113	68.0 ± 0.66	70.8 ± 0.73	60
Instrumental Precision	CFC-12	10	43	
	CFC-11	32	8.7	
	CFC-113	1.8	4.2	

The values given in Table 4.1 are relative to the SIO (CFCs 11 and 12) and PML (CFC-113) scales, but include uncertainties based on random instrumental errors only. Using the estimated accuracy of the tertiary standard from Table 3.5 the absolute accuracy of these figures can be implied. This systematic calibration uncertainty is about 10, 4 and 1.9pptv for CFCs 12, 11 and 113 respectively. The IPCC values in Table 4.1 are referenced to an unknown standard, and based on extrapolations from 1988 and 1989 assuming constant atmospheric growth rates. The field observations reported here do not vary significantly for CFC-12, but cannot be reconciled within errors for CFCs 11 and 113. Warner (88) reports that the uncertainty in CFC-11 and CFC-12 atmospheric mixing ratios is about 2% since 1983, whilst the data presented here suggests the values in Table 4.1 are known to within about 3.7% for CFC-12 and CFC-113 and 2% for CFC-11 in 1990 (CFC-12 and CFC-113 only) and 1991.

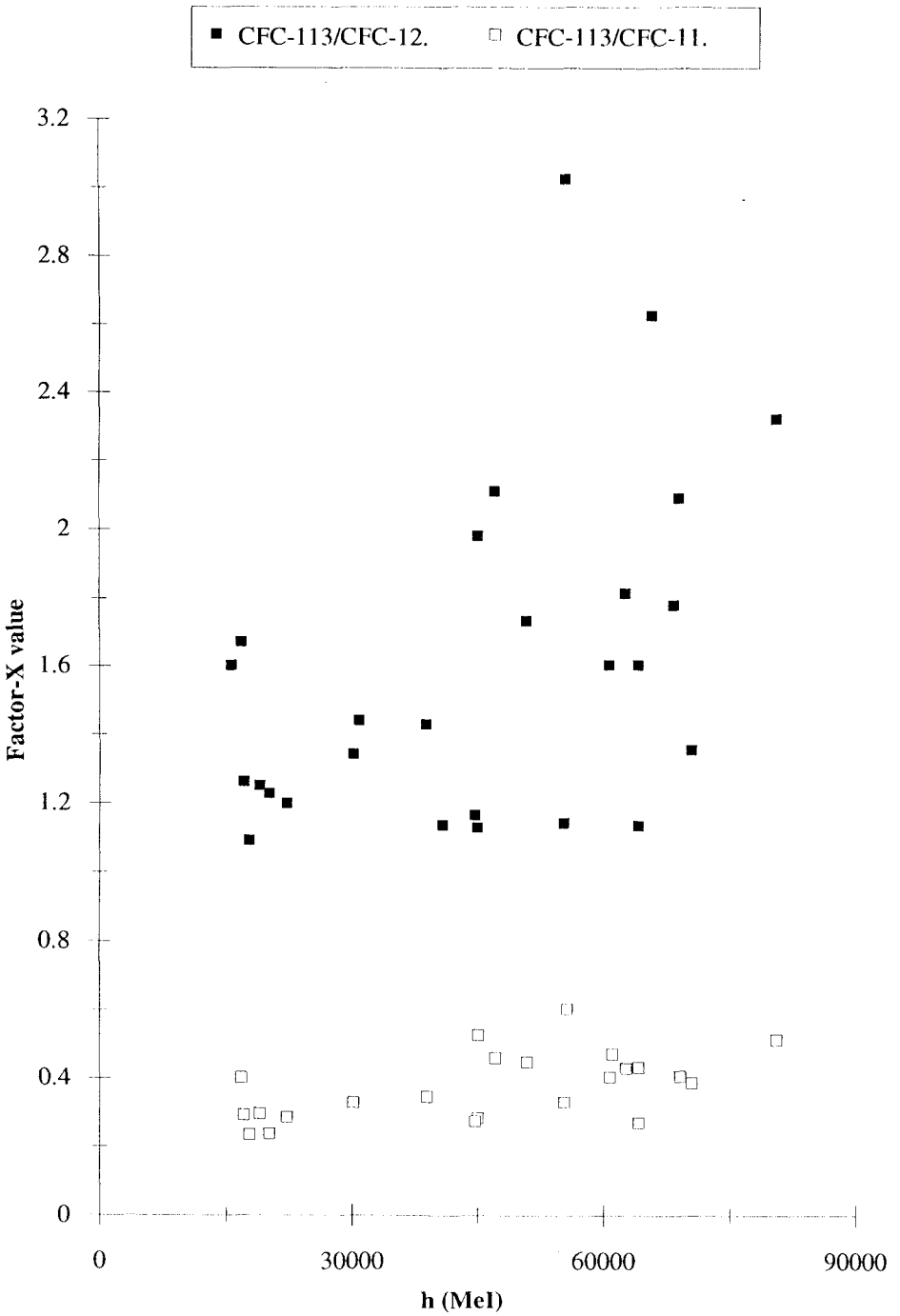

Figure 4.6. Scatter plot of $_{113}X_{12}$, and $_{113}X_{11}$ against modelled contribution of MeI peak to CFC-113, h(MeI) in peak height units, as defined by Equation 4.2.3b.

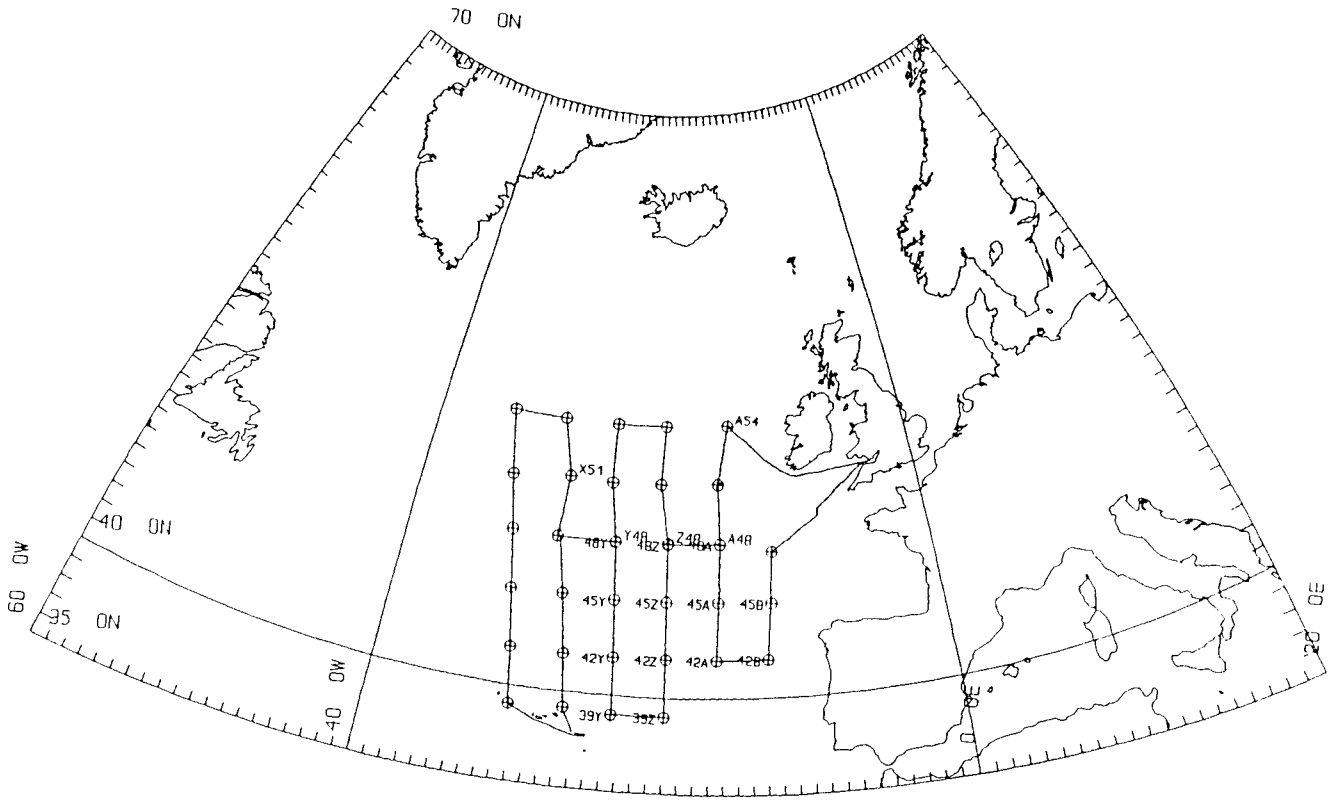

Figure 4.7. Map of VIVALDI '91 cruise track showing stations with reliable CFC-113 data. Three stations were not sampled for CFCs, three had no surface samples, but were removed due to implausibly high CFC-113/CFC-12 ratios deeper in the cast, and thirteen were removed because their MeI contamination was too great (i.e. h(MeI) > 10; see Section 4.2.2).

4.2.4. Detection limits, precisions and dynamic ranges.

The detection limit for the instrument, evaluated by consideration of deep water samples with very low CFC burdens (Antarctic Bottom Water in the deep Porcupine and Iberian Abyssal plains) was 0.03-0.05pMol/l for CFC-12 and 0.003-0.004pMol/l for CFC-113. No sample contained what was considered to be undetectable concentrations of CFC-11, although the minimum recorded value was 0.04pMol/l. The true detection limit is considered to be approximately 0.02pMol/l by comparison with system blanks for this species which are no larger than 0.01pMol/l. The seawater sampling precision, as determined by comparing samples from different bottles closed at the same depths and at different depths within the well-mixed layer, are 0.02, 0.09, and 0.01pMol/l for CFC-12, CFC-11 and CFC-113 respectively. These represent fractions of 1.2, 2.4 and 2.9% of typical surface water concentrations. The precision to consecutive samples of standard gas was 1.9, 0.97 and 2.8% for the 94 injections examined. Consideration of the ratios of saturated cold surface waters to the minimum detection limits reveals dynamic ranges of 100:1, 350:1 and 200:1 for CFC-12, CFC-11 and CFC-113 respectively. (This calculation for 2°C, 35‰ seawater at saturation in 1991, and assuming a solubility for CFC-113 of 0.30 times the CFC-11 solubility. See Section 4.3.2.)

Fortunately, some VIVALDI stations on leg 1 were repeated on leg 2. These were 48Y, Y48; 48Z, Z48 and 48A, A48 on Figure 4.1; cast 48X was missed on leg 1 due to bad weather. Figure 4.8 shows the repeat station data for each CFC species. For those bottles closed at the same depths the CFC-11 and CFC-12 discrepancies are not significantly different from the combined uncertainty of seawater sampling precision and replicate calibration injections. Figure 4.8(c) shows the CFC-113 data which has not been corrected for MeI contamination. The second cast at each station pair demonstrates consistently higher CFC-113 values in the top 1000db as a result of the contribution to this peak from MeI. The same profiles with corrections described in Section 4.2.2 applied is shown in Figure 4.8(d). Again, the discrepancies at the same depths for the repeat stations do not vary significantly from the expected uncertainty. Figure 4.9 shows data from the repeat stations for potential temperature, salinity and bottle oxygen concentration for comparison (Pollard *et al.*, 1991) The analytical uncertainties for these measurements are much smaller than for the CFC observations, and so Figure 4.9 is included in order to allow an estimate of any real changes in the ocean during the period between observations. The top 1500db show significant changes in particular which can cause some of the observed discrepancies in the CFC profiles of Figure 4.8.

Figure 4.8. Plots of repeated stations from VIVALDI. (a) CFC-12, (b) CFC-11, (c) CFC-113 uncorrected for MeI contamination, and (d) CFC-113 corrected for MeI contamination as described in Section 4.2.2. Dates and positions of stations are respectively; Y48, 48Y 29/5/91, 11/5/91 48 00.0'N 24 02.0'W; Z48, 48Z 4/9/91, 3/5/91 48 00.0'N 19 57.0'W; A48, 48A 2/5/91, 5/6/91 48 00.0'N 15 58.0'W. Y-axis is in-situ concentration in pMol/l offset by steps of (a) 1.5, (b) 3.0, and (c), (d) 0.4 pMol/l.

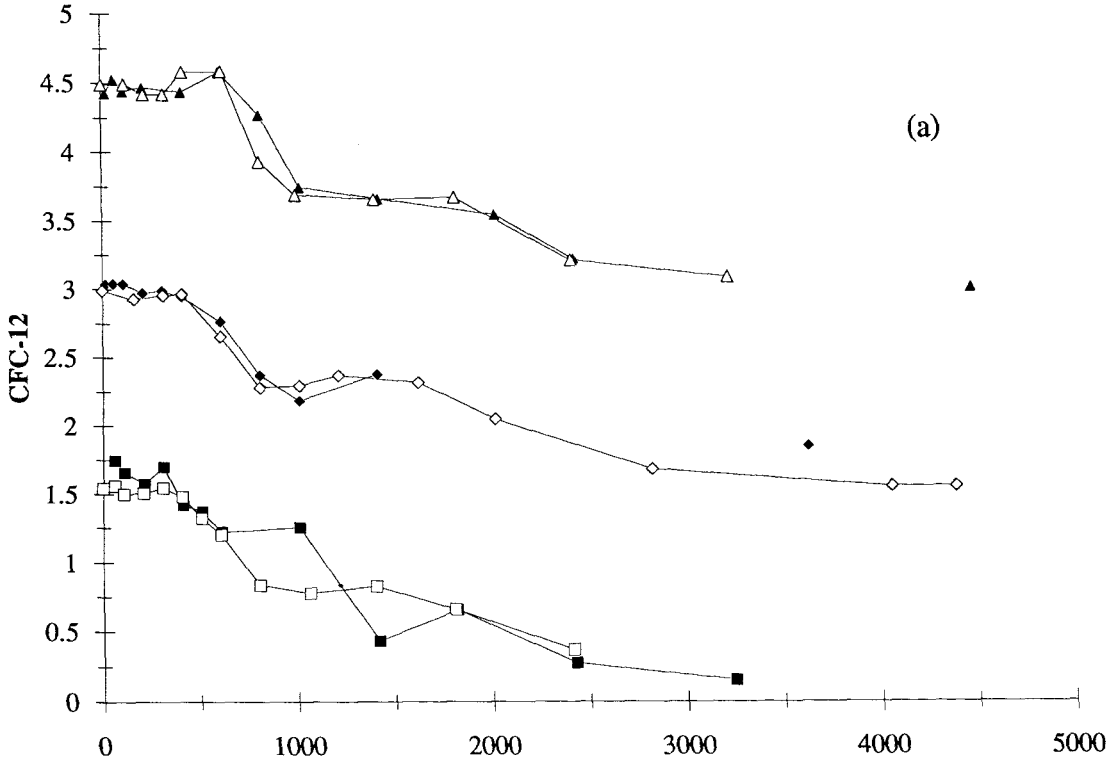
(a)
CFC-12
5
4.5
4
3.5
3
2.5
2
1.5
1
0.5
0
0
1000
2000
3000
4000
5000

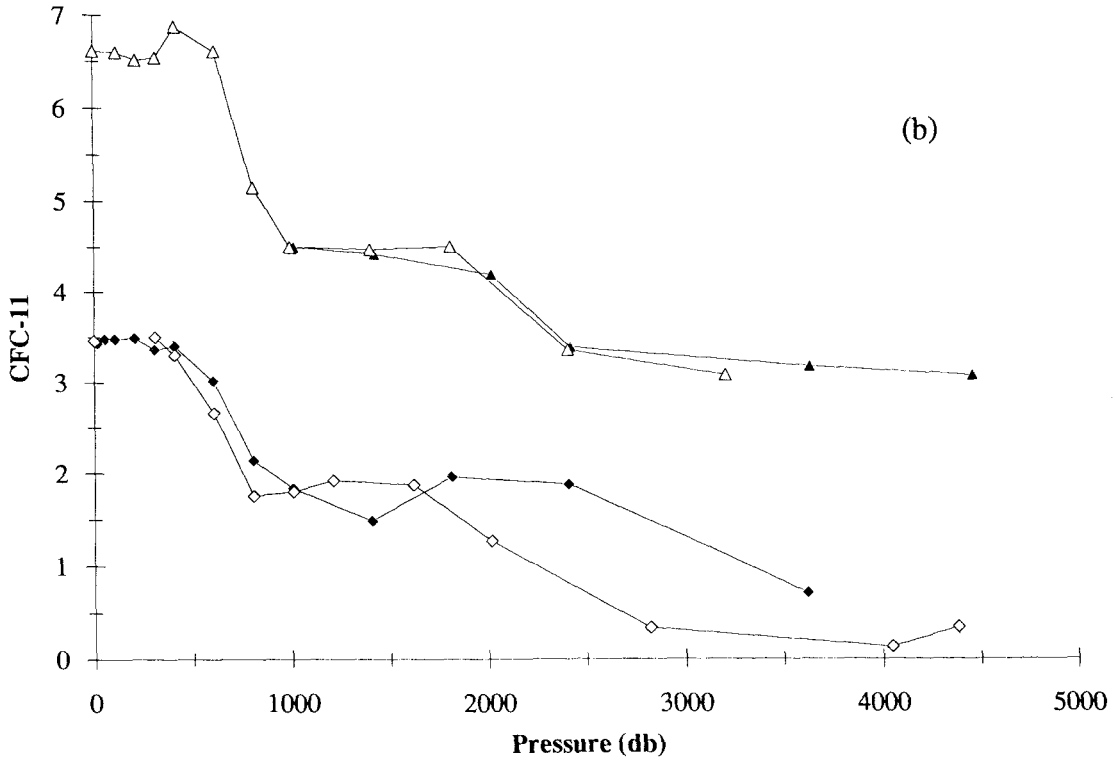
(b)
CFC-11
7
6
5
4
3
2
1
0
0
1000
2000
3000
4000
5000
Pressure (db)

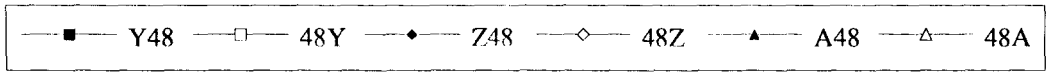
Y48
48Y
Z48
48Z
A48
48A

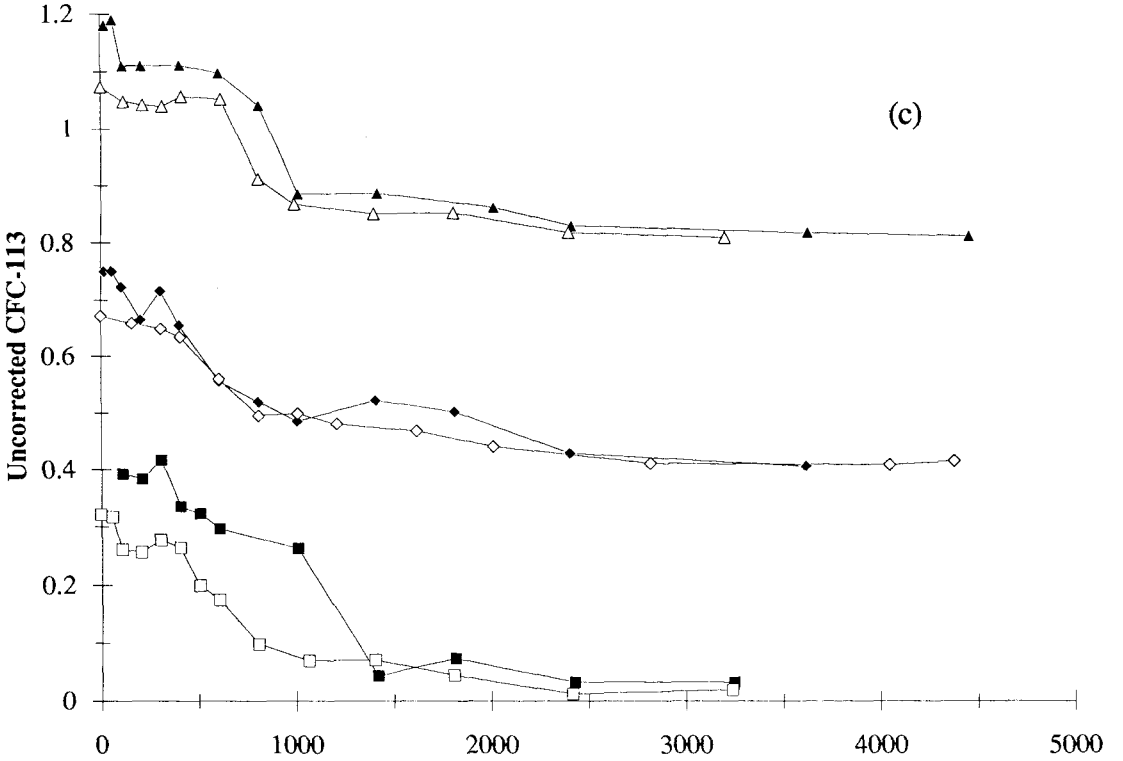
(c)
Uncorrected CFC-113
1.2
1
0.8
0.6
0.4
0.2
0
0
1000
2000
3000
4000
5000

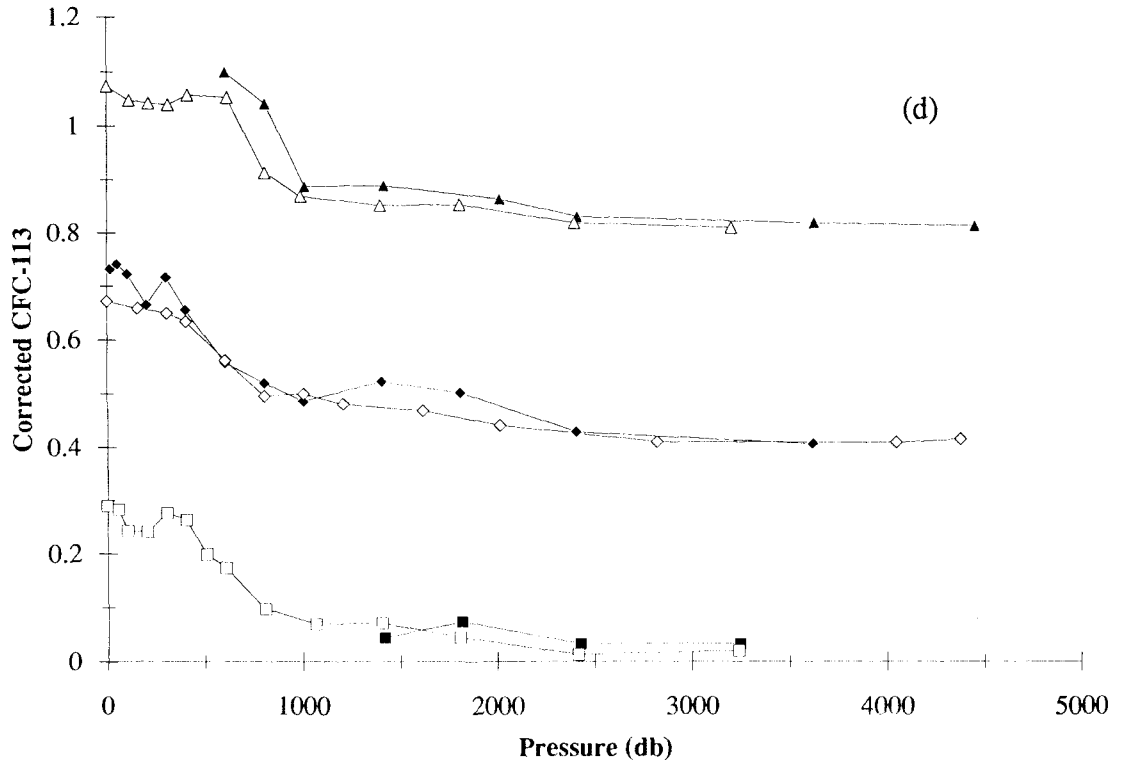
(d)
Corrected CFC-113
1.2
1
0.8
0.6
0.4
0.2
0
0
1000
2000
3000
4000
5000
Pressure (db)

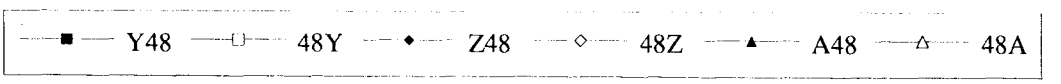
Y48
48Y
Z48
48Z
A48
48A

Figure 4.9. Plots of repeated stations from VIVALDI. (a) Potential temperature referenced to 0db (°C), (b) salinity (‰), and (c) bottle dissolved oxygen (ml/l). Dates and positions of stations as per Figure 4.8. Y-axis offset in steps of (a) 8°C, (b) 0.7‰ , and (c) 1.25ml/l.

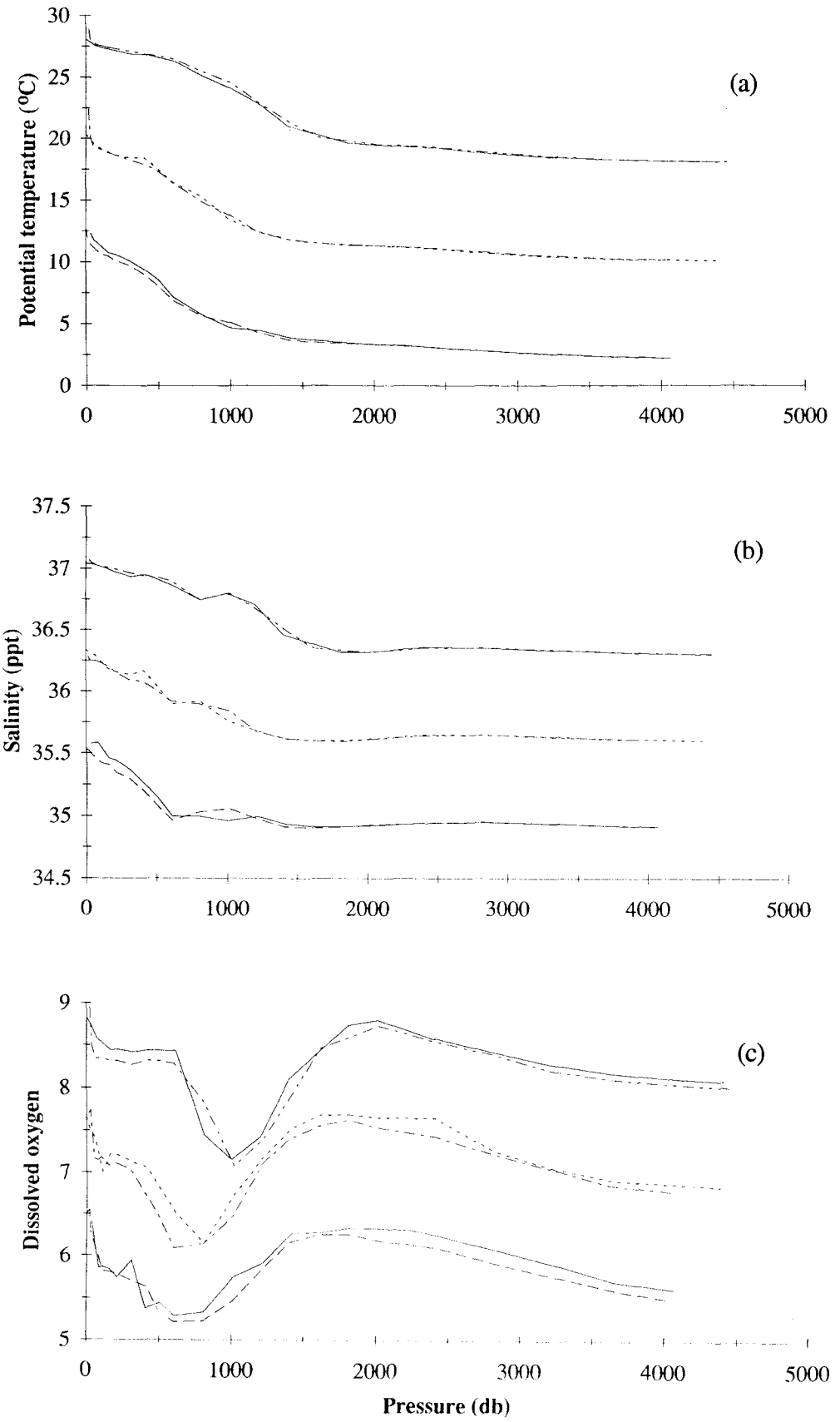
(a)
Potential temperature (°C)
30
25
20
15
10
5
0
0
1000
2000
3000
4000
5000
(b)
Salinity (ppt)
37.5
37
36.5
36
35.5
35
34.5
0
1000
2000
3000
4000
5000
(c)
Dissolved oxygen
9
8
7
6
5
0
1000
2000
3000
4000
5000
Pressure (db)
Y48
48Y
48Z
Z48
A48
48A

4.3. Calculation of CFC-113 Ventilation Ages and Results from the VIVALDI Survey.

This Section reports some of the CFC fields obtained during VIVALDI. Initially, the current state of knowledge on the hydrography and circulation of the north east Atlantic is reviewed, to put the survey area into an oceanographic context (Section 4.3.1). Section 4.3.2 is concerned with the details of calculating CFC-113 ventilation ages, and the approximation used to substitute for the unknown CFC-113 solubility. Finally Section 4.3.3 reports some of the data gathered during the VIVALDI cruise, and brief comments are made concerning possible interpretation of these fields, although a more complete description is postponed until Chapter 7.

4.3.1. Hydrography of the North East Atlantic Ocean.

The oceanography of the North Atlantic has been extensively studied. Recent publications of climatological atlas data include Fukumori *et al.* (1991), Woods (1987) and Levitus (1982). Harvey (1982), in describing a θ-S analysis of water masses in the eastern North Atlantic, identifies four deep water types ($\theta < 4^oC$) and three intermediate water types ($4^oC < \theta < 12^oC$); Table 4.2 describes some of their characteristics. Leetmaa & Bunker (1978) show the zero Ekman pumping line crosses the North Atlantic in a roughly east to west fashion at about 52°N, east of the mid-Atlantic ridge. Worthington (1976) describes the gyre circulation in the western basin consisting of a rapid jet (the Gulf Stream) running North along the eastern United States, then turning out to sea, losing velocity to become the North Atlantic Current (NAC) which forms the axis of the Sub-Polar Front, separating the sub-tropical and sub-polar gyres. This jet is consistent with the observed mean wind forcing (Ekman pumping), and the region to the east of this western boundary current is one of more quiescent recirculation, heading south then west. The Kiel atlas (Woods, 1987) shows much reduced eddy kinetic energies in the eastern basin, based on Seasat observations, consistent with this postulated slow return flow.

Several authors have attempted to describe and account for the eastern North Atlantic circulation. In a study of the eastern basin, between 9 and 38°N, Stramma (1984) used the conservation of mass theory of Fiadeiro & Veronis (1982) to derive a level of no motion for geostrophic calculations, and found good agreement between maps of linear potential vorticity and geostrophic transport. Sy (1988) also used this technique in a study of the mid-Atlantic ridge circulation (22-53°N) with a refinement on the reference level calculation following the inverse method of Wunsch (1977). He implied a surface flow crossing the ridge between 24 and 53°N in two distinct currents; the NAC and the Azores Current (AC). At intermediate depths ($27.55 < \sigma_T < 27.65$) a wedge of Mediterranean Water (MW) flows westward to be increasingly altered by enhanced mixing with Sub-Arctic Intermediate Water (SAIW) and underlying Labrador Sea Water (LSW) over the

mid-Atlantic Ridge, and by the increased shear due to the divergent NAC and AC streams (see Figure 18, Sy, 1988).

Table 4.2. Water masses in the eastern North Atlantic. Characteristics taken from Harvey (1982) and Wright & Worthington (1970)

Name	θ (°C)	S (‰)	Characteristics
Deep Mediterranean Water	> 2.6	> 34.95	High salinity, near Gibraltar
Labrador Sea Water (LSW)	3.2 - 3.9	< 34.94	Fresh, cold, deep water spreading from the west.
Iceland-Scotland overflow water	< 3.0	> 34.98	High salinity northern contour following current.
Bottom Water	< 2.4	< 34.94	Antarctic Bottom water spreading north from the western basin through the Romanche Gap.
Mediterranean Water (MW)	9.5	> 35.7	Characteristic core MW at 600-1700m.
Sub-Arctic Intermediate Water (SAIW)	5.0 - 9.0	< 35.0	Fresh water, ventilated in sub-Arctic gyre.
Eastern North Atlantic Water (ENAW)		35.0 -> 35.7	Intermediate water mass between MW & SAIW.

Leetmaa *et al.* (1977) and Stommel *et al.* (1978) test the theory that the North Atlantic east of the mid-Atlantic ridge is in Sverdrupian balance (see, for example, Gill (1982)), and conclude that this is so. Saunders (1982) uses this assertion to make an estimate of the level of no motion for a geostrophic calculation of meridional velocities in the eastern basin between 30 and 50°N, with inferred large scale velocities of order 1cm/s. The flow of MW according to Saunders (1982) is almost entirely zonal. A reasonable eastern extension of anticyclonic recirculation is found south of 45°N in the top 850m, and an east to west flux across the mid-Atlantic ridge between 1200 and 3500m fed by overflow waters from the North is also inferred. Ríos *et al.* (1992) found that MW moving towards the mid Atlantic ridge is connected with the AC, restricting the southward penetration of Eastern North Atlantic Water (ENAW) formed in the sub-polar gyre. They also found a subsurface front along 42°N separating ENAW into two types; one of sub-polar, origin, and one of sub-tropical origin. In a study of various aspects of

the North Atlantic northeast of the Azores, Pollard & Pu (1985) report a salty wedge (salinity > 35.7‰) penetrating to the north, from the wind driven anticyclonic gyre, and outcropping near 45°N. They found the eastward flow of this water between 36°N and 46°N to be of order 2-4cm/s, converging towards the east. North of this outcrop the majority of the subpolar mode water is ventilated then subducted to the south, beneath the saline wedge, at rates of order 0.2-0.5cm/s.

4.3.2. Factor-X Values and CFC-113 Ventilation Ages.

Section 1.3.2 explains that the solubility of CFC-113 in seawater as a function of temperature and salinity is unknown, whereas those of CFC-11 and CFC-12 are well established (Warner & Weiss 1985, Wisegarver & Cline 1985). Wisegarver & Gammon (1988) used a factor (X) to relate the solubility of CFC-113 to that of CFC-11, required to estimate CFC-113 ventilation ages. This section examines the use of factor-X values, and shows how ventilation ages are evaluated.

For the unknown CFC-113 solubility, $F_{113}(\theta,S)$, and the solubility of either CFC-11 or CFC-12, $F_a(\theta,S)$ (a $\Leftrightarrow$ 11 or 12), there exists a quantity ${}_{113}X'_a(\theta,S)$ such that,

$$F_{113} = {}_{113}X'_a F_a \qquad 4.3.1.$$

It is likely that ${}_{113}X'_a$ is a slow function of (θ,S), since ${}_{11}X'_{12}$ varies by only 12% for $\Delta\theta$ = 20°C, and by 0.3% for ΔS = 2‰ (Warner & Weiss, 1988). For the present purposes ${}_{113}X'_a$ will be assumed to be constant, based on this evidence.

In general, the relationship between atmospheric and aqueous concentrations is given by

$$[a]_{surf} = F_a\,[a]_{atm}\,\xi_a \qquad 4.3.2$$

with square brackets expressing concentrations in appropriate units and where Equation 1.3.2 has been extended to include saturations, ξ_a, other than unity (equilibrium). Wisegarver & Gammon (1988) *estimate* ${}_{113}X'_{11}(\theta,S)$ by writing,

$${}_{113}X'_{11} \approx {}_{113}X_{11} = \frac{[113]_{surf}\,[11]_{atm}}{[113]_{atm}\,[11]_{surf}} \qquad 4.3.3.$$

They calculate ${}_{113}X_{11}$, using their surface data, and obtain the value 0.49. Equations 4.3.1, 4.3.2 and 4.3.3 yield an important relationship, viz.

$${}_aX_b = {}_aX'_b \frac{\xi_a}{\xi_b} \qquad 4.3.4$$

which will be used shortly.

One needs to know the CFC-113 solubility to calculate ventilation ages and the CFC-113 ventilation age, τ', of a fluid parcel is defined to be,

$$\tau' = t - f\left(\frac{p_{113}}{p_a}\right) \qquad 4.3.5$$

where the function f is shown in Figure 1.2 (Section 1.3.1), p refers to the dissolved partial pressure in the fluid parcel and a represents either CFC-11 or CFC-12. Although Wisegarver & Gammon (1988) use the quantity $f\left(\frac{p_{113}}{p_a}\right)$ directly for their 'ventilation age' it seems more appropriate to refer to this as a 'vintage'; Equation 4.3.5 also bears a closer resemblance to the tritium/helium-3 age defined by Jenkins (1988). Dissolved partial pressures are defined simply by,

$$p_a = \frac{[a]}{F_a} \qquad 4.3.6$$

where [a] is the dissolved gas concentration (see Section 5.1 too), and so Equation 4.3.5 leads one to

$$\tau' = t - f\left(\frac{[113]}{[a]\ {}_{113}X_a'}\right) \qquad 4.3.7$$

and thus,

$$\tau' = t - f\left(\frac{[113]\ \xi_{113}}{[a]\ {}_{113}X_a\ \xi_a}\right) \qquad 4.3.8$$

Here ξ_{113} and ξ_a refer to the saturation values at the time of permanent subduction of the water parcel. It is clear that τ' is a good proxy of the 'true' time since sequestration if $\xi_a = \xi_{113}$, although anticipating the comments of Section 5.1, in general, ξ values are strong functions of time and position in the ocean.

Table 4.3 shows the values of factor-X parameters from the VIVALDI and ARANDA expeditions, from Wisegarver & Gammon (1988) and from the AJAX dataset (CFC-11 and CFC-12 only). The previous estimate of 0.49 for ${}_{113}X_{11}$, is too high according to the work reported here. This result is important, and although the CFC-113 solubility is unknown it is worth persevering with the calculation of ventilation ages. This is done by approximating Equation 4.3.8 with

$$\tau' \approx \tau = t - f\left(\frac{[113]}{[a]\ {}_{113}X_a}\right) \qquad 4.3.9$$

used throughout this work. The factor-X values from Table 4.3 (VIVALDI expedition) are used for ${}_{113}X_{11}$ and ${}_{113}X_{12}$, with a scheme of interpolation between the annually reported atmospheric concentrations of Figure 1.2 used for f(r). Further, discussion of these concepts can be found in Section 4.3.3 where a profile of ventilation

ages is examined, and in Section 5.1 where the surface ξ_{11} and ξ_{12} are reported. Although the factor-X technique is approximate (Wisegarver & Gammon (1988) estimate a 4% error applying the same method to CFC-12) the values of $_{113}X_{11}$ and $_{113}X_{12}$ are not sensitive to the MeI correction technique described in Section 4.2.2.

Table 4.3. Factor-X values for various expeditions and techniques. N-E Pacific data from Wisegarver & Gammon (1988). AJAX data from stations 96-135, Weddell Sea, Weiss *et al.* (1990). The criteria of Section 4.2.2 were used to correct these data.

Expedition	$_{113}X_{11}$	$_{113}X_{12}$	$_{11}X_{12}$	#	Technique
VIVALDI 1991 N-E Atlantic	0.303	1.22	4.3	10, 15, 24	(This work)
ARANDA 1990 Denmark Straits	0.27	1.3	4.9	5	Liddicoat *et al.* (in prep.)
N-E Pacific 1986	0.49			3	Wisegarver & Gammon (1988)
AJAX 96-135 1984 Weddell Sea			4.2	40	Bullister & Weiss (1988)

4.3.3. CFC-113 Ventilation Age Fields in the North East Atlantic.

Figure 4.10 shows a cast profile from Leg 1 which is one of the best obtained, showing that the CFC-11/CFC-12 ratio is inadequate in resolving ventilation ages at depths less than 1800db at this station, since its ratio stopped varying more than fourteen years ago. Both the CFC-113/CFC-11 and CFC-113/CFC12 ratios exhibit substantial variation over this interval, however. Figure 4.10(c) shows these ratios in terms of ventilation ages. The relatively constant profiles of concentration, and ventilation ages down to the sample at 628db suggest that this fluid is mixed seasonally, with permanently stratified water evident to depths of around 1000db. For the next ~1000db of the water column there is a stad in the CFC concentration, with an increase in ventilation ages, before the concentrations drop again to the sample at 2408db. At this point the CFC-113 concentrations are too small for precise ventilation age evaluation, since errors dominate the concentration ratio, and the ventilation age for the deepest sample on this cast is not shown in Figure 4.10(c). It is not until the sample at 2408db is reached that that the CFC-11/CFC-12 ratio starts to decrease, and use of this ratio for ventilation age dating might be attempted.

Figure 4.10. (a) CFC concentration, (b) CFC ratio profiles, and (c) CFC-113/CFC-11 and CFC-113/CFC-12 ventilation ages for station 11008 (48A on Figures 4.1 and 4.7) taken on 2/5/91 above the Porcupine Abyssal Plain (48 01.4'N 15 59.1'W). Errors are shown in figure (c); long dashes for CFC-113/CFC-11 age; short dashes for CFC-113/CFC-12 age.

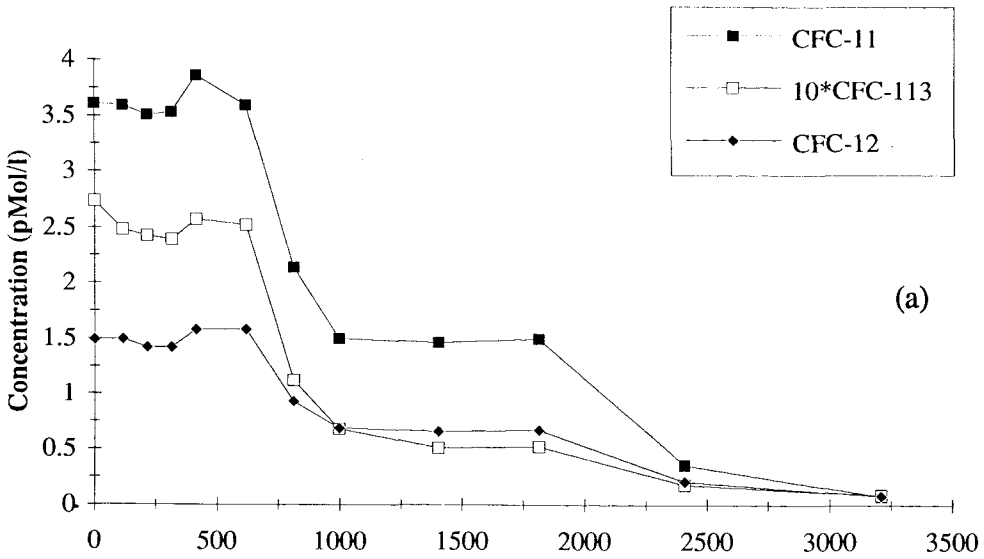
CFC-11
10*CFC-113
CFC-12
Concentration (pMol/l)
4
3.5
3
2.5
2
1.5
1
0.5
0
0
500
1000
1500
2000
2500
3000
3500

(a)

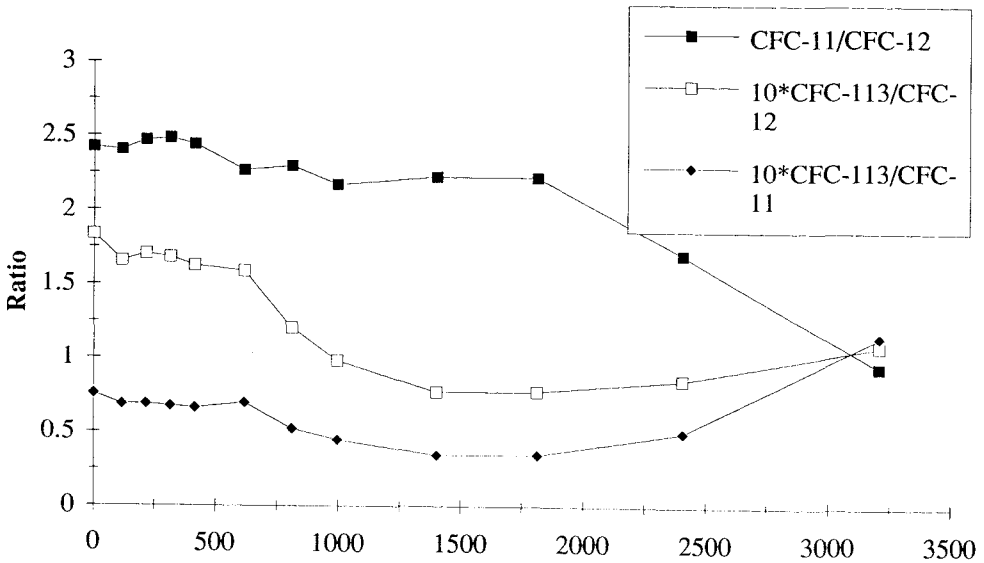
CFC-11/CFC-12
10*CFC-113/CFC-12
10*CFC-113/CFC-11
Ratio
3
2.5
2
1.5
1
0.5
0
0
500
1000
1500
2000
2500
3000
3500

(b)

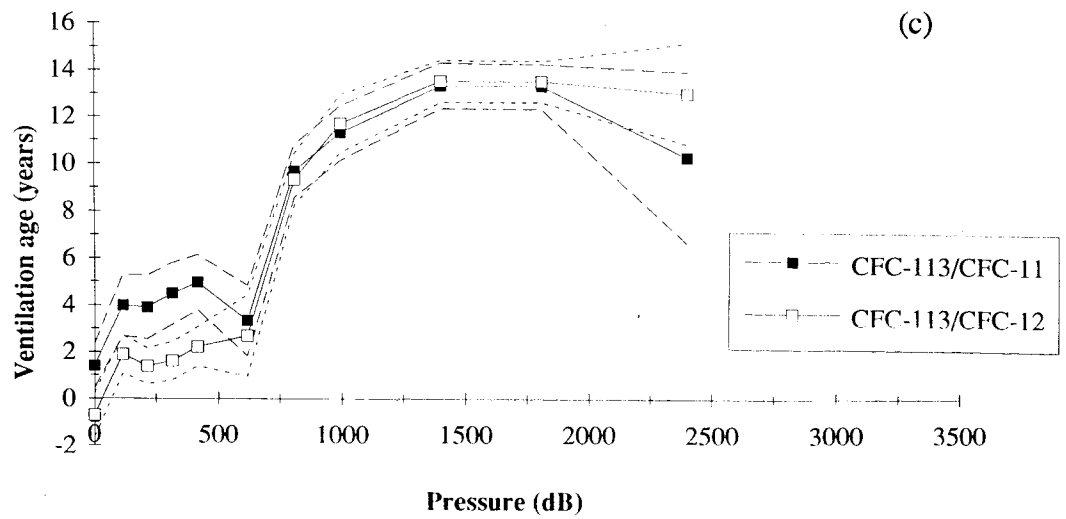
CFC-113/CFC-11
CFC-113/CFC-12
Ventilation age (years)
16
14
12
10
8
6
4
2
0
-2
0
500
1000
1500
2000
2500
3000
3500
Pressure (dB)

(c)

By using the information in both the CFC-113/CFC-11 and CFC-113/CFC-12 ratios the ventilation age can be well constrained, providing a powerful check of consistency. Figure 4.10(c) shows the two sets of ventilation ages agree well between 628db and 1800db. At shallower depths, the curves diverge by a maximum of 2.9 years. Errors on the ventilation age at these depths are ± 1.5 years based on the values quoted in Section 4.2.4 for seawater sampling precisions. The error on the ventilation age is a minimum of ± 0.9 years at depths of 1500-2000db; below this it increases because the absolute concentrations become small, while towards the surface the fractional change in the ratio is less with each passing year, i.e. using the definitions of Section 6.3, $\frac{d^2f}{dr^2} > 0$.

There appears to be a systematic discrepancy between the two ventilation age curves in Figure 4.10(c) close to the surface, although the agreement is formally insignificant (Figure 4.10(c) shows error bars). The CFC-113/CFC-11 age is consistently older than the CFC-113/CFC-12 age. Indeed, the mean ventilation age profile shown in Figure 6.2(c) (Section 6.4) shows this too. There are several possible reasons for this which are discussed below.

i) The calculation of ${}_{113}X_{12}$ and ${}_{113}X_{11}$, as Section 4.3.2 and Table 4.3 suggest, is an approximate technique. In particular, the values used for these parameters are prone to uncertainty based on errors in the observations, and, to a lesser extent, errors in the MeI correction technique explained in Section 4.2.2. However, perturbation of the ${}_{113}X_{12}$ or ${}_{113}X_{11}$ values by constant errors merely offsets the whole ventilation age profile as Equation 4.3.9 implies. Since the ${}_{113}\tau_{11}$ and ${}_{113}\tau_{12}$ ages agree for the thermocline and deeper samples, but disagree for the seasonal thermocline, offsetting the whole profile, by varying ${}_{113}X_{12}$ or ${}_{113}X_{11}$, will not explain this discrepancy.

ii) The first assumption made in Section 4.3.2 is that ${}_{113}X_a'$ is not a function of (θ,S). If however, this premise is relaxed, then it is possible that ${}_{113}X_{11}$, (for example) could vary with θ, and hence co-vary with pressure, sufficiently to resolve the discrepancy between the two ventilation age curves of Figure 4.10(c) Although this mechanism does refine estimates of factor-X, it is unlikely to provide sufficient variation to be important. Indeed, correlation of surface ${}_{113}X_{11}$ and ${}_{113}X_{12}$, with temperature yielded linear coefficients of r = 0.277 and 0.185 respectively; statistically insignificant, and sufficient evidence to vindicate this possible explanation of ventilation age divergence.

iii) Although Wisegarver & Gamon (1988) cite various sources to support the premise of a linear increase of atmospheric concentration since 1973, lack of manufacturer's data on release makes the source function for CFC-113 less certain than for CFCs 11 or 12 (Section 1.3.1). Errors in the CFC-113 source function cannot cause discrepancies between CFC-113/CFC-11 and CFC-113/CFC-12 ages however; but

inaccuracies in the recent atmospheric concentrations of CFCs 11 and 12 could. This requires changes in the shape of the atmospheric source function however, rather than mere changes in the rate of increase, since changing the current value of $[a]_{atm}$ also alters ${}_{113}X_a$ in the way prescribed in part i) above (Equation 4.3.3) and cannot account for the differences of ventilation ages down their profiles. It is unlikely, however, that the uncertainty in the shape of the atmospheric source function is sufficient to cause this discrepancy. Even in the pathological case that the CFC-11 concentration in the atmosphere is constant for the period 1985-1988, then resumes the values shown in Figure 1.1, the effect on the CFC-113/CFC-11 ventilation age is only about 1.5 years.

iv) Equation 4.3.3 is used to estimate a value for ${}_{113}X_a'$, and is in error by the factor $\frac{\xi_{113}}{\xi_a}$ as Equation 4.3.4 shows. Specifically it is in error by $\left.\frac{\xi_{113}}{\xi_a}\right|_{VIV}$ the value of the saturation ratio at the time of the VIVALDI cruise. However, the fluid is entrained at a different time, when $\left.\frac{\xi_{113}}{\xi_a}\right|_{entrain}$ is the relevant ratio, and in general $\left.\frac{\xi_{113}}{\xi_a}\right|_{VIV} \neq \left.\frac{\xi_{113}}{\xi_a}\right|_{entrain}$. This, indeed, causes an incorrect estimate of the value of the appropriate factor-X, it is, however, no more than another mechanism to vary these quantities as is outlined in part i). Only if $\left.\frac{\xi_{113}}{\xi_a}\right|_{entrain}$ varies with depth, can this process explain the discrepancy between the CFC-113/CFC-11 and CFC-113/CFC-12 ventilation ages. One possibility is that $\left.\frac{\xi_{113}}{\xi_{11}}\right|_{entrain}$ is smaller in the seasonal thermocline than the corresponding value in the water > 600db, for example, this would bring the two ventilation curves of Figure 4.10(c) more into coincidence. The fact that the CFC-113/CFC-11 age is older than the CFC-113/CFC-12 age, and the latter age is close to zero through the seasonal thermocline, is consistent with the saturation values at entrainment being such that $\xi_{113} \sim \xi_{12} < \xi_{11}$. This disagrees with the results of modelling work described in Section 5.6.

v) A final possibility to reconcile the differences in ventilation ages through the seasonal thermocline in Figure 4.10 is that the CFC-11 peak is boosted by coelution with another compound in this depth region (but not present in atmospheric samples), so as to make the CFC-113/CFC-11 ratio smaller than it otherwise would be. If this contamination decreased with depth, so too would the difference in age between the estimates based on CFC-113/CFC-11 and CFC-113/CFC-12. This mechanism, however, requires a candidate compound for the contaminant to be treated seriously. Several possible species are tested on the analytical system of Chapter 2, with no problem of CFC-11 peak resolution (Figure 2.2). Moreover, the surface saturation values for CFC-11 are reasonable based on Warner's (1988) data (Section 5.1).

Although none of the individual processes mentioned above seem to adequately explain the differences between the CFC-113/CFC-11 and CFC-113/CFC-12 ventilation ages, the effect of i)-iv) in combination may well do. Until the CFC-113 solubility is known, these factors will remain obscure. Option v) can only be rigourously investigated by a period in the field when an established CFC-11, CFC-12 instrument is also operational. As far as this thesis is concerned a pragmatic decision to use CFC-113/CFC-12 ages in preference to CFC-113/CFC-11 is made, based on the fact that the CFC-12 data is superior to the CFC-11.

Figure 4.11 is a map of a σ_θ surface which outcrops in the VIVALDI survey area. The vertical direction in the figure is pressure and the CFC-113/CFC-12 ventilation age colours the net. Two features stand out specifically. Firstly, the pressure and ventilation age fields are remarkably well correlated (linear correlation coefficient, r = 0.947, for 12 data pairs). Secondly, there is a large range of ages on this surface (13.5 years). The mixed layer depths observed during the VIVALDI cruise are of order 30-40m, and so most of the north-eastern area of this density surface is outcropping. The fact that the ventilation age is so spatially coherent, reinforces the confidence in the reproducibility of the analytical technique.

However, it is not so manifest how the ventilation age distribution relates to oceanographic features. This question of how CFC-113 ventilation age fields should be interpreted is the motive for the remainder of this thesis. After theoretical ideas have been developed in Chapters 5 and 6 the discussion returns to Figure 4.11. In the meantime however, let us make two initial comments. Firstly, one might expect that fluid in the actively mixed layer of the winter immediately preceeding the VIVALDI survey would have a ventilation age of between 0-1 years. Based on this, a line of outcropping for the σ_θ = 27.1 isopycnal can be traced from the age field at a pressure of about 100db, following the blue to green colour scale of Figure 4.11. (If, indeed, the fluid of (say) τ = 0.5 years was ventilated the previous winter, the true depth of the mixed layer at that time is twice the pressure shown in Figure 4.11, i.e. ~ 200db. This is because Figure 4.11 shows *mean* pressure on the σ_θ = 27.10 isopycnal.). Secondly, judging by the lines of constant age, one might diagnose the flow on the surface of Figure 4.11 to be towards the southwest with a speed of about 0.2 cm/s. Incidentally, this is consistent with the estimate of Pollard & Pu (1985). These comments are reappraised in the light shed by the proceeding two chapters in Section 7.2.

Figure 4.11. Pressure (db) on isopycnal σ_θ = 27.10, with CFC-113/CFC-12 ventilation age (years) colouring the surface. Station positions are shown for this region in Figure 4.7; there are twelve data points in the figure.

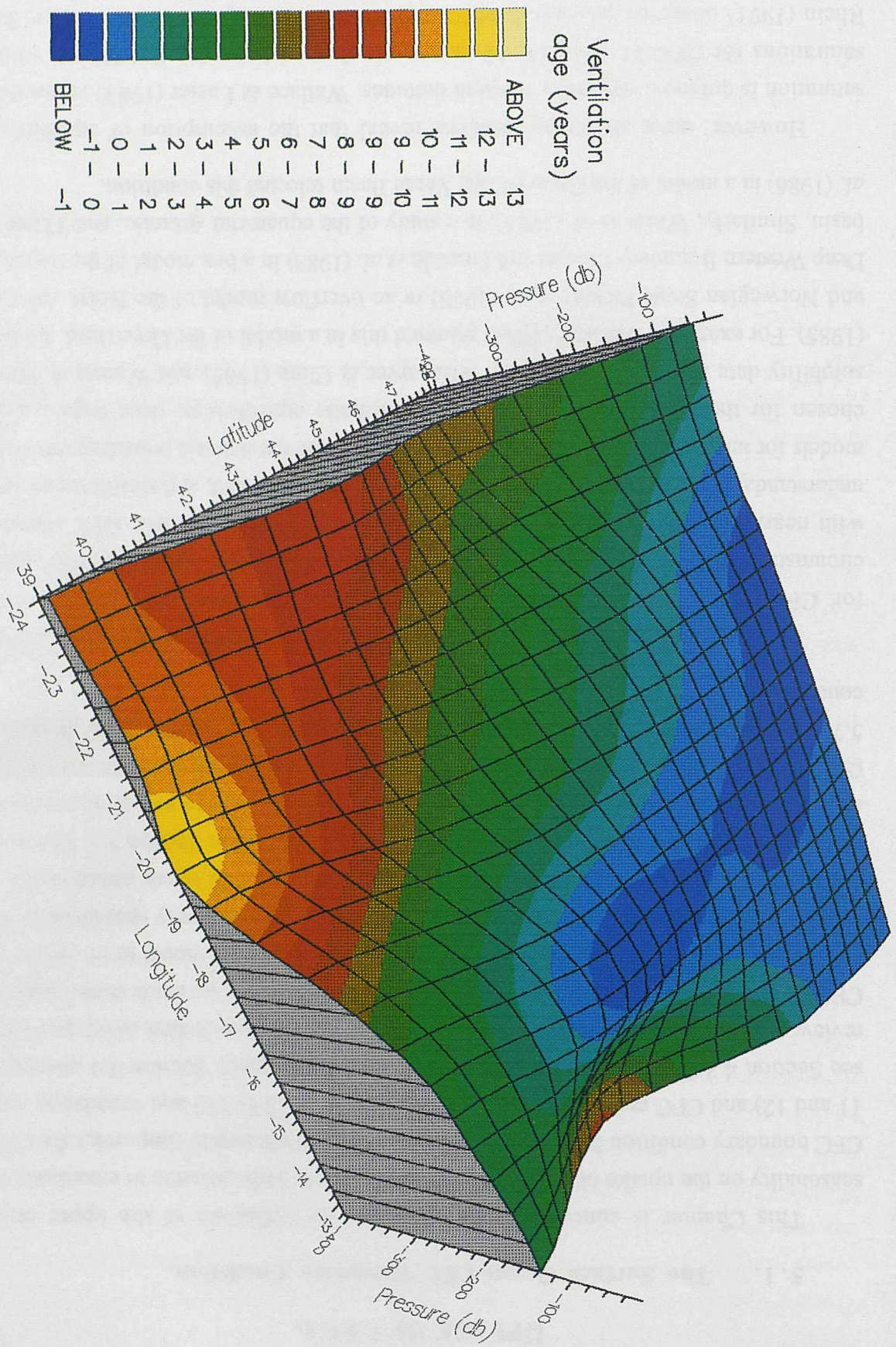
Ventilation age (years)
ABOVE 13
12 – 13
11 – 12
10 – 11
9 – 10
8 – 9
7 – 8
6 – 7
5 – 6
4 – 5
3 – 4
2 – 3
1 – 2
0 – 1
–1 – 0
BELOW –1
Pressure (db)
Latitude
Longitude
Pressure (db)

CHAPTER 5

THE INFLUENCE OF SEASONALLY MIXED LAYERS ON OCEANIC UPTAKE OF CFCS.

5.1. The Surface Ocean CFC Boundary Condition.

This Chapter is concerned with assessing the influence of the upper ocean seasonality on the uptake of CFCs from the atmosphere. This amounts to examining the CFC boundary condition for the interior ocean. Both concentration (important for CFCs 11 and 12) and CFC ratios are considered (important for CFC-113 and ventilation ages; see Section 4.3.2 for an introduction to CFC ventilation ages). Section 5.1 contains a review of recent literature relevant to this question. A discussion is then developed using CFC-11 and CFC-12 data from various sources, and deductions are made concerning the behaviour of CFC-113. Section 5.2 examines a simple analytical model to introduce the air/sea exchange parameterisations and explore the behaviour in a very special case. The rest of the Chapter is involved with use of a physically realistic upper ocean model in which a tracer model is embedded; the model itself is discussed in Section 5.3. The tracer response to perturbation of the model parameters (Section 5.4) and to initial conditions (Section 5.5) is examined. Section 5.6 compares model results with real data and Section 5.7 draws conclusions about the limits of certainty for the oceanic CFC boundary condition.

The CFC boundary condition for the atmosphere is reasonably well known, at least for CFCs 11 and 12, as Section 1.3.1 explains. However, the corresponding circumstances in the upper ocean, in intimate contact with the atmosphere, are not known with nearly so much certainty (see also Section 1.3.2). Early oceanic CFC research understandably concentrated on the analytical techniques required, and simple conceptual models for interpreting sparse data were employed. Often the oceanic boundary condition chosen for these problems was one of atmospheric equilibrium, once high quality solubility data had been obtained by Wisegarver & Cline (1985) and Warner & Weiss (1985). For example, Bullister (1984) assumed this in a model of the Greenland, Iceland and Norwegian Seas, Pickart *et al.* (1989) in an overflow model of the North Atlantic Deep Western Boundary Current and Smethie *et al.* (1988) in a box model of the Eurasian basin. Similarly, Weiss *et al.* (1985), in a study of the equatorial Atlantic, and Thiele *et al.* (1986) in a model of the Canary-Cape Verde Basin selected this condition.

However, more recent publications reveal that the assumption of equilibrium saturation is dubious, especially for high latitudes. Wallace & Lazier (1988) report 0.60 saturations for CFC-11 and CFC-12 in recently formed Labrador Sea Water, whilst Rhein (1991) observed saturations of 0.79±0.05 in Greenland Sea surface water. Her results are from a deep convection episode revealing homogenisation of the water

column, but no equilibration with the atmosphere during the event. She also reports dissolved oxygen saturations of 0.919-0.948 demonstrating that the ventilation process was closer to completion for this gas than for the chlorofluoromethanes (CFMs), consistent with its larger piston velocity (Broecker & Peng, 1982, p123). In the Ross Sea Trumbore *et al.* (1991) believe a surface under-saturation of 10-12% for CFCs 11 and 12 occurs at sequestration. Schlitzer *et al.* (1991) found typical super-saturations of +10% in the eastern Mediterranean, and occasional CFC-12 values as high as +21%, whilst Warner (1988), in a review of a large dataset from various oceans, reports that surface saturation is not temperature dependent, and that in general CFC-11 is further from equilibrium than CFC-12. Rhein (1991) compares four incompatible CFC studies of the turnover time for Greenland Sea Deep Water and Norwegian Sea Deep Water with different boundary conditions (her Table 1), and asserts that "The convective turnover rate of Eurasian Basin Deep Water is strongly dependent on the CFM boundary conditions" (presumably as inferred from her box models). In the same vein, Trumbore *et al.* (1991) note "Disequilibrium in surface waters at the time of entrainment appears to be the most likely explanation for discrepancies in 11/12 ratios between our model and the observations".

Comparing the variation in saturation boundary condition at the sea surface with typical instrumental precisions of 1-2% highlights an important point. It is the spatial and temporal uncertainty in the surface CFC saturation which currently limits the utility of CFC-11 and CFC-12 as oceanic tracers, and this uncertainty is greatest in those regions where the largest volumes are ventilated. Figure 5.1 shows surface CFC-11 and CFC-12 from both the ARANDA and VIVALDI cruises. It confirms the assumption of equilibrium saturation is poor, which is borne out by Warner's (1988) data too (his Figure 3.2).

The work of Wisegarver & Gammon (1988) promised an amelioration of this problem by introducing CFC-113 as a third CFC tracer. The advantage of this compound, as they explain, is that a combination of CFC-113 and CFC-11 or CFC-12 fields can yield a ventilation age tracer (Section 4.3.2) which cannot be achieved by use of CFC-11 and CFC-12 alone (at least since circa 1975; see Section 1.3.1). The reason that this age tracer may reduce the boundary condition uncertainty is that the assertion age = 0 at the surface may be more robust. This requires that each CFC species used to form the age tracer is in the same state of saturation, although they need not be at atmospheric equilibrium. In this way the ratio (and hence the ventilation age) is still a reliable proxy of the atmosphere. However, this is not, in general, the case either; essentially because the rate of relaxation to atmospheric equilibrium for each species is different. Figure 5.1 shows this for the CFC-11 and CFC-12 pair. The boundary condition age = 0 requires CFC-12 saturation = CFC-11 saturation, the locus of which is the straight line in the figure (although CFC-11/CFC-12 ages are not monotonic with time since 1975 this

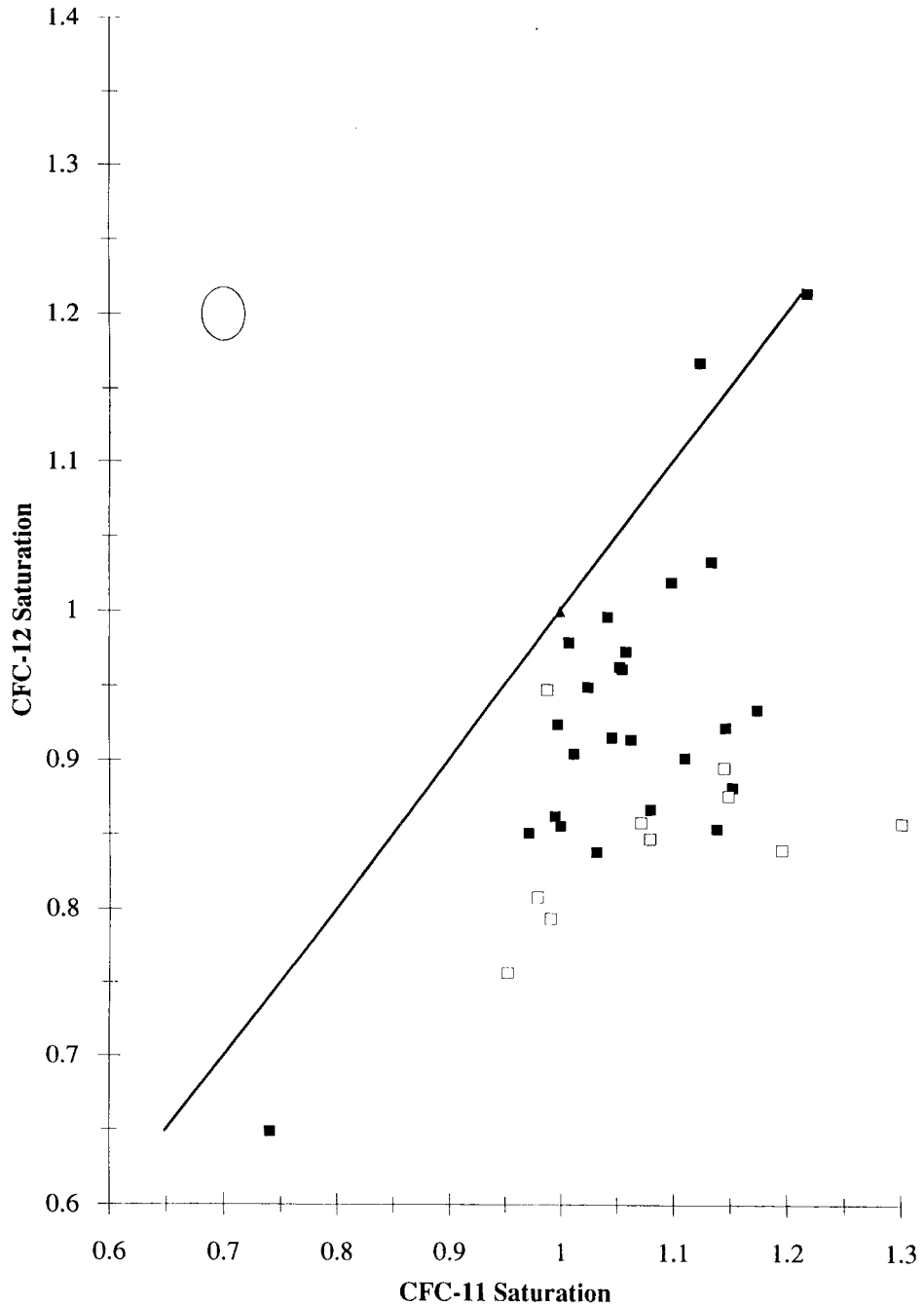

Figure 5.1. Scatter plot of surface CFC-11 saturation versus surface CFC-12 saturation for the VIVALDI '91 and ARANDA cruises (filled and open symbols respectively; see Section 4.1). The ellipse represents one standard deviation on the scatter plot from the instrumental uncertainties explained in Section 4.2.4. No error due to inaccuracy in the primary standard calibration propagates to the calculation of saturations. The triangular symbol represents the condition of atmospheric equilibrium for each species, and the solid line is a segment of the locus of points for which the CFC-11 and CFC-12 saturations are equal. These represent the two surface boundary conditions discussed in Section 5.1.

comment is still valid, see below for further discussion). Indeed, data from the AJAX cruises in 1983/1984 (Weiss *et al.*, 1990) tend to confirm this. Figures 5.2(a) and (b) show plots of the implied atmospheric CFC-11/CFC-12 ratio for a meridional (Figure 5.2(a)) and a zonal (Figure 5.2(b)) section from the AJAX data set. In these figures the implied atmospheric CFC-11/CFC-12 ratio is defined as

$$ {}_{a}r_{b} = \frac{[a]_{surf}\, F_b}{[b]_{surf}\, F_a} \equiv \frac{p_a}{p_b} \equiv \frac{\xi_a [a]_{atm}}{\xi_b [b]_{atm}} \qquad 5.1.1a $$

where square brackets are concentrations, F is solubility, ξ is saturation and p dissolved partial pressure. This is the ratio which is used to calculate the fluid ventilation age as explained in Section 4.3.2. It is compared to the atmospheric ratio $\frac{[a]_{atm}}{[b]_{atm}}$, represented by the dashed lines in Figure 5.2. These two quantities are equal if $\xi_a = \xi_b$, as Equation 5.1.1a shows. In this case a and b refer to CFC-11 and CFC-12 respectively, although Equation 5.1.1a yields

$$ {}_{a}r_{b} \approx \frac{[a]_{surf}}{[b]_{surf}\, {}_{a}X_{b}} \qquad 5.1.1b $$

by use of Equations 4.3.1 and 4.3.3 which must be used when a represents CFC-113, since F_{113} is currently unknown.

Both Figures 5.2(a) and (b) demonstrate the significant departure from the assumed state of equal saturation, also suggested by the VIVALDI and ARANDA data of Figure 5.1. The observed variation in surface ${}_{11}r_{12}$ values is 2.8 and 3.3 times the respective analytical uncertainties in this quantity for these expeditions. Moreover, Figure 5.1 shows that the mean ${}_{11}r_{12}$ is not equal to the atmospheric value; it is significantly higher (the locus $\xi_{11} = \xi_{12}$ lies above the cluster of data points). Warner's (1988) data shows this bias too, although it is less pronounced and includes surface samples from many different oceanic regimes (see his Figure 3.2).

The VIVALDI and AJAX data thus show a discrepancy between the atmospheric ratio and the ratio implied by surface waters for the CFC-11 and CFC-12 pair. The relative variability expressed by ${}_{113}r_{12}$ or ${}_{113}r_{11}$ is expected to be greater than that for ${}_{11}r_{12}$ for several reasons. Firstly the piston velocity of CFC-113 is likely to be lower than that of either CFC-11 or CFC-12 since it is a substituted ethane molecule rather than a methane derivative (see Section 5.3 for estimates of piston velocities). This decreases the rate of transfer of CFC-113 across the air/sea interface with respect to either CFC-11 or CFC-12, and consequently reduces the value of ${}_{113}r_{12}$ or ${}_{113}r_{11}$ when saturation equilibrium is not reached. Secondly, fluid entrained each winter into the mixed layer has ${}_{113}r_{12}$ and ${}_{113}r_{11}$ values which are lower than the current atmospheric ratios since it has been out of contact with the atmosphere. Although the mixing of ratios, ${}_{a}r_{b}$, is complicated and non-conservative, it can only serve to reduce the ratio in the mixed layer in this case. This however, is not so for ${}_{11}r_{12}$ since the CFC-11/CFC-12 ratio in the

Figure 5.2. Implied atmospheric CFC-11/CFC-12 ratio ($_{11}r_{12}$, see Equation 5.1.1a) for (a) section north/south along the Prime Meridian (AJAX stations #1-52 and #65-93), and (b) section east/west at 60°S through the Weddel Sea (AJAX stations #96-137) in the austral summer of 1983/1984 (Weiss *et al.*, 1990). The dashed lines in each diagram are the ambient atmospheric ratios as observed during the cruises. The solid lines represent one standard deviation in the value of $_{11}r_{12}$ as reported by Warner (1988).

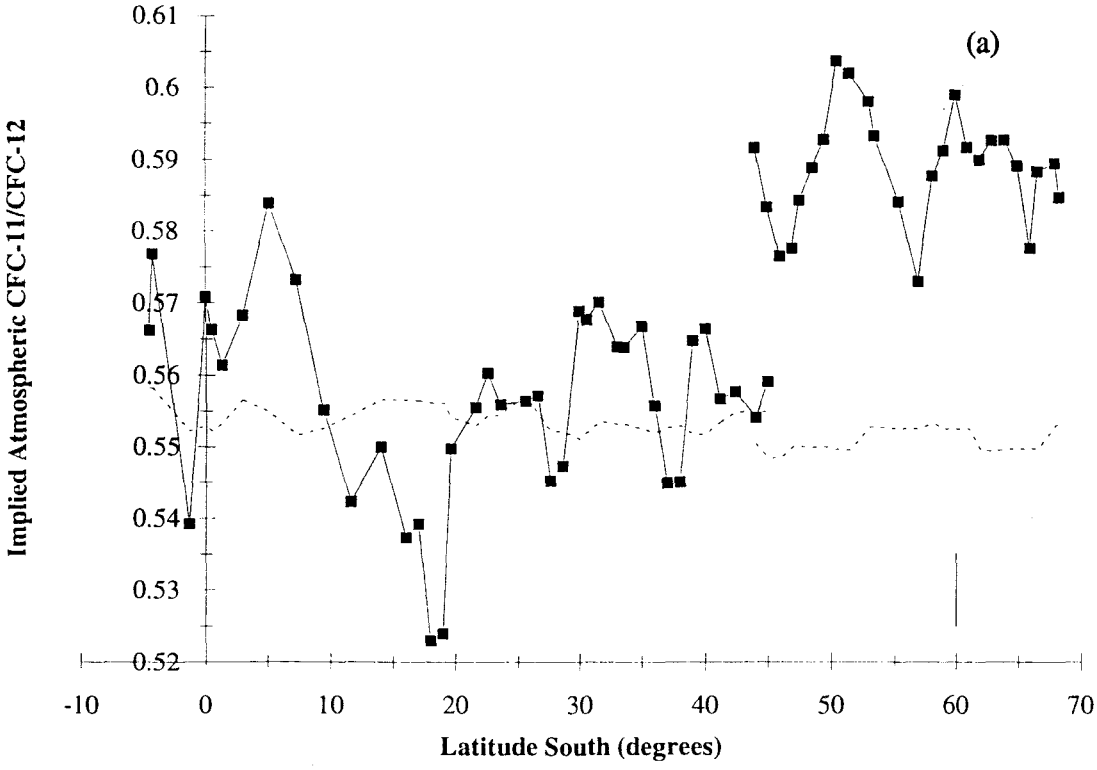
(a)
Implied Atmospheric CFC-11/CFC-12
0.61
0.6
0.59
0.58
0.57
0.56
0.55
0.54
0.53
0.52
-10
0
10
20
30
40
50
60
70
Latitude South (degrees)

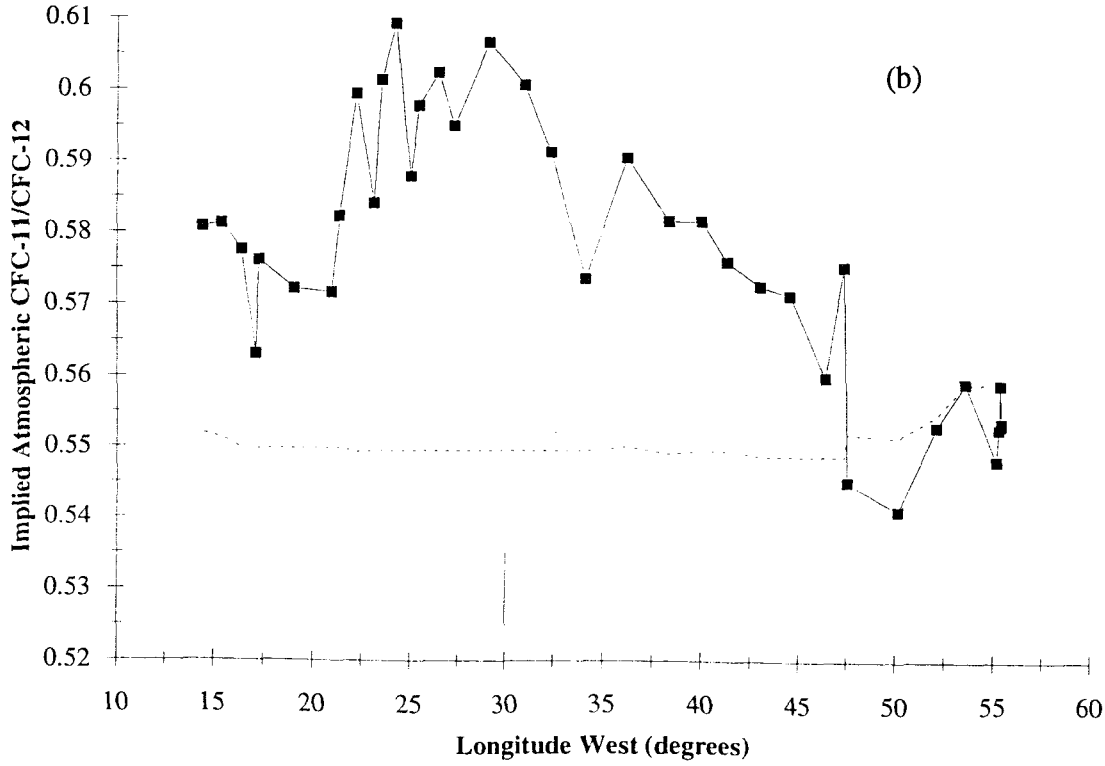
(b)
Implied Atmospheric CFC-11/CFC-12
0.61
0.6
0.59
0.58
0.57
0.56
0.55
0.54
0.53
0.52
10
15
20
25
30
35
40
45
50
55
60
Longitude West (degrees)

atmosphere has not changed in the period 1975-1992, and thus the underlying fluid will have a ratio which is not systematically depressed in the way described for $_{113}r_{12}$ or $_{113}r_{11}$. Finally, the rate of atmospheric increase for CFC-113 is greater than that for either CFC-11 or CFC-12. This also tends to mean that CFC-113 is further from equilibrium because the timescale for atmospheric equilibration is closer to the timescale for atmospheric increase for CFC-113 than for either CFC-11 or CFC-12 (this mechanism is discussed in more detail in Section 5.2).

As Figure 5.1 shows, $\xi_{11} > \xi_{12}$ in general, and hence the derived $_{11}X_{12}$ is greater than the true ratio of solubilities (see Section 4.3.2). Indeed, the calculated values of $_{11}X_{12}$ based on Equation 4.3.1 are 3.85 and 3.67 for the ARANDA and VIVALDI cruises, compared to values estimated in the manner of Equation 4.3.3 of 4.9 and 4.3 respectively (Table 4.3).

It is worthwhile to outline a comparison between CFC tracers and another established transient tracer pair; anthropogenic tritium and helium-3 (^{3}He). Fuchs *et al.* (1987) in particular, examine the excess ^{3}He in the upper ocean and deduce a corresponding initial tritium/helium age which is non-zero. (See Section 1.5 and the work of Jenkins (1980), for example, for a discussion of the details of this transient tracer pair.) Of particular relevance to the present context is Fuchs *et al.*'s (1987) comment "Ventilation implies aeration of the water, but apparently even ^{3}He, the gas with the highest ocean-atmosphere equilibration rates of all, falls short of attaining a full ocean-atmosphere equilibrium". The similarities between tritium/helium and CFC tracers are pursued further in Chapter 6.

5.2. Analytical Model of Tracer Invasion.

As a first step in understanding the ocean response to a transient atmospheric tracer, consider invasion into a layer of homogeneous fluid with constant depth. There is exchange as described in Section 1.3.2, between the atmosphere and ocean, of concentrations C_{atm} and C respectively. This exchange is driven by the air/sea gradient in concentration, with a characteristic transfer coefficient (piston velocity) k, and so,

$$h \frac{dC}{dt} = k [C_{atm} F - C] \qquad 5.2.1$$

with depth h, and F defining solubility. Non-dimensionalising the time variable, t, with t^* such that,

$$t^* = \frac{t k}{h} \qquad 5.2.2$$

and scaling the oceanic concentration by the solubility F (i.e using partial pressures for the ocean concentration) gives

$$\frac{dC^*}{dt^*} = C_{atm} - C^* \qquad 5.2.3.$$

The solution of Equation 5.2.3 is straightforwardly given by

$$C^* \exp\{t^*\} = \int_0^{t^*} C_{atm} \exp\{\gamma\}\, d\gamma \qquad 5.2.4$$

(γ is the dummy variable of integration). Table 5.1 lists a few simple functions C_{atm}, and the solutions to Equation 5.2.3 for the ocean concentration, C^*. Combining two of these functions allows us to examine the behaviour of a pair of tracers sequestered into the fluid layer, and so form the ratio in this layer, corresponding to the age of the surface ocean. Taking the quotient of two concentration variables gives one a value of the ratio which is directly analogous to that defined in Equation 5.1.1a, since the factors of solubility are already accounted for. For example, let us model two CFC-like tracers by exponential rises of the form $A\left[\exp\left\{\frac{t^*}{\delta}\right\} - 1\right] : \delta > 0$, with different rates for each species. The symbol δ is the ratio of timescales for atmospheric increase to the fast fluid response, and in general $\delta >> 0$. Initially assume that $k_1 = k_2$; the gases exchange equally easily. The fluid ratio is then,

$$\frac{C_1^*}{C_2^*} = \frac{A_1\left[\frac{\delta_1}{\delta_1 + 1}\left(\exp\left\{\frac{t^*}{\delta_1}\right\} - \exp\{-t^*\}\right) - 1 + \exp\{-t^*\}\right]}{A_2\left[\frac{\delta_2}{\delta_2 + 1}\left(\exp\left\{\frac{t^*}{\delta_2}\right\} - \exp\{-t^*\}\right) - 1 + \exp\{-t^*\}\right]} \qquad 5.2.5$$

with which we wish to compare the atmospheric ratio,

$$\frac{C_{atm1}^*}{C_{atm2}^*} = \frac{A_1\left[\exp\left\{\frac{t^*}{\delta_1}\right\} - 1\right]}{A_2\left[\exp\left\{\frac{t^*}{\delta_2}\right\} - 1\right]} \qquad 5.2.6.$$

For dimensional time scales which are large compared to the response time of the fluid (say $t^* > 5$) we can simplify Equation 5.2.5 to

$$\frac{C_1^*}{C_2^*} \approx \frac{A_1\left[\frac{\delta_1}{\delta_1 + 1}\exp\left\{\frac{t^*}{\delta_1}\right\} - 1\right]}{A_2\left[\frac{\delta_2}{\delta_2 + 1}\exp\left\{\frac{t^*}{\delta_2}\right\} - 1\right]} \qquad 5.2.7.$$

Table 5.1. Some simple functions, C_{atm}, and the corresponding solutions to Equation 5.2.3, evaluated by Equation 5.2.4.

C_{atm}	C^*
α	$\alpha\ [1 - \exp\{-t^*\}]$
$\beta\ t^*$	$\beta\ [t^* - 1 + \exp\{-t^*\}]$
$\gamma\ t^{*2}$	$\gamma\ [t^{*2} - 2\ (t^* - 1 + \exp\{-t^*\})]$
$A\left[\exp\left\{\frac{t^*}{\delta}\right\} - 1\right] : \delta > 0$	$A\left[\frac{\delta}{\delta + 1}\left(\exp\left\{\frac{t^*}{\delta}\right\} - \exp\{-t^*\}\right) - 1 + \exp\{-t^*\}\right]$

Equation 5.2.7 shows that the rates of increase of atmospheric concentration of the tracer pair can influence the surface ratio (and hence the surface age), even when the two tracers exchange at the same rate. Choosing $k_1 = k_2 \approx 1$m/day, $h \approx 100$m gives the timescale for fast response of the fluid layer as 100 days. If we also have $\delta_1 \approx 25$, and $\delta_2 \approx 50$, then the fluid ratio is about 1.4% smaller (older in this example) than the atmospheric value at time $t^* = 50$ (about 16 years). Although these particular values do not correspond to a specific CFC tracer pair, they are included for comparison with the results reported below. Figure 5.3(a) shows a plot of the ratio of $\frac{C_1^*}{C_2^*}$ to $\frac{C_{atm1}^*}{C_{atm2}^*}$ against $\frac{\delta_1}{\delta_2}$.

In general, however, $k_1 \neq k_2$ and thus there is no longer a single characteristic timescale t^*, in which case the fluid ratio is given by,

$$\frac{C_1^*}{C_2^*} = \frac{A_1\left[\frac{\delta_1}{\delta_1 + 1}\left(\exp\left\{\frac{k1\ t^*}{k2\ \delta_1}\right\} - \exp\left\{-\frac{k1\ t^*}{k2}\right\}\right) - 1 + \exp\left\{-\frac{k1\ t^*}{k2}\right\}\right]}{A_2\left[\frac{\delta_2}{\delta_2 + 1}\left(\exp\left\{\frac{t^*}{\delta_2}\right\} - \exp\{-t^*\}\right) - 1 + \exp\{-t^*\}\right]} \qquad 5.2.8$$

where the characteristic time is chosen such that,

$$t^* = \frac{k_2\ t}{h} \qquad 5.2.9.$$

The analogous version of Equation 5.2.7 in this example, when t^* is large, and $k_1 \approx k_2$ is,

Figure 5.3. Plots from the simple analytical mixed layer model of Section 5.2. Quotient of mixed layer tracer ratio with atmospheric tracer ratio versus, (a) δ_1/δ_2, and (b) k_1/k_2. In (a) $k_1 = k_2$ and in (b) $\delta_1 = \delta_2$. In both figures $t^* = 50$.

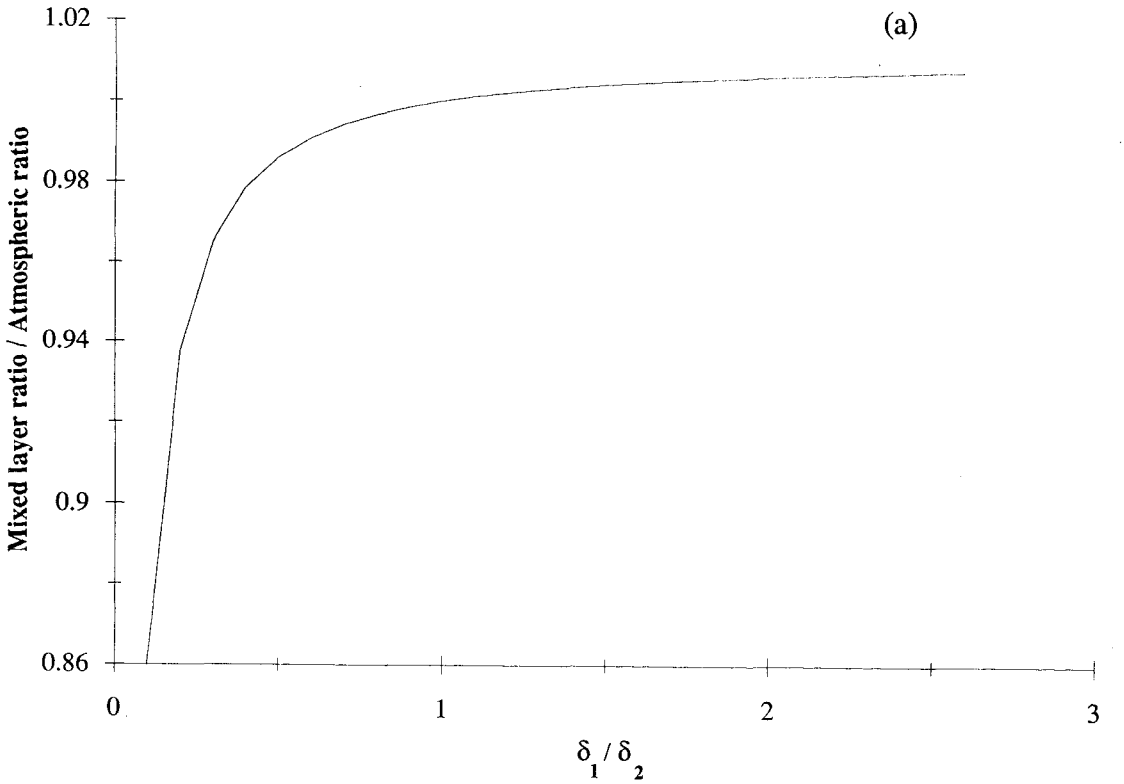
(a)
1.02
0.98
0.94
0.9
0.86
Mixed layer ratio / Atmospheric ratio
0
1
2
3
δ1 / δ2

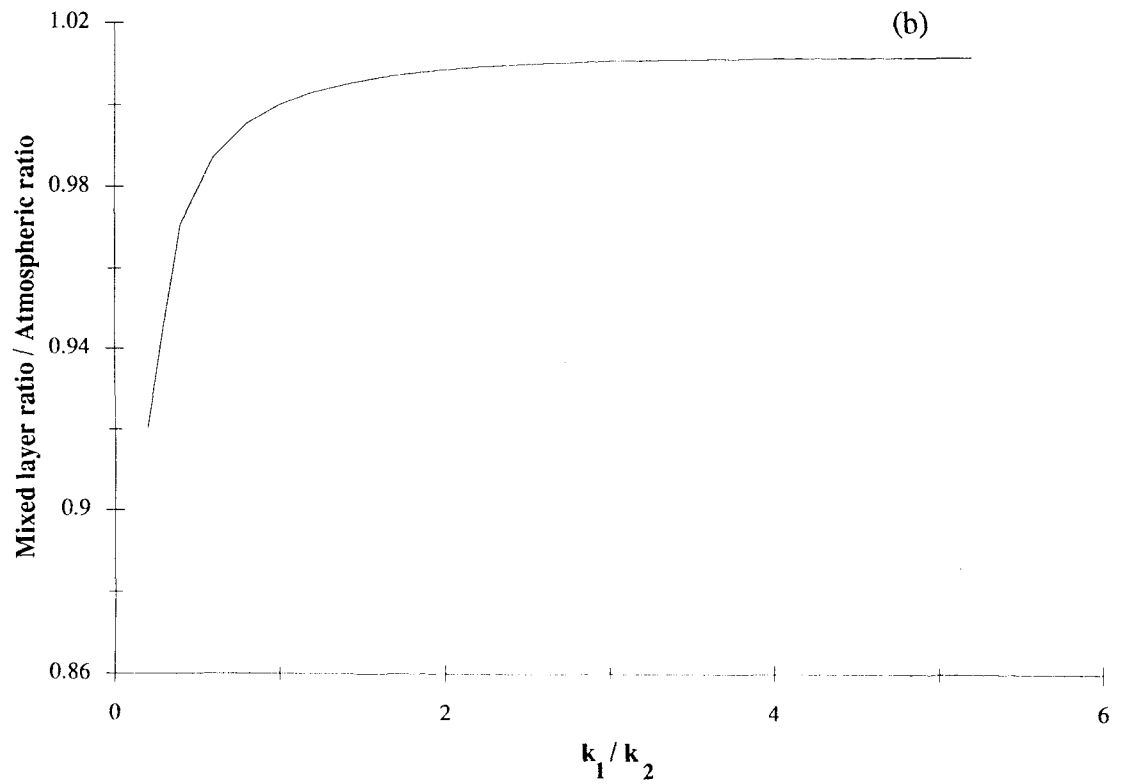
(b)
1.02
0.98
0.94
0.9
0.86
Mixed layer ratio / Atmospheric ratio
0
2
4
6
k1 / k2

$$\frac{C_1^*}{C_2^*} = \frac{A_1\left[\frac{\delta_1}{\delta_1 + 1}\exp\left\{\frac{t^*}{\delta_1}\right\} - 1\right]}{A_2\left[\frac{\delta_2}{\delta_2 + 1}\exp\left\{\frac{k_2\, t^*}{k_1\, \delta_2}\right\} - 1\right]} \qquad 5.2.10.$$

Using this expression, with the parameters given above except k_1 = 0.6m/day, k_2 = 1m/day, gives a fluid ratio about 2.7% smaller than the atmospheric value. These values are appropriate for CFC-113/CFC-12 and correspond to a fluid ventilation age of 0.5 years. Putting k_1 = 0.8m/day, k_2 = 1m/day, and $\delta_1 = \delta_2 = 50$, gives a fluid ratio 0.5% smaller than the atmospheric value, a reasonable choice for the CFC-11/CFC-12 pair with similar atmospheric timescales and piston velocities. Figure 5.3(b) is a plot of the ratio of $\frac{C_1^*}{C_2^*}$ to $\frac{C_{atm1}^*}{C_{atm2}^*}$ against $\frac{k_1}{k_2}$. Comparison of this figure with Figure 5.3(a) shows that the rates of atmospheric increase and the air/sea exchange are important factors influencing the mixed layer discrepancy.

Obviously the conditions modelled in this analytical example do not prevail in the real ocean. In particular, the depth of the fluid layer, h, and the solubility F are not constant. They vary on many timescales, and can significantly affect the flux of tracer in a few days. There is no simple solution to Equation 5.2.3 for general h(t) and F(t) and so it must be found numerically. This is the problem which Section 5.3 examines.

5.3. Introduction to Mixed Layer Model.

Sections 5.3, 5.4 and 5.5 deal with a physically realistic mixed layer model of the seasonal ocean used in conjunction with an inert tracer model. Section 5.6 attempts to compare the model results with real data. Obviously there is no interaction between the physics or the tracer simulation and distinction is made in the discussion between each component. In this Section the details of the model are introduced (physics, then tracer) and then a typical run is discussed. Finally, the point in the seasonal cycle most important for the CFC boundary condition is identified; it turns out to be when the tracer is furthest from equilibrium. Throughout the rest of this chapter 'thermocline' should be regarded as synonymous with 'pycnocline'; no explicit salinity forcing is considered.

More realistic models are required to investigate the effect of seasonality on the oceanic uptake of CFCs than the analytical treatment described in Section 5.2. A one dimensional slab mixed layer model as described by Kraus & Turner (1967) is suitable for this purpose (see the papers of Niiler (1977) and Niiler & Kraus (1977) for reviews). This sort of model parameterises turbulence in the upper ocean by postulating a well mixed layer, homogeneous in its characteristics. The temperature and depth of this slab are diagnosed by consideration of the interfacial fluxes of buoyancy and mechanical

stirring energy. No physical processes are simulated in the fluid beneath the mixed layer. A model of this type was used in the experiments described in the remainder of this Chapter (W Barkmann provided the code). The model resolves diurnal and seasonal changes in the upper ocean with a realistic solar absorption model (Woods *et al.*, 1984). Buoyancy fluxes through the surface affect the stability of the water column and when appropriate a convective adjustment is made in order to recover a marginally stable layer. Mechanical stirring is achieved by the wind in a way that decreases exponentially with depth. This particular Kraus Turner model has been used extensively before in the publications of Woods & Strass (1986), Woods & Barkmann (1986a, b), and Woods *et al.*, 1984. A turbulence closure model is considered unnecessarily complicated for the purpose of oceanic tracer invasion, and use of an upper ocean time series (derived from either real data or a more sophisticated model) is also deemed inappropriate. The slab model employed is flexible in the range of upper ocean environments represented, whilst being computationally efficient enough to allow a thorough investigation of the model sensitivity to tracer parameterisations.

Into the physical model is embedded a tracer simulation. The physical model diagnoses the depth of the mixed layer, h, and its temperature, T, from which the instantaneous solubility is derived. The tracer is conserved throughout the model domain with no physical processes represented in the fluid below the mixed layer. With this tracer model there are two critical parameterisations. The first is the variation of piston velocity, k, with windspeed, u, and the second the ease of transfer intrinsic to each species considered, quantified in terms of Schmidt numbers, S_c (Jähne *et al.*, 1987). In particular,

$$k = f(u, S_c^{-1/2}) \qquad 5.3.1$$

where $S_c = \frac{\eta}{D}$, the ratio of kinematic viscosity to molecular diffusivity, is a function of temperature.

The formulae of Liss & Merlivat (1986) are used to derive the piston velocity variation with windspeed, of which the rough regime nearly always applies ($3.6 < u$ (m/s) ≤ 13), and thus for species a,

$$k = (2.85\,u - 9.65)\sqrt{\frac{S_c(CO_2,20^oC)}{S_c(a,T)}} \qquad 5.3.2$$

where $S_c(CO_2,20^oC) = 600$ and $S_c(a,T)$ is taken from Wanninkof's (submitted, 1991) cubic fits for CFC-11 and CFC-12. S_c(CFC-113,T) is unknown, and so the method of Wilke & Chang (1955), adjusted for the revised association factor of water (Hayduk & Laudie, 1974) is used. This bases the molecular diffusivity on the molal volume of the solute and its viscosity. Use of Dupont (Report) data yielded

$$S_c(\text{CFC-113,T}) = 1.16\ S_c(\text{CFC-11,T}) \qquad 5.3.3.$$

The values of the Schmidt numbers at 25°C are 824, 822 and 959 for CFCs 11, 12 and 113 respectively. The solubilities of Warner & Weiss (1985) are used for CFC-11 and CFC-12, and following Equation 4.3.3, with the value of $_{113}X_{11}$ given in Table 4.3 (VIVALDI data), the CFC-113 solubility is derived, although no assumption of equal saturation is made. The results of the mixed layer model are not sensitive to the particular value of solubility chosen as the renormalisation of Equation 5.2.1 to yield Equation 5.2.3 suggests, and so no experiments varying this parameter have been performed.

Figure 5.4 shows a sample run of the mixed layer model where analytical functions are used for wind and buoyancy forcing (windspeed constant, buoyancy annually periodic with near-zero seasonal mean). Generally, monthly mean values of windstress, cloud cover, surface heat and water flux are used to integrate the model, taken from the climatology of Isemer & Hasse (1985), except where specifically stated to the contrary. The mixed layer depth and temperature response is typical of the north east Atlantic, deepening with time (40°N 37°W). A nine year mean loss of 12.5Wm^{-2} causes the steady deepening and cooling of the mixed layer shown in Figure 5.4(a) and (b). Numerical integrations with steps of 1 hour begin on day 81, 1980. Starting at the time of deepest mixing avoids problems with the model physics slowly spinning up, since the seasonal thermocline laid down in the spring of the first model year is a consequence of the forcing alone, with no memory of the previous year. The initial condition for the tracer profiles was one of atmospheric equilibrium throughout the mixed layer (hence age = 0) and zero in the fluid below. Although the boundary condition for the abyss is undoubtedly incorrect it has little effect on the age of the mixed layer since both tracers are equally diluted by mixing with the fluid below (Section 5.5 examines the model sensitivity to this initial condition). As the mixed layer deepens annually there is a corresponding increase in the annual maximum surface age (Figure 5.4(c)). Figure 5.4(c) and (d) shows how the tracer field is spun up after ~ 600 days, and most results are taken from around day 2000. Based on a tracer budget the accumulated fractional error after 2356 days of integration is 2.8 and 0.76% for CFC-113 and CFC-12 respectively, corresponding to an excess age of 0.4 years. In a more typical run (maximum annual depth of mixing is 200-300m) these errors are -0.32%, -0.49% and 0.03 years respectively.

The peaks in mixed layer age shown in Figure 5.4(d) are significant because it is fluid with this characteristic which is left at depth as the mixed layer shallows in spring. For those areas of the ocean where the maximum depth of mixing the following year is shallower, some of this fluid will be too deep to be entrained in the mixed layer next winter. (See Nurser & Marshall, 1991; Marshall & Nurser, 1992; Marshall *et al.*, 1992; Woods & Barkmann, 1986a; and Woods, 1985, for a discussion of this mechanism. The latter two citations show that mode water formation depends more on the decreasing depth of winter convection than on Ekman pumping.) The peaks in age in Figure 5.4(d),

Figure 5.4. Typical mixed layer model run, showing,

(a) mixed layer depth (m),

(upper,lower) ⇔ (minimum,maximum) diurnal depth,

(b) mixed layer temperature (^{o}C),

(c) mixed layer tracer saturations (dimensionless; 1.0 = equilibrium saturation),

(upper,lower) ⇔ (CFC-12,CFC-113),

(d) mixed layer CFC-113/CFC-12 ventilation age (years) and

(e) buoyancy fluxes (Wm^{-2}),

(upper,middle,lower) ⇔ (noon solar radiation,net interfacial,total oceanic heat loss).

The total oceanic heat loss consists of sensible heat, latent heat and longwave radiation. In this integration the windspeed was constant at $10ms^{-1}$, with seasonal changes of the length of day simulated for 40^{o}N, 37^{o}W. There is a net, 9 year mean, heat loss of $12.5Wm^{-2}$.

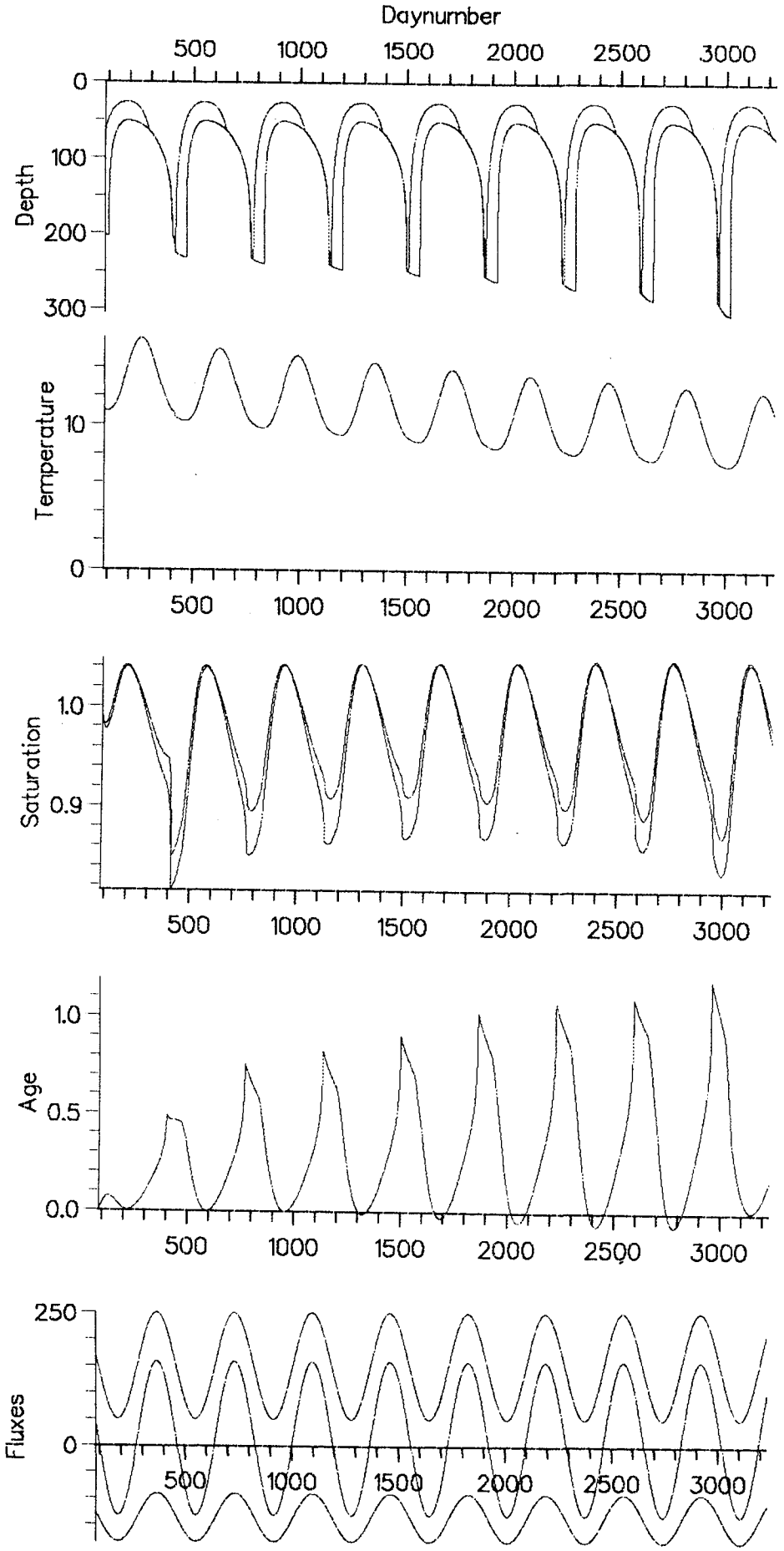
Daynumber
500
1000
1500
2000
2500
3000
0
100
200
300
Depth
(a)
Temperature
10
0
(b)
Saturation
1.0
0.9
(c)
Age
1.0
0.5
0.0
(d)
Fluxes
250
0
(e)

therefore, correspond to the age boundary condition for waters ventilated in this way. The model run shows a period of several weeks each year when the mixed layer depth slowly increases by erosion of the strong stratification beneath (Figure 5.4(a)). During this period the tracer age decreases as the deep mixed layer is ventilated, although this process does not have time to complete before the mixed layer suddenly shallows in spring (the exchange during this phase is the fast response of Section 5.2). A competition of timescales thus prevails. The initial deepening through the weakly stratified seasonal thermocline is too rapid for the tracer to exchange and so saturation falls and the mixed layer age increases (this, incidently, is also the time of greatest model inaccuracy). There follows a time of slow increase in depth, of entrainment of dense water from below, during which the tracer can exchange fast enough to increase saturation and reduce the mixed layer age. As the net buoyancy forcing changes sign (Figure 5.4(e)) a rapid shallowing of the mixed layer occurs, leaving fluid at depth with non-zero age. Should this fluid travel to a place where the next deepest seasonal mixed layer is shallower, then some of it will not be re-entrained and can thus be considered to have formed part of the permanent thermocline. Section 5.6 returns to the subject of seasonal cycles, with specific reference to the saturation conditions.

5.4. Sensitivity to Model Tracer Parameterisations.

This section reports the results of three sensitivity studies. In each of these the characteristic tracer quantity used for comparison is the mixed layer age, taken at the time of deepest mixing (following comments in Section 5.3). Firstly the sensitivity to tracer piston velocity is examined, and secondly to the windspeed parameterisation of piston velocity. Finally the effect of the maximum depth of annual mixing is investigated.

To gauge the model sensitivity to the parameterised tracer exchange at the air/sea boundary the Schmidt numbers, S_{c1} and S_{c2}, are systematically varied from their best guess values reported in Section 5.3. No sensitivity analysis on the Schmidt number temperature dependence is performed, and so the Schmidt number for each tracer is simply multiplied by a 'Schmidt number multiplier'. Figure 5.5 is a contour plot derived from 18 model runs with identical physical forcing functions (constant windspeed and annually periodic buoyancy fluxes). It shows a smooth variation between -0.2 and 1.6 years with the values of the perturbed Schmidt numbers. The tracer pair notionally considered is CFC-113 and CFC-12, although the results are not expected to vary considerably if CFC-11 is used as the other species paired with CFC-113 (see Section 5.6). The same data is used to examine the behaviour to windspeed parameterisation by modifying both k_1 and k_2 by a constant multiplier (Figure 5.6(a)). Again there is a smooth variation between 0.4 and 1.3 years; higher 'piston velocity multipliers' correspond to more rapid exchange than expected by Liss & Merlivat's (1986) formulae, and yield smaller values of maximum annual mixed layer age. So, to the extent that the parameterisation of Equation 5.3.1 applies, there exists a well defined f, albeit uncertain.

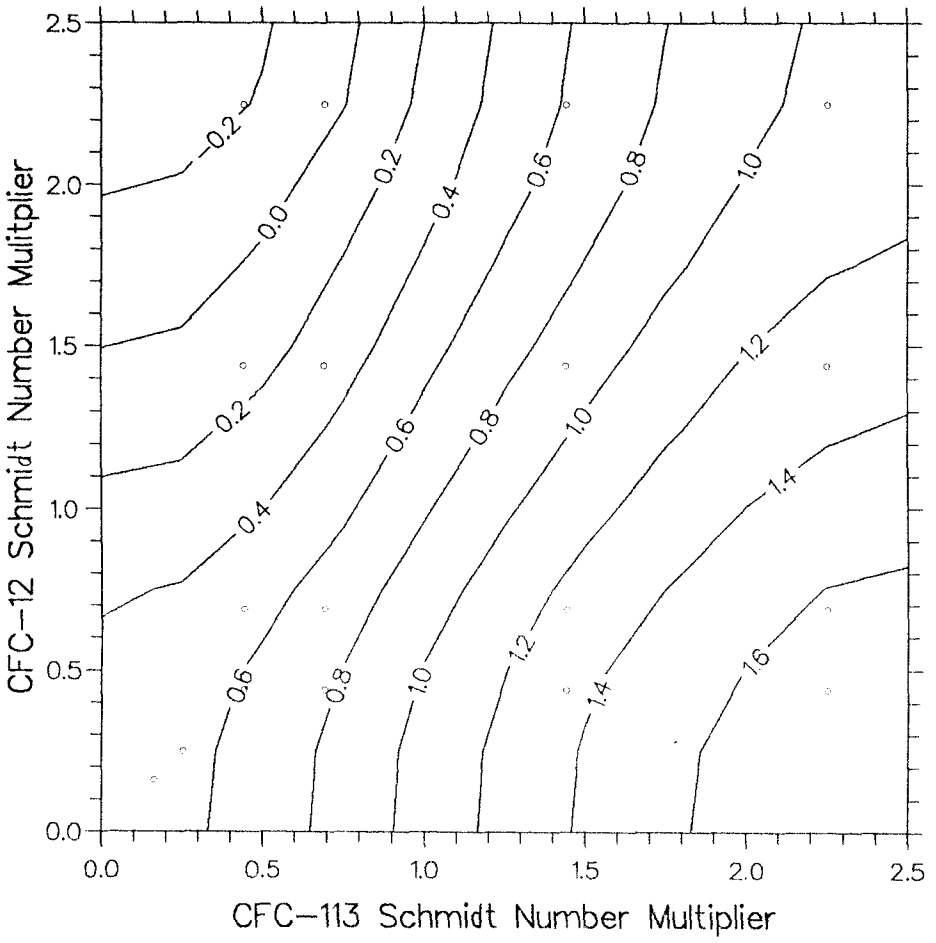

Figure 5.5. Contour plot of the maximum CFC-113/CFC-12 mixed layer age (years) as a function of Schmidt number multipliers (see Section 5.4). Model physics is identical for each run with the age taken after 5 years of integration for an annually repeating cycle of mixing to 206m.

A plausible range for uncertainty in the Schmidt numbers and in the windspeed parameterisation is ± 50%. Figures 5.5 and 5.6(a) show the corresponding uncertainty in the mixed layer age is of order a few tenths of a year.

Figure 5.6(b) shows the results of a series of model runs where the buoyancy forcing was varied in an attempt to assess the influence of the depth of maximum annual mixing on the maximum mixed layer age. As the arguments of Section 5.3 suggest, the mixed layer age depends in a sensitive way on the mixed layer history. Consequently, it is difficult to choose a new maximum depth of mixing by simply adjusting the buoyancy forcing, without also altering the shape of the mixed layer versus time curve. This is the reason that the data of Figure 5.6(b) do not lie as close to the fitted function as do those of Figure 5.6(a), for example. Nevertheless, the plot shows that in this simulation, for reasonably realistic annual mixed layer cycles, the CFC-113/CFC-12 age departs from the condition of age = 0 by 0.5-2.5 years at the time of ventilation. Deeper mixed layers have older CFC ventilation ages. This is a key point since the depth of maximum annual mixing varies considerably with space in the real ocean. The simple model of Section 5.2 predicts that the mixed layer CFC-113/CFC-12 age for a 100m deep slab is of order 0.5 years, and this is comparable to the results of the more realistic seasonal model, shown in Figure 5.6(b). This suggests that, as far as the tracer is concerned, seasonality has little influence for mixed layers which do not deepen seasonally by more than 100m.

These three sensitivity studies indicate that the current Haney parameterisation of tracer exchange is adequate (Equations 5.3.1 and 5.3.2). This is because the mixed layer age uncertainties caused by perturbing the exchange parameterisation are considerably smaller than those as a result of the variation of the depth of maximum annual mixing.

As an aside it is worth comparing the data shown in Figure 5.6(b) with a plot of modelled tritium/helium ages against convection depth reported by Fuchs *et al.* (1987; their Figure 7). These authors used a different model to simulate the effect of seasonality on the surface value of tritium/helium age. Their predicted response of surface tritium/helium age to maximum annual convection depth is a comparable curve to that of Figure 5.6(b), but with values for the mixed layer age approximately half of those for the CFC-113 ventilation age. Fuchs *et al.* (1987) argue that neither diapycnal mixing nor realistic Ekman pumping velocities contribute significantly to the mixed layer budget of ^{3}He in comparison to the seasonal exchange of fluid as a result of mixed layer migrations. The first two of these mechanisms are not included in the mixed layer model formulation described in this chapter, and the results of Fuchs *et al.* (1987) suggest that this simplification is reasonable.

Figure 5.6. (a) Graph of the maximum annual mixed layer age (years) versus piston velocity multiplier, showing the dependence of surface age on windspeed parametisation. These data are taken from some of the runs in Figure 5.5, for which the Schmidt number multipliers are equal. Note that piston velocity, k, and Schmidt number, S_c, are related such that $k \sim S_c^{-1/2}$. (b) Graph of maximum annual mixed layer age (years) versus depth of maximum annual mixing (m). Fitted curves in both figures are quadratic.

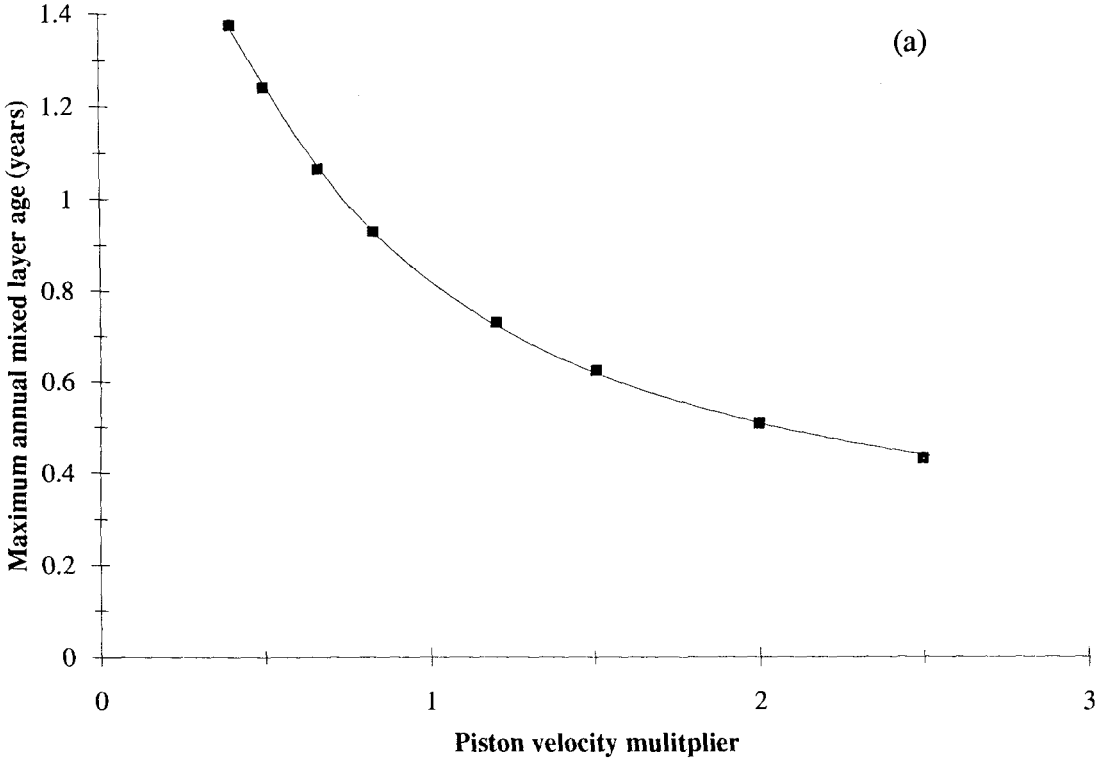
(a)
Maximum annual mixed layer age (years)
1.4
1.2
1
0.8
0.6
0.4
0.2
0
0
1
2
3
Piston velocity mulitplier

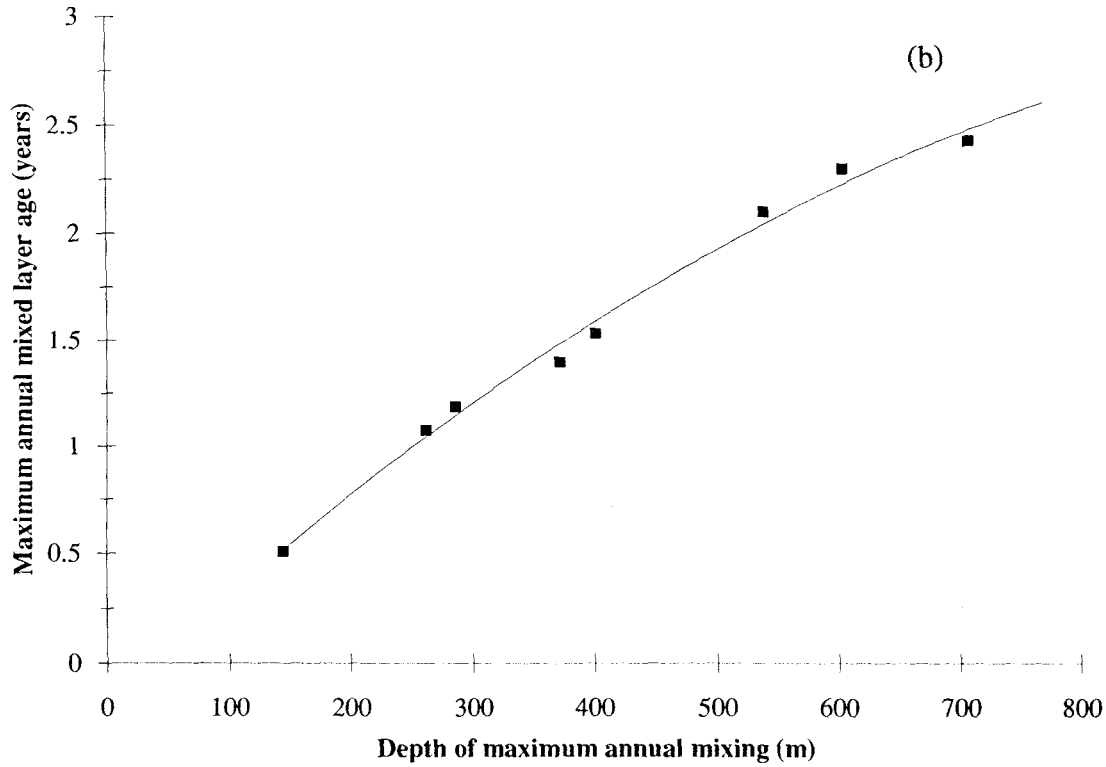
(b)
Maximum annual mixed layer age (years)
3
2.5
2
1.5
1
0.5
0
0
100
200
300
400
500
600
700
800
Depth of maximum annual mixing (m)

5.5. Model Sensitivity to Initial Conditions. Lagrangian Simulations.

This section examines the initial tracer condition for the permanent thermocline by using Lagrangian integrations of the mixed layer model (Woods & Barkmann, 1986a). Obviously there is no unambiguous initial condition for this domain of the model, which in general requires a three dimensional simulation, well beyond the scope of the present context. Initially the results of a Lagrangian run are presented where the mixed layer depth decreases annually, and some general comments are made. Following this are the results of two Lagrangian integrations where the mixed layer depth increases annually, then decreases. These are used to assess the effect of the initial tracer condition of the permanent thermocline on the CFC boundary condition.

Figure 5.7 shows a contour plot of ventilation age for a Lagrangian integration of the mixed layer model following a conceived path which travels south through the VIVALDI region (details of the physical forcing are unnecessary in the present context; the March mixed layer depth varies between about 500-150m in a North-South fashion based on evidence from several sources in the Kiel atlas (Woods, 1987)). Mixing to ~450m for five years allows the tracer fields to spin up properly, before there is a net oceanic heat gain and the depth of maximum annual mixing decreases for four successive years. Because the deep part of the seasonal thermocline is so weakly stratified the depth of maximum mixing around day 2250 strongly depends on the exact value of the net oceanic heat gain in the year before. Indeed, as this quantity tends to zero the maximum mixed layer depth, and consequently the volume of fluid ventilated that year, changes rapidly. (For the runs in Figures 5.5, and 5.6, there is a very small net, annual, oceanic heat loss, ensuring that the seasonal maximum depth increases very slightly each year.) Therefore the lengths of time of each phase in the annual cycle, the variation from year to year and hence the boundary condition for tracer entering the permanent thermocline, depend critically on the buoyancy forcing and the local background stratification. This is an important point because it admits the possibility that slight inter-annual variability in the buoyancy forcing can have a large impact on the tracer boundary condition.

For all the runs considered so far the initial condition for fluid in the main thermocline has had little influence. This is because these integrations simulate depths of maximum annual mixing which do not increase substantially during the run, i.e. very little of the fluid from the main thermocline is ever entrained into the mixed layer. This will not be the case, however, when a run has a considerable annual increase in the depth of maximum mixing. Figure 5.8 shows data from such a run, where the deepest mixing depth increases, then shallows after five model years. The initial condition for main thermocline fluid in this simulation is an exponential decrease of concentration with depth from the value of atmospheric equilibrium in the mixed layer. The length scale of this relaxation was chosen to be 150m, after the work of Gammon *et al.* (1982) on a similar

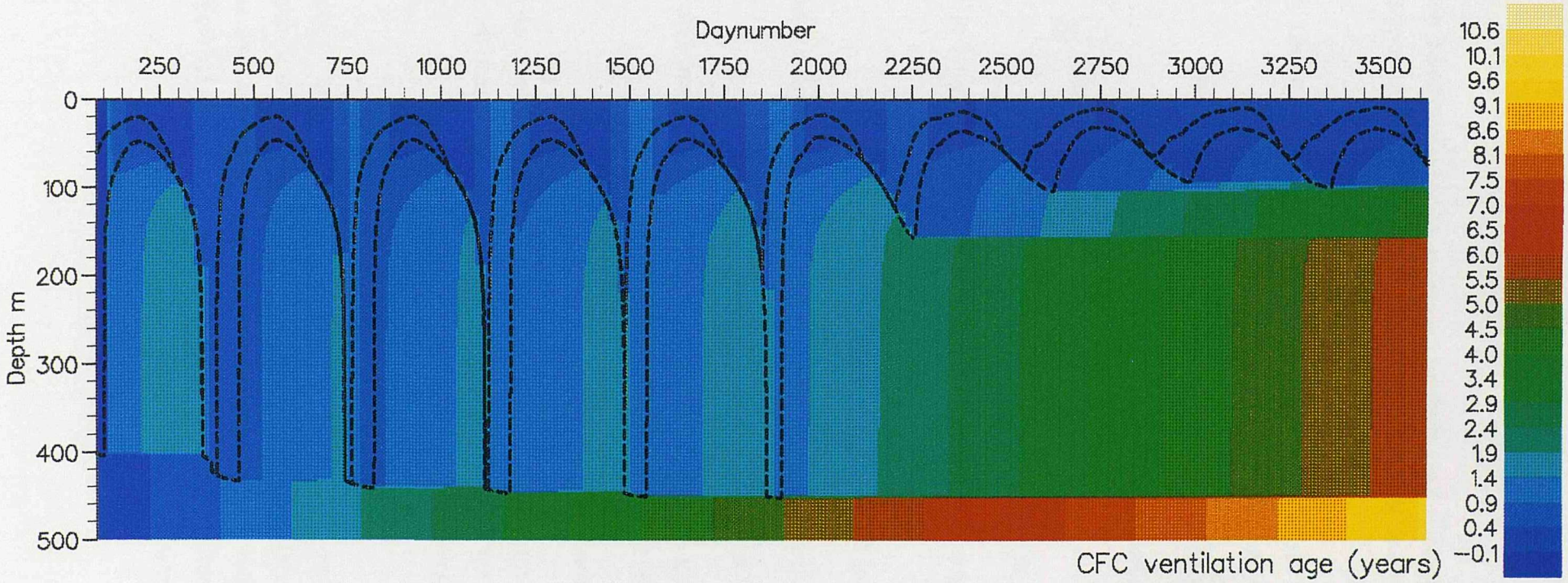

Figure 5.7. Plot of mixed layer depth (upper curve, diurnal minimum; lower curve diurnal maximum) as a function of model daynumber, coloured with CFC-113/CFC-12 ventilation age (years) for a Lagrangian integration of the mixed layer model. The initial condition in the fluid below the mixed layer is an exponential decrease with depth (scale 150m) for each species.

Figure 5.8. Data from a Lagrangian mixed layer model run where the annual depth of maximum mixing deepens, then shallows over the ten year integration.

(a) Plot of mixed layer depth as a function of model daynumber, coloured with CFC-113/CFC-12 ventilation age (years),

(upper,lower) $\Leftrightarrow$ (minimum,maximum) diurnal depth,

(b) mixed layer depth (m),

(upper,lower) $\Leftrightarrow$ (minimum,maximum) diurnal depth,

(c) mixed layer temperature (^{o}C),

(d) mixed layer tracer saturations (dimensionless; 1.0 = equilibrium saturation),

(upper,lower) $\Leftrightarrow$ (CFC-12,CFC-113),

(e) mixed layer CFC-113/CFC-12 ventilation age (years) and

(f) buoyancy fluxes (Wm^{-2}),

(upper,middle,lower) $\Leftrightarrow$ (noon solar radiation,net interfacial,total oceanic heat loss),

(g) windspeed (m/s).

The total oceanic heat loss consists of sensible heat, latent heat and longwave radiation. The initial condition in the fluid beneath the mixed layer is one of exponential decrease with scale 150m (see text).

Figure 5.9 (over). Plot of CFC-113 mixed layer saturation (solid line; no units), CFC-12 saturation (long dashes; no units) and mixed layer age (short dashes; years) differences between model run described in Figure 5.8 and an identical integration, except the initial condition for fluid below the mixed layer is zero concentration for each tracer.

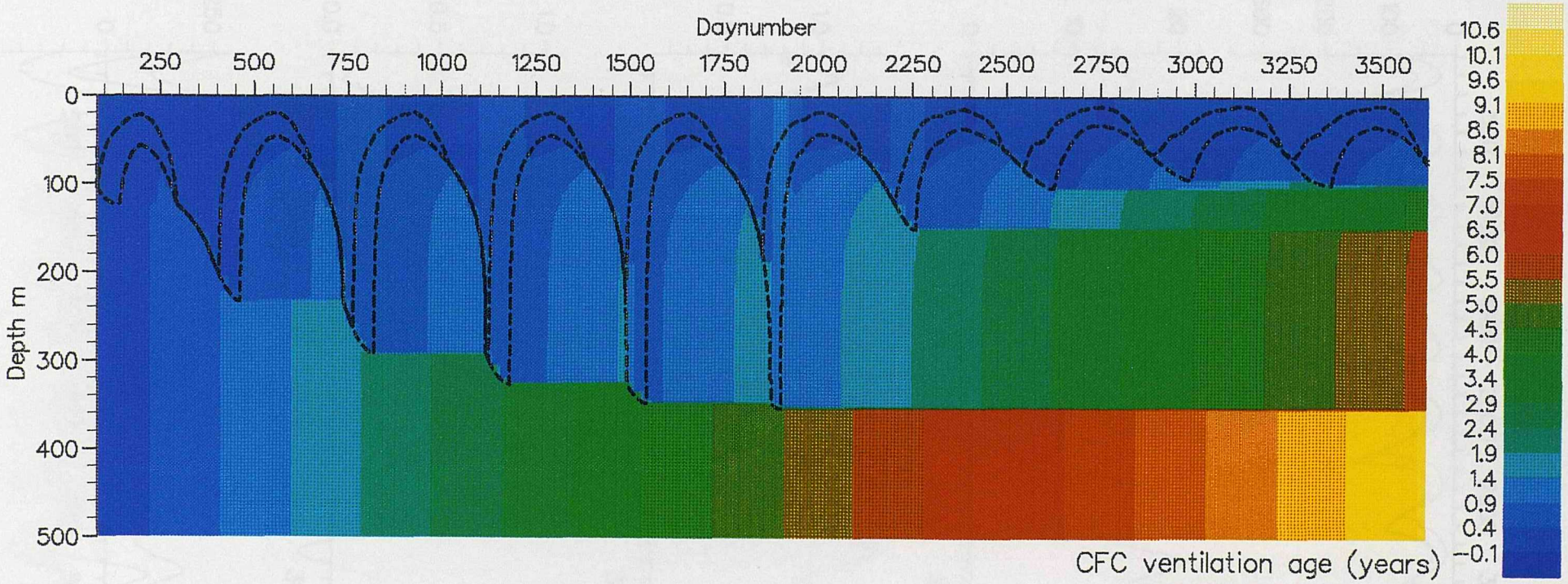
Daynumber
250
500
750
1000
1250
1500
1750
2000
2250
2500
2750
3000
3250
3500
Depth m
0
100
200
300
400
500
CFC ventilation age (years)
10.6
10.1
9.6
9.1
8.6
8.1
7.5
7.0
6.5
6.0
5.5
5.0
4.5
4.0
3.4
2.9
2.4
1.9
1.4
0.9
0.4
−0.1

(a)

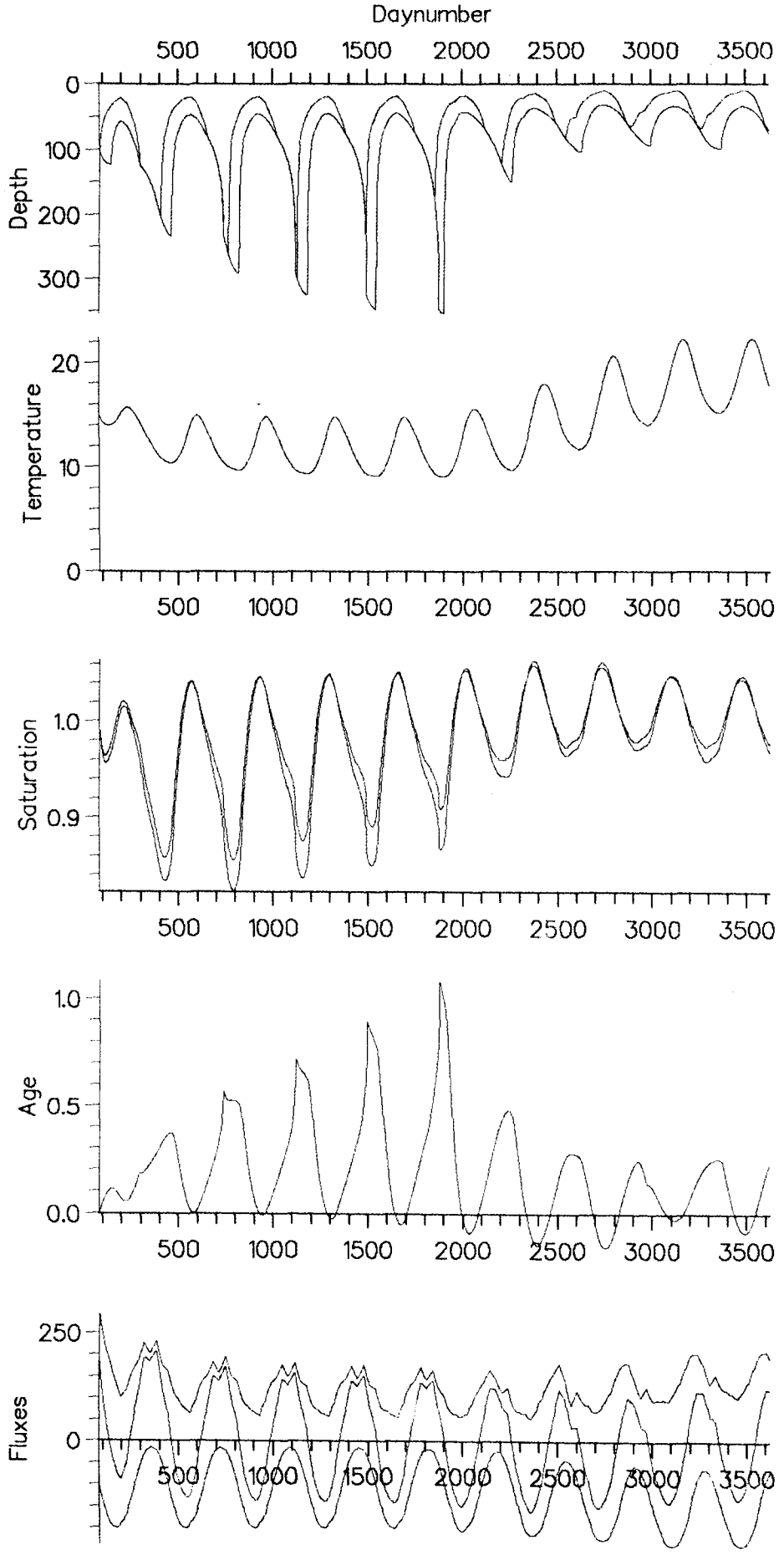
Daynumber
500
1000
1500
2000
2500
3000
3500
Depth
0
100
200
300
Temperature
20
10
0
Saturation
1.0
0.9
Age
1.0
0.5
0.0
Fluxes
250
0

(b)

(c)

(d)

(e)

(f)

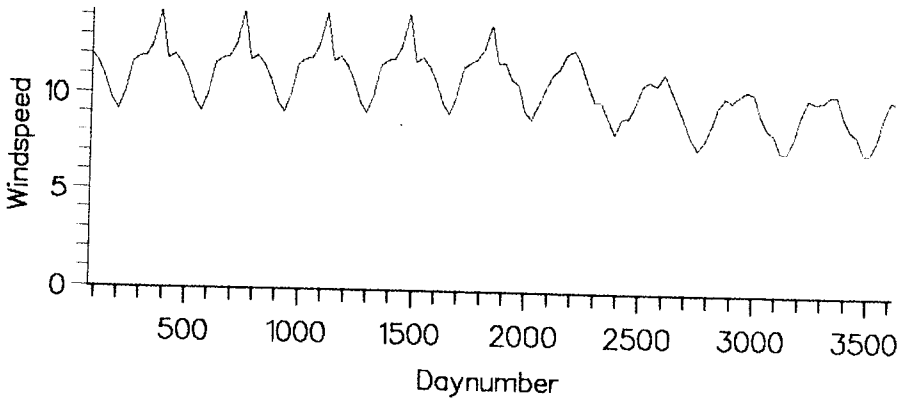
Windspeed
10
5
0
500
1000
1500
2000
2500
3000
3500
Daynumber

(g)

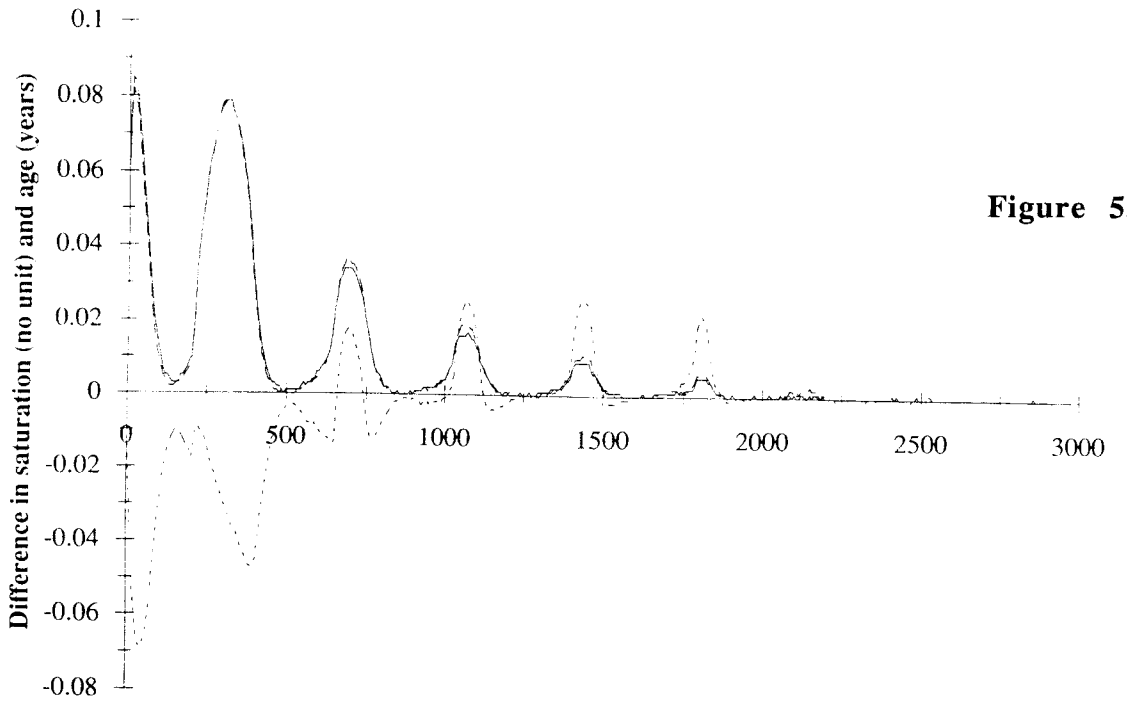
0.1
0.08
0.06
0.04
0.02
0
-0.02
-0.04
-0.06
-0.08
Difference in saturation (no unit) and age (years)
0
500
1000
1500
2000
2500
3000
Daynumber

Figure 5.9.

problem. The initial profile of age through the deep levels is thus age = 0, the same as for the mixed layer, since the decrease in concentration with depth for each species is compensated for in the ratio, and hence in the age. Clearly, mixing with this fluid will influence both age and concentration of the mixed layer in the modelled winters of daynumbers 450, 800, 1150 and 1500 (Figure 5.8(a)). Figure 5.9 compares these results with the CFC-113 and CFC-12 saturations and the mixed layer ventilation age of a similar model run where the initial condition is concentration = 0 throughout the main thermocline. This will leave the mixed layer age unaffected by mixing, since each species is diluted in equal amounts, but will reduce the saturations compared to the model integration of Figure 5.8. Figure 5.9 shows the response of the mixed layer saturations seems to be on a timescale of order 600 days; not significantly different from the tracer spin-up time mentioned in Section 5.3 The model tends to suggest, therefore, that the mixed layer has a 'memory' of order ~ 18 months with respect to mixing with thermocline water below, and the mixed layer tracer characteristics are no longer affected by details of mixing events three or four years previously.

5.6. Comparison of Mixed Layer Model Results with VIVALDI Data.

This section attempts to compare and contrast the results of the mixed layer model described in this chapter with observations made in the field. The most suitable quantity for comparison in this context is tracer saturation. CFC-113 model results are included although no direct comparison can be made for this species since the solubility is currently unknown. An obvious, generic problem exists when one tries to compare a time series with quasi-synoptic data, gathered at different times of the year and places in the ocean. To make this task more straightforward the seasonal cycles of saturation, mixed layer depth and CFC-113 age are described initially.

The data in Figure 5.10 show annual cycles from four simulations with maximum depths of mixing of approximately 200, 400, 600 and 800m (the cycles are offset in Figures 5.10(a) and (b)). In the saturation : saturation plots of Figures 5.10(a) and (b) the annual excursion begins at day 6, which is approximately half way along the lower branch of each cycle in each figure, and at about 0.5 years on the upper branches of each cycle in Figure 5.10(c). (Figure 5.10(c) is a plot of mixed layer depth against mixed layer age for each run.) The mixed layer is rapidly deepening at this stage (see also Figure 5.4(a) from a similar run) and both tracer concentrations are dropping as fluid from the seasonal thermocline is entrained. When this process is complete the CFC-113/CFC-12 mixed layer age is maximum, and the tracer saturations minimum. There follows a period of about 20 days (in these particular simulations) when the strong stratification of the main thermocline is eroded and there is a slow increase in the depth of mixing. This is accompanied by an increase in tracer saturations and a drop in age. When the net buoyancy forcing goes positive there is a very rapid decrease in mixed layer depth with

Figure 5.10. Plots of one annual cycle from four mixed layer model runs with different, annually repeated, depths of maximum mixing. (a) CFC-12 versus CFC-113 mixed layer saturation, (b) CFC-12 versus CFC-11 mixed layer saturation, and (c) mixed layer depth versus mixed layer age. In figures (a) and (b) the CFC-12 data are offset by multiples of 0.05, and in each figure the symbols are separated by 7 days. A saturation of unity (dimensionless) is the equilibrium saturation.

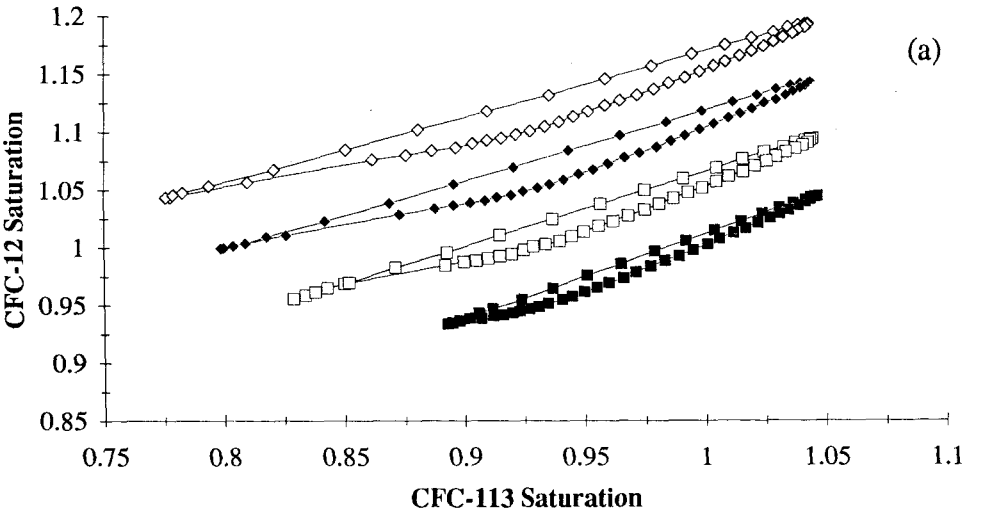
(a)
CFC-12 Saturation
1.2
1.15
1.1
1.05
1
0.95
0.9
0.85
0.75
0.8
0.85
0.9
0.95
1
1.05
1.1
CFC-113 Saturation

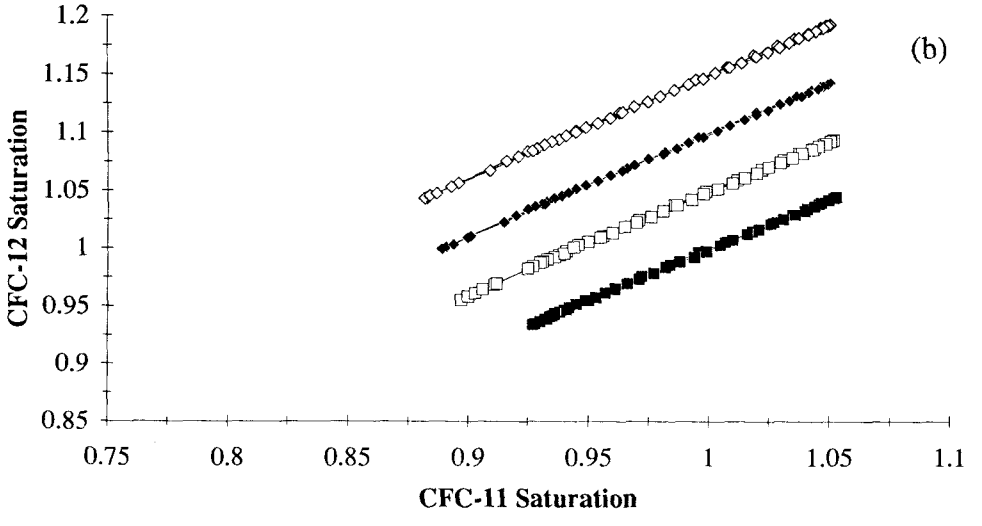
(b)
CFC-12 Saturation
1.2
1.15
1.1
1.05
1
0.95
0.9
0.85
0.75
0.8
0.85
0.9
0.95
1
1.05
1.1
CFC-11 Saturation

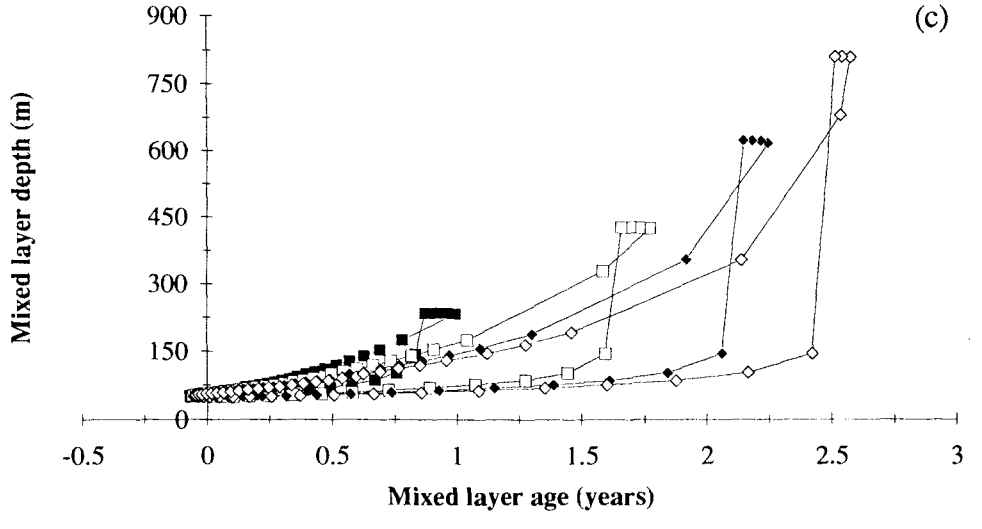
(c)
Mixed layer depth (m)
900
750
600
450
300
150
0
-0.5
0
0.5
1
1.5
2
2.5
3
Mixed layer age (years)

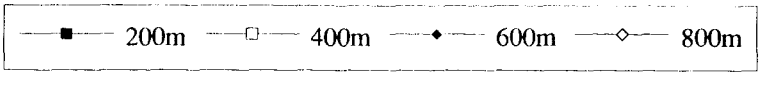
200m
400m
600m
800m

no opportunity for any significant tracer exchange. As spring progresses the mixed layer saturations increase and age decreases, more rapidly than when the layer was deep, until the summer, when ~ 5% super-saturations prevail. Approximately 30-40 days later the minimum age of ~ -0.1 years and then, after another 30 days, the maximum annual temperatures (*cf* Figure 5.4(b)) occur. The autumn is a period of mixed layer deepening; slowly to begin with, then with increasing speed; decreasing tracer saturations and increasing mixed layer age, until the cycle is completed at New Year.

The separation of data points from the locus of equal saturation reflects the condition of non-zero CFC-113/CFC-12 age in the mixed layer (Figure 5.10(a)). However, the corresponding plot for CFC-12 against CFC-11 does not show this to nearly the same extent, mainly as a result of the much smaller difference in Schmidt numbers for these gases (Figure 5.10(b), but also see the comments below). Hence the mixed layer CFC-11/CFC-12 ratio is a reliable atmospheric proxy in these simulations, and if a ventilation age could be formed with these two tracers its value in the mixed layer would be close to zero. Figure 5.10(b) is the basis for assuming that differences in CFC-113/CFC-12 and CFC-113/CFC-11 ages are slight, and throughout this chapter the CFC-113/CFC-12 ventilation age is used.

Model data in Figure 5.10(b) can be compared to observations reported by the workers cited in Section 5.1. The range of absolute values of under-saturation are reasonably well reproduced by the model. One notes that they vary as a consequence of different physical forcing functions, and so a detailed comparison cannot be attempted. However, two important points are revealed by closer examination using the VIVALDI and ARANDA data shown in Figure 5.1 (Figures 5.10(a) and (b) cannot be compared directly with Figure 5.1; Figure 5.10(a) and (b) are seasonal cycles, offset in the y-direction, whilst Figure 5.1 shows quasi-synoptic data from a large region). Firstly the model is not able to reproduce the difference in saturations between CFC-11 and CFC-12. The mean difference in saturations between these species is $14 \pm 10\%$ from the VIVALDI data of Figure 5.1, and the corresponding value calculated from the discrepancies in CFC-11/CFC-12 ratio from Weiss *et al.*'s (1990) data in Figure 5.2(b) is $5 \pm 4\%$. The VIVALDI data were gathered between days 118 and 159, and those from AJAX between austral daynumbers 213 - 228. During the period between daynumbers 118 - 228 the greatest discrepancy in model CFC-11 and CFC-12 saturations is less than 1%, considering all of the runs in Figure 5.10. Moreover, Figure 5.10(a) suggests that merely changing the Schmidt number of CFC-11 or CFC-12 in an attempt to resolve this difference will fail since the modelled saturation of CFC-113 is almost identical to that of CFC-11 around this daynumber. So the model is incapable of simulating the difference in saturations between CFCs 11 and 12. The second feature to note is that the model exhibits a maximum super-saturation of +5% in summer, which is unaffected by change in depth of mixing, or tracer exchange (Figures 5.10(a) and (b)). However, there is no

corresponding upper limit to the observed saturations of CFCs 11 or 12 based on either the VIVALDI data of Figure 5.1, or those studies cited in Section 5.1 which report super-saturations. There is no clear indication of the reason for these model shortcomings, although one may speculate that the solubilities, or temperature dependence of the solubilities and Schmidt numbers, may contribute to this behaviour. It is also possible that a one dimensional, barotropic, model is too simple to faithfully represent this behaviour in the real ocean. Further investigation is considered beyond the scope of the present context.

5.7. Conclusions of Mixed Layer Modelling.

The mixed layer modelling described in this chapter reveals several things with regard to the boundary condition for CFC tracer entering the main oceanic thermocline. A simple analytical model of tracer invasion into a slab of homogeneous fluid suggests that both the rates of atmospheric increase and the rates of tracer exchange are important in biasing the mixed layer tracer ratio. A physically realistic simulation of the upper ocean seasonality with the best estimates of tracer exchange parameters yields saturation estimates for CFCs 11 and 12 which are plausible, at least in their magnitudes. The numerical integrations agree with the simple analytical model for the case of a shallow mixed layer. Model experiments with CFC-113 show a mixed layer ventilation age which varies seasonally. It appears to be weakly dependent on the transfer parameters used with respect to the variation as a result of the maximum annual depth of mixing. This can be up to 2.5 years for a 700-800m deep winter mixed layer, and represents the tracer age boundary condition for the main thermocline. The mixed layer age is very sensitive to the annual details of buoyancy and wind forcing, as well as the ambient density stratification, implying that the CFC saturation and age boundary conditions vary significantly with space and time in the real ocean. Tests with different initial conditions in the deep fluid beneath the mixed layer suggest that, for the mixed layers simulated, information about previous mixing details is lost after three or four years. Although it is very difficult to contrast the model results with field data, there seems to be a systematic discrepancy between the model and observations comparing differences in CFC-11 and CFC-12 saturations in spring, and also in the maximum value of supersaturation.

CHAPTER 6

CFC VENTILATION AGE EVOLUTION.

6.1. Introduction.

Chapter 5 focuses on the boundary condition for CFC tracer entering the main thermocline from the surface ocean. It shows how the seasonal cycle of mixing can significantly affect the concentration and age boundary condition. This chapter is concerned with the behaviour of CFC ventilation age in the ocean away from the surface layers. Initially (Section 6.2), a very simple diagnostic model is described which allows an investigation of ventilation age in a diffusively dominated regime. This provides a basis for analysing the behaviour of CFC-113 age in diffusive flows. Section 6.3 is a derivation of a more accurate and general expression for the evolution of ventilation age with time, which is especially simple in the case of an advectively dominated regime. Appropriate approximations are considered in Section 6.4 by estimating orders of magnitudes for the various terms in the evolution equation using CFC-113 and CFC-12 data from the VIVALDI survey. This material is a corollary of work with the tritium/helium-3 age reported by Jenkins (1980, 1987, 1988) and Roether & Fuchs (1987). Section 6.5 extends this by considering the effects of error propagation, Section 6.6 discusses a generic difficulty with interpreting ventilation age fields by recourse to a simple example with a summary and conclusion in Section 6.7. This chapter explores concepts which underpin the interpretation of ventilation age fields in the ocean interior, although this is not actually attempted until chapter 7.

6.2. Simple Diffusive Mixing Model.

Jenkins (1980) introduces the tritium/helium-3 dating technique by examining a simple box model of oceanic mixing. The model attempts to simulate circumstances where transport of fluid is accomplished by diffusion only. It is a limiting case of the true oceanic evolution, but is reported because it is simply understood, and exhibits features which may well be important in the real ocean. Results from essentially the same model appear here, using CFCs 11, 12 and 113 as the tracers of investigation.

Consider an instantaneously well-mixed volume of water which has a characteristic flushing, or renewal, time T. At regular intervals, Δt, an appropriate amount of tracer-tagged fluid is injected into the volume which has the properties of fully saturated surface ocean water. At time $t + \Delta t$ the concentration, C, of the inert tracer in the well-mixed box is thus,

$$C(t + \Delta t) = \left(1 - \frac{1}{T}\right) C(t) + \frac{C_{atm}(t)\, F}{T} \qquad 6.2.1$$

where F is the solubility of the tracer species (taken as constant), and $C_{atm}(t)$ is the atmospheric source function. And so,

$$C_N = \left(1 - \frac{1}{T}\right)^N C_0 + \frac{F}{T} \sum_{i=0}^{N} C_{atm,i-1} \left(1 - \frac{1}{T}\right)^{N-i} \qquad 6.2.2$$

where the discretisation relates C_n to C(t) by

$$C_n = C(n\Delta t) \qquad 6.2.3$$

and similarly for $C_{atm}(t)$ and $C_{atm,n}$.

By simulating CFCs 11, 12 and 113 in this way the ventilation ages derived from the three ratios CFC-11/CFC-12, CFC-113/CFC-11 and CFC-113/CFC-12 can be examined as functions of t ($\Leftrightarrow$ N) and T. Figure 6.1(a) shows the model concentrations and ventilation ages for T = 8 years, where the calculation commences in 1930. The ventilation ages underestimate T. Figure 6.1(b) is a plot derived from several runs showing how each CFC ventilation age depends on the flushing time T. As Jenkins (1980; his Figure 4) found for tritium/helium-3 the tracer age always underestimates the model age. Indeed, Figure 6.1(b) shows how the ages asymptotically tend to a constant value for large T. One notes that the CFC-11/CFC-12 ratio age is close to this plateau once T is sufficiently large for the age to be unambiguously determined. (The ventilation ages in Figure 6.1(b) are taken from model year 1991.) In this model then, this quantity is a very poor indicator of the fluid age. The CFC-113/CFC-11 and CFC-113/CFC-12 ages are almost indistinguishable and the age difference is of order 10% for T ~ 6.5 years.

This model is a diffusive limit to the more complicated problem of ventilation age behaviour in the ocean. This is because the mixing in the postulated box is complete and instantaneous; in no sense is 'old' fluid segregated from 'young' fluid. Indeed, the definition of the true fluid age is somewhat ambiguous in this regime too, and the true fluid age, T, is an averaged value. That the tracer age plateaus is no surprise as consideration of Equation 6.2.2 readily reveals. Each tracer source function has a characteristic time scale, be it an exponential type (CFCs) or a pulse (tritium/helium-3). If this time scale is long compared with T then the expression in the sum of the right hand side of Equation 6.2.2 will be dominated by the behaviour of the $\left(1 - \frac{1}{T}\right)^{N-i}$ term, which will reduce the influence of the $C_{atm,i-1}$ term on C_N, and so on the tracer age. This corresponds to the region of Figure 6.1(b) for which T < 7 years. If, however, T is larger than the inherent tracer timescale then the $\left(1 - \frac{1}{T}\right)^{N-i}$ term will not diminish in magnitude as rapidly as the value of $C_{atm,i-1}$ multiplying it. Thus the effect of $C_{atm,i-1}$ on C_N at

Figure 6.1. Plots from a simple box mixing model. (a) CFC ventilation ages (years ; symbols) and CFC concentrations (pMol/l ; curves) against model year for the case of the true fluid renewal time, T, equal to 8 years. (b) CFC ventilation ages (years) against true renewal time, T, (years). This figure is based on many calculations with varying T and the ages shown are observed in model year 1991. The full line represents the true age, T.

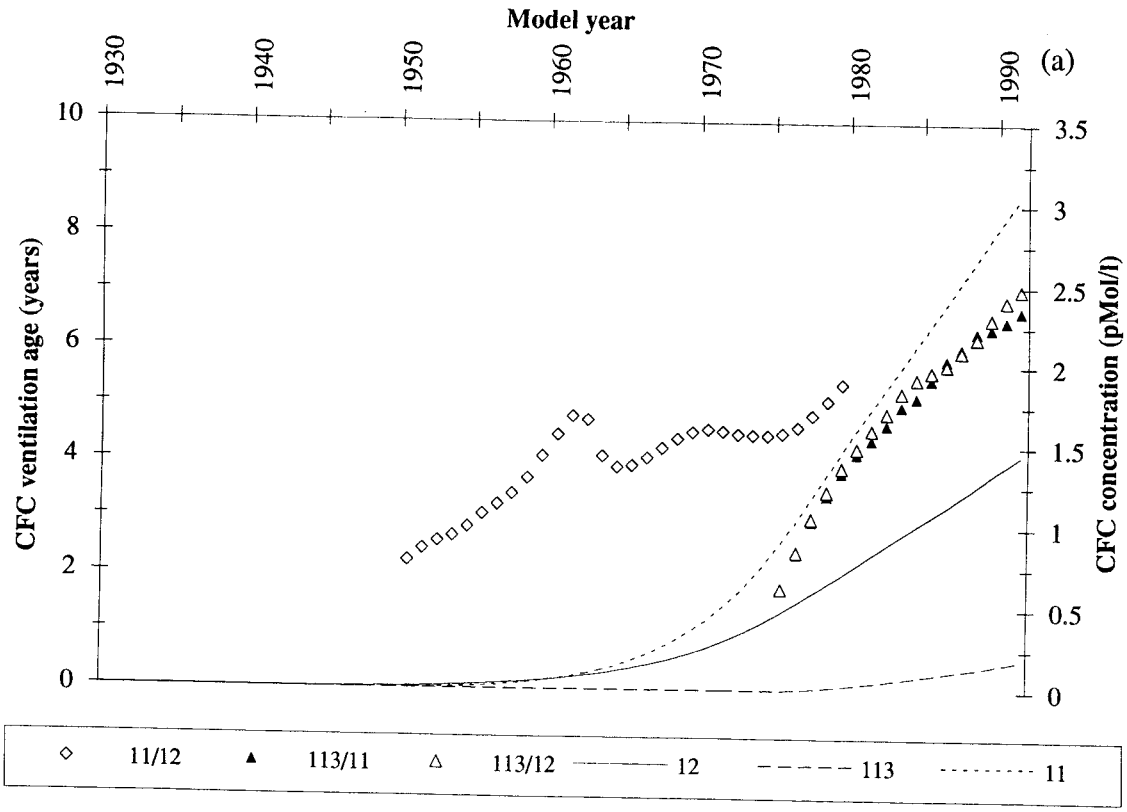
Model year
1930
1940
1950
1960
1970
1980
1990
(a)
CFC ventilation age (years)
CFC concentration (pMol/l)
0
2
4
6
8
10
0
0.5
1
1.5
2
2.5
3
3.5
11/12
113/11
113/12
12
113
11

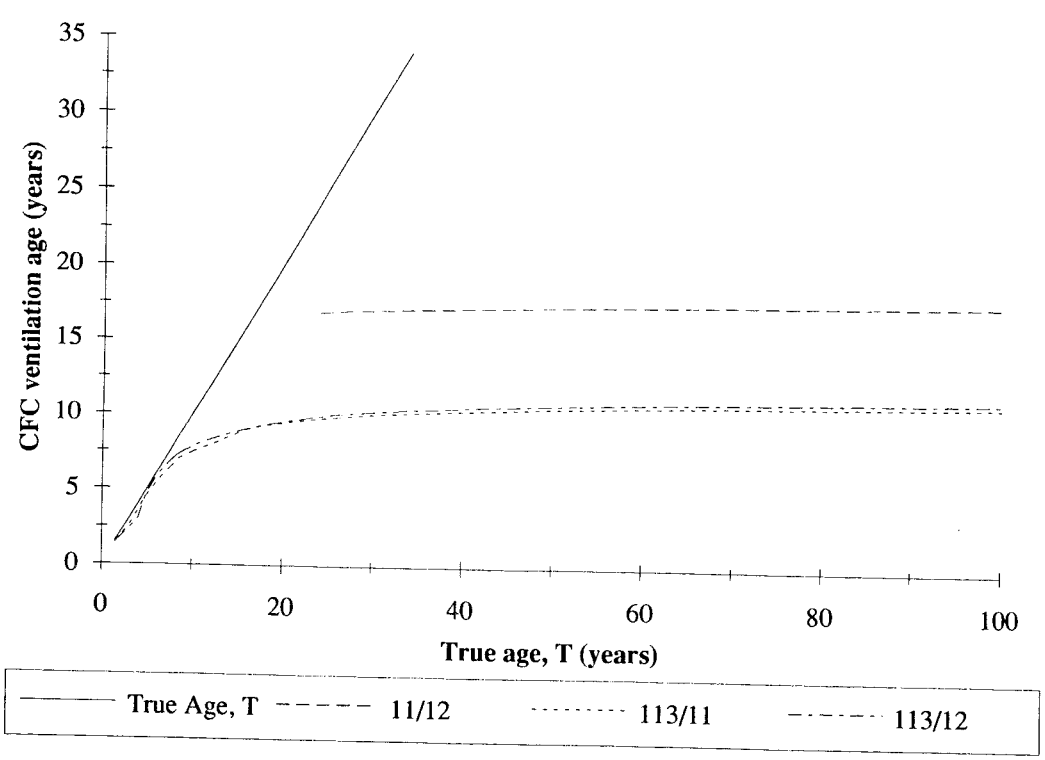
(b)
CFC ventilation age (years)
0
5
10
15
20
25
30
35
0
20
40
60
80
100
True age, T (years)
True Age, T
11/12
113/11
113/12

times much larger than the tracer timescale will be very slight, even if $\left(1 - \frac{1}{T}\right)^{N-i}$ is not small. The tracer age will then reflect the characteristic tracer time scale, rather than the mixing time, a regime which corresponds to the plateau of Figure 6.1(b).

One last comment on the simple box model is worthwhile. Figure 6.1(a) shows that the ventilation age varies with the model year. As one might expect, there is a period of spin-up for the tracer age, which increases as does the model mixing time. For T = 8 years, Figure 6.1(b) shows the difference between the CFC-113 ventilation age and T is only ~ 15% in model year 1991. However, Figure 6.1(a) also shows that the age was significantly lower in previous years. In the nomenclature of Section 6.3, $\frac{\partial \tau}{\partial t} \neq 0$; its magnitude may be several tenths, the significance of which is explained in Section 6.4.1.

6.3. Ventilation Age Evolution Equation.

In this section an expression for the evolution of CFC ventilation age is derived. The details are different for the behaviour of tritium/helium-3 age, which Jenkins (1987; henceforth JK) and Thiele & Sarmiento (1990) describe, but the motivation is very similar.

Consider the dissolved partial pressures of two tracers θ and ϕ which are scalar functions of position $\underline{x}$, and time, t. From Equation 4.3.5 the age tracer of interest is a function of the ratio of θ to ϕ, and so this analysis can be applied to CFC tracers where θ and ϕ are CFC-113 and CFC-12, or CFC-113 and CFC-11, or CFC-11 and CFC-12. To a good approximation θ and ϕ are conservative (they are, in fact, functions of the in-situ solubility, as Equation 4.3.6 shows. For the purposes of this argument, however, this extra complication is neglected). Thus their behaviour in the ocean away, from the surface boundary, is a simple balance of advection and diffusion. Namely,

$$\frac{\partial \theta}{\partial t} = D(\theta), \quad \frac{\partial \phi}{\partial t} = D(\phi) \qquad 6.3.1a,b$$

where D() is an advection diffusion operator, which has an anisotropic diffusion coefficient, and is given by,

$$D() = K_i \nabla_i^2() + K_z \frac{\partial^2}{\partial z^2}() - \underline{v}_i . \nabla_i() - w \frac{\partial}{\partial z}(). \qquad 6.3.2.$$

Here, then, subscript i refers to an isopycnal surface (free horizon; JK discusses this choice briefly) and z is the diapycnic direction, not necessarily vertical. The tracer ventilation age is given the symbol τ, and is defined in terms of the function f of the ratio $\frac{\theta}{\phi}$;

$$\tau(\underline{x},t) = t - f(r), \qquad r(\underline{x},t) = \frac{\theta}{\phi}. \qquad 6.3.3a,b.$$

(See Sections 1.3.1, 4.3.2, Figure 1.2 and Equation 4.3.5. Strictly the argument below applies to the quantity τ' of Section 4.3.2, which is estimated in this chapter by τ, defined by Equation 4.3.9, and given the same symbol for convenience.) With these definitions what we require is an expression for the ventilation age evolution, i.e. $\frac{\partial\tau}{\partial t}$, in the manner of Equation 6.3.1. Proceeding, one has,

$$\frac{\partial\tau}{\partial t} = 1 - \frac{\partial f}{\partial t} \qquad 6.3.4$$

by straightforward differentiation of Equation 6.3.3a. Expanding the left hand side of this expression yields, with Equation 6.3.3b,

$$\frac{\partial\tau}{\partial t} = 1 - \frac{\partial f}{\partial r}\left[\frac{1}{\phi}\frac{\partial\theta}{\partial t} - \frac{\theta}{\phi^2}\frac{\partial\phi}{\partial t}\right] \qquad 6.3.5.$$

The values of $\frac{\partial\theta}{\partial t}$ and $\frac{\partial\phi}{\partial t}$ are given by Equation 6.3.1, and after they have been substituted into Equation 6.3.5 rearranging yields the CFC ventilation age evolution equation,

$$\frac{\partial\tau}{\partial t} = 1 + D(\tau) - K_i\nabla_i r.\left[\frac{2}{\phi}\frac{df}{dr}\nabla_i\phi - \frac{d^2f}{dr^2}\nabla_i r\right] - K_z\frac{\partial r}{\partial z}\left[\frac{2}{\phi}\frac{df}{dr}\frac{\partial\phi}{\partial z} - \frac{d^2f}{dr^2}\frac{\partial r}{\partial z}\right] \qquad 6.3.6.$$

Inspection of Equation 6.3.6 reveals several things. Firstly, the rate of change of ventilation age is affected by a chronological term; the '1' on the right hand side of Equation 6.3.6. This reflects the tendency of the ventilation age to increase by one unit of time for each unit of time that goes by. Secondly, the ventilation age is advected and diffused by the operator D() in the same way as θ and ϕ. Thirdly there are two non-linear terms which affect $\frac{\partial\tau}{\partial t}$; one isopycnic term and one diapycnic. They have a characteristic form of a diffusion coefficient multiplying a function of the gradients of the tracer fields with the first and second derivatives of f also appearing in order to scale the gradients appropriately.

In the case where the ventilation age is constant in time, and when the effects of diffusion can be regarded as sufficiently small to be ignored Equation 6.3.6 is particularly simple. That is, from Equation 6.3.2,

$$\underline{v}_i.\nabla_i\tau = 1 \qquad 6.3.7$$

In other words, in advectively dominated flows, the balance of terms in Equation 6.3.6 is dominated by the advection of ventilation age with the chronological term. This simple expression is the focus of the rest of this chapter. If Equation 6.3.7 is an appropriate surrogate of Equation 6.3.6 then fields of CFC ventilation ages on isopycnal surfaces can reveal information about the velocities on those surfaces.

6.4. Balance of Terms in the Ventilation Age Evolution Equation.

There are six terms in Equation 6.3.6 whose magnitudes need to be estimated in order to investigate the fidelity of Equation 6.3.7. Namely,

two isopycnic terms; $K_i \nabla_i^2 \tau$ and $K_i \nabla_i r . \left[\frac{2}{\phi} \frac{df}{dr} \nabla_i \phi - \frac{d^2 f}{dr^2} \nabla_i r \right]$ and

two diapycnic terms; $K_z \frac{\partial^2 \tau}{\partial z^2}$ and $K_z \frac{\partial r}{\partial z} \left[\frac{2}{\phi} \frac{df}{dr} \frac{\partial \phi}{\partial z} - \frac{d^2 f}{dr^2} \frac{\partial r}{\partial z} \right]$,

the diapycnic advection of age; $w \frac{\partial \tau}{\partial z}$

and the Eulerian derivative of age with time; $\frac{\partial \tau}{\partial t}$.

In estimating these quantities eight density surfaces (σ_θ) in the seasonal and permanent thermocline are chosen and CFC data from the VIVALDI expedition are used to derive the necessary tracer gradients. In Section 6.4.1 the details of the tracer gradient calculations are explained whilst the choice of diffusion coefficients is discussed in Section 6.4.2. In Section 6.4.3 the balance of terms is evaluated and appropriate approximations discussed.

At this stage it is worth remarking that, in general, there is no unambiguous way to proceed in calculating the values of either the tracer gradients or the diffusion coefficients. The magnitudes of these quantities depend strongly on the length scale over which they are measured. One would anticipate large K_i and small gradients for length scales which are large compared to the characteristic length of the geostrophic turbulence. Much smaller K_i and correspondingly larger gradients would be expected when these quantities are estimated over shorter length scales, however. The form of the two non-linear terms in Equation 6.3.6 demonstrates how this effect is compensated for, since K_i multiplies functions of the gradients, and therefore the manner in which the total magnitudes of these terms vary with length scale is not clear. In practice there is no difficulty in choosing a length scale since the data available are not capable of simultaneously resolving many scales. Figure 4.7 shows the grid of points which can be used to estimate values of the CFC-113 gradients. The appropriate length used in determining representative values of K_i and the tracer gradients is thus of order 500km.

6.4.1. Calculation of Tracer Gradients.

The tracer gradients required for the balance of terms comparison include isopycnic gradients of tracer concentration and ratio, and the isopycnic Laplacian of age. The diapycnic gradients of concentration, ratio and age plus the second derivative of age are also needed. In addition the first and second derivatives of the function f with r are necessary. Throughout this analysis the CFC concentrations are expressed in dissolved partial pressures, derived by dividing the molar concentration by the relevant in-situ solubility. The solubility is based on the local potential temperature and salinity with the factor-X technique described in Section 4.3.2 used for CFC-113. The original profiles are interpolated onto each density surface. Plane fits for θ, ϕ, r and τ are determined and a representative profile of these quantities is found by evaluating the fitting functions at the centre of the region covered by usable data (about 45°N 20°W). The plane fits can also be differentiated to yield the values of $\nabla_i r$ and $\nabla_i \phi$, required for the isopycnic non-linear term. A quadratic function of horizontal position is fitted to ventilation age in order to estimate the magnitude of the isopycnic Laplacian. The typical profile is used to derive values for $\frac{\partial^2 \tau}{\partial z^2}$, $\frac{\partial \tau}{\partial z}$, $\frac{\partial r}{\partial z}$ and $\frac{\partial \phi}{\partial z}$ by fitting cubic and quadratic functions of z and differentiating appropriately. All that is finally required to compute the diffusive terms listed above are the first and second derivatives of f(r), for each tracer ratio considered (i.e. CFC-113/CFC-12 and CFC-113/CFC-11). These are found by fitting cubic polynomials to the atmospheric source functions shown in Figure 1.2. These techniques are similar to those described by JK in his study of tritium/helium-3 age evolution.

6.4.2. Choice of Diffusion Coefficients, K_i and K_z.

Estimating the values of diffusion coefficients is a notorious problem. K_i and K_z are properties of the flow rather than the fluid and one rarely has sufficient data to completely describe the flow. JK describes a method to render a value for K_i based on work by Armi & Stommel (1983) and Tennekes & Lumley (1972). The technique presupposes an underlying smooth gradient in property (e.g potential temperature, salinity or dissolved oxygen) which is being mixed by homogeneous and isotropic turbulence with a single characteristic length scale. By sampling the property at intervals greater than the characteristic length scale one obtains an incoherent field. From a knowledge of the underlying field the anomalies in these observations can be used to estimate the characteristic mixing length. An additional assumption is that the turbulence is vertically coherent. The mixing length can be used to estimate K_i by an expression due to Tennekes & Lumley (1972) based on three-dimensional turbulence in a shear flow. This method is used by JK and Armi & Stommel (1983) for the β-triangle region of the north east Atlantic and results in a value of $500 m^2 s^{-1}$ for K_i. The same technique has been used on the temperature and dissolved oxygen fields of the VIVALDI data set, although the details are not reported here (Cunningham & Haine, in prep.). Calculations including

all the VIVALDI stations were compared with results from the subset of casts, shown in Figure 4.7, where good CFC-113 data is available. These did not significantly differ from each other, or from JK's estimate, and so a value of $500 m^2 s^{-1}$ is used in this chapter.

The value of K_z used is $10^{-5} m^2 s^{-1}$, again based on JK's work, who cites Garrett (1979), Schmitt (1981), Schott & Zantrop (1980) and Jenkins (1980) in defence of this choice. The effect of different K_i and K_z on the various diffusive terms in Equation 6.3.6 is readily apparent; they simply scale in proportion to the perturbation (see also the discussion in Section 6.4.3 and 6.7). It is interesting to consider that in a numerical simulation of CFC-113 age invasion the values of the diffusion coefficients are actually prescibed. The balance of terms in the ventilation age evolution equation is a worthwhile area of future study in a model such as this.

6.4.3. Orders of Magnitude in the CFC Ventilation Age Evolution Equation.

Table 6.1 shows the isopycnal surfaces chosen for the analysis, and the values of pressure and the required tracer variables taken from the centres of the planes fitted to each variable. These are representative profiles for the region considered, and plotted in Figure 6.2. The profiles of ventilation age as calculated by use of CFC-113/CFC-12 and CFC-113/CFC-11 ratios closely resemble the profile at 48°N 16°W shown in Figure 4.10(c). No further discussion of the discrepancy between these two ages appears here (see Section 4.3.3). Figure 6.3 shows plots of $K_i \nabla_i^2 \tau$, $K_i \nabla_i r \left[\frac{2}{\phi} \frac{df}{dr} \nabla_i \phi - \frac{d^2 f}{dr^2} \nabla_i r \right]$, $K_z \frac{\partial^2 \tau}{\partial z^2}$, $K_z \frac{\partial r}{\partial z} \left[\frac{2}{\phi} \frac{df}{dr} \frac{\partial \phi}{\partial z} - \frac{d^2 f}{dr^2} \frac{\partial r}{\partial z} \right]$ and, $\frac{\partial \tau}{\partial z}$. Of these the isopycnic diffusion term dominates, with a magnitude of several tenths. Indeed, the error in this term is of this order too, even when the error in K_i is neglected (and this is undoubtedly substantial). The other terms are all at least one order of magnitude smaller and so it is reasonable to disregard these. The diapycnic velocity, w, is strictly zero in the formalism of Equation 6.3.2, at least in the absence of internal heating (i.e. where absorption of solar radiation at depth is small). Even for the shallowest surface ($\sigma_\theta = 27.1$, pressure ~ 145db) this has a slight influence, and so $w \frac{\partial \tau}{\partial z}$ is neglected too.

An appropriate approximation to Equation 6.3.6 is thus,

$$\frac{\partial \tau}{\partial t} \approx 1 - \underline{v}_i . \nabla_i \tau + K_i \nabla_i^2 \tau \qquad 6.4.1$$

CFC-113/CFC-12 and CFC-113/CFC-11 ventilation ages are therefore good substitutes for 'ideal age' in the terminology of Thiele & Sarmiento (1990) since they are merely advected and diffused with the extra chronological term included too. This is true

Figure 6.2. Plots of mean profiles taken from plane fits to isopycnic data from the VIVALDI stations shown in Figure 4.7. (a) 10 * CFC-113, CFC-12 and CFC-11 partial pressures (pptv). (b) CFC-113/CFC-12 and CFC-113/CFC-11 ratios. (c) CFC-113/CFC-12 and CFC-113/CFC-11 ventilation ages (years). The figures in italics are the σ_θ surfaces used in the isopycnic analysis.

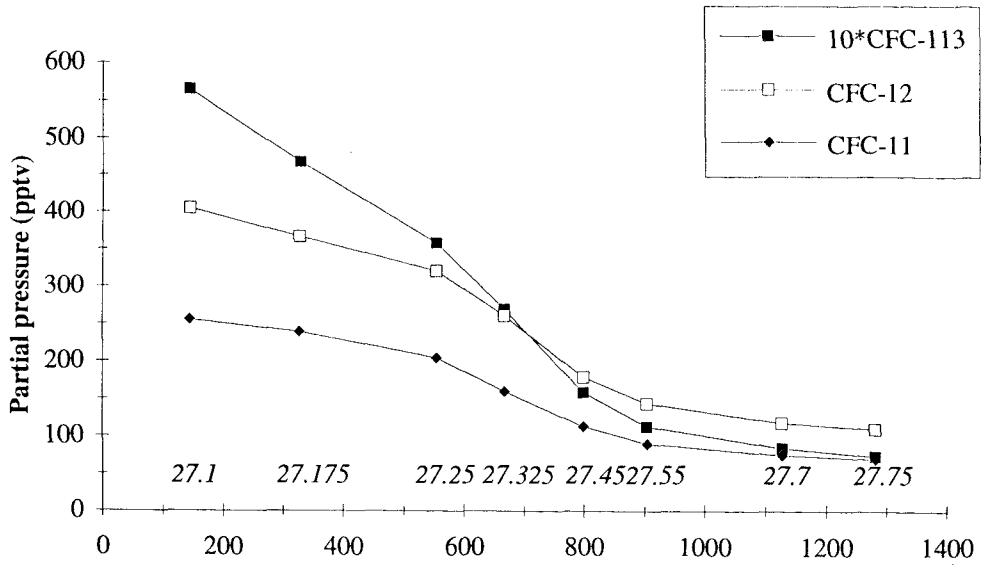
10*CFC-113
CFC-12
CFC-11
Partial pressure (pptv)
600
500
400
300
200
100
0
27.1
27.175
27.25
27.325
27.45
27.55
27.7
27.75
0
200
400
600
800
1000
1200
1400

(a)

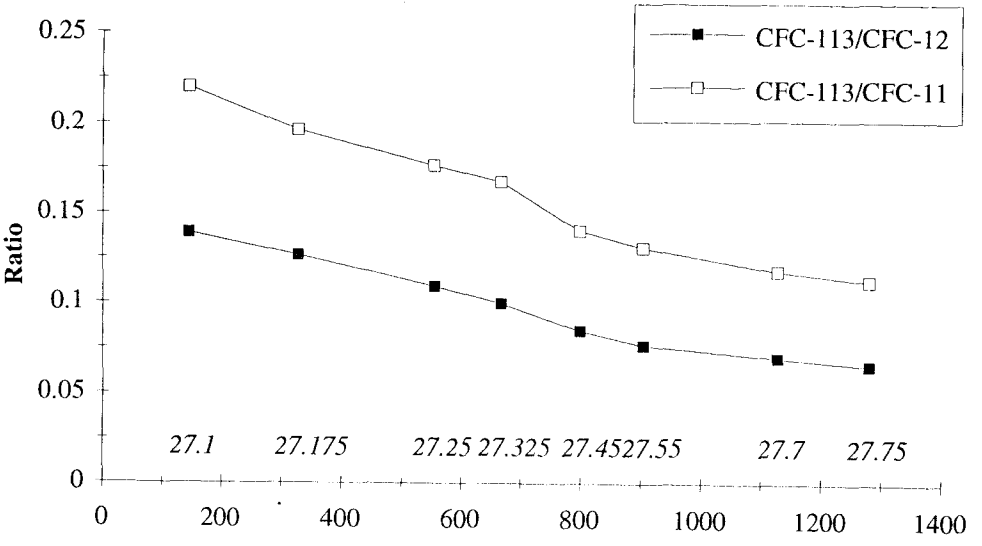
CFC-113/CFC-12
CFC-113/CFC-11
Ratio
0.25
0.2
0.15
0.1
0.05
0
27.1
27.175
27.25
27.325
27.45
27.55
27.7
27.75
0
200
400
600
800
1000
1200
1400

(b)

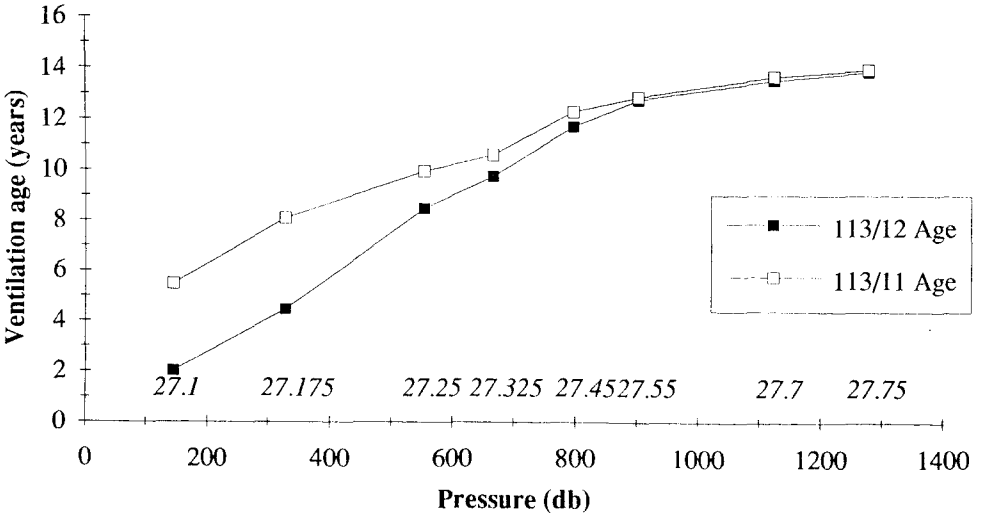
113/12 Age
113/11 Age
Ventilation age (years)
16
14
12
10
8
6
4
2
0
27.1
27.175
27.25
27.325
27.45
27.55
27.7
27.75
0
200
400
600
800
1000
1200
1400
Pressure (db)

(c)

Figure 6.3. Profiles of terms in the CFC ventilation age evolution equation (Equation 6.3.6) with $K_i = 500 m^2 s^{-1}$ and $K_z = 10^{-5} m^2 s^{-1}$.

(a) Isopycnic diffusion, $K_i \nabla_i^2(\tau)$,

(b) isopycnic non-linear, $K_i \nabla_i(r).\left[\frac{2}{\phi}\frac{df}{dr}\nabla_i(\phi) - \frac{d^2f}{dr^2}\nabla_i(r)\right]$,

(c) diapycnic diffusion $K_z\frac{\partial^2\tau}{\partial z^2}$; (squares),

diapycnic non-linear, $K_z\frac{\partial r}{\partial z}\left[\frac{2}{\phi}\frac{df}{dr}\frac{\partial\phi}{\partial z} - \frac{d^2f}{dr^2}\frac{\partial r}{\partial z}\right]$; (diamonds),

and

diapycnic gradient of age, $\frac{\partial\tau}{\partial z}$; (triangles).

The figures in italics are the σ_θ surfaces used in the isopycnic analysis. Filled symbols are for τ defined in terms of CFC-113/CFC-12, open in terms of CFC-113/CFC-11. The dashed lines in (a) and (b) are standard errors based on the fits described in Section 6.4.1. No error in function f or the value of the diffusion coefficient is accounted for. The effect of perturbing the diffusion coefficients is readily apparent; the y-axes simply scale in proportion.

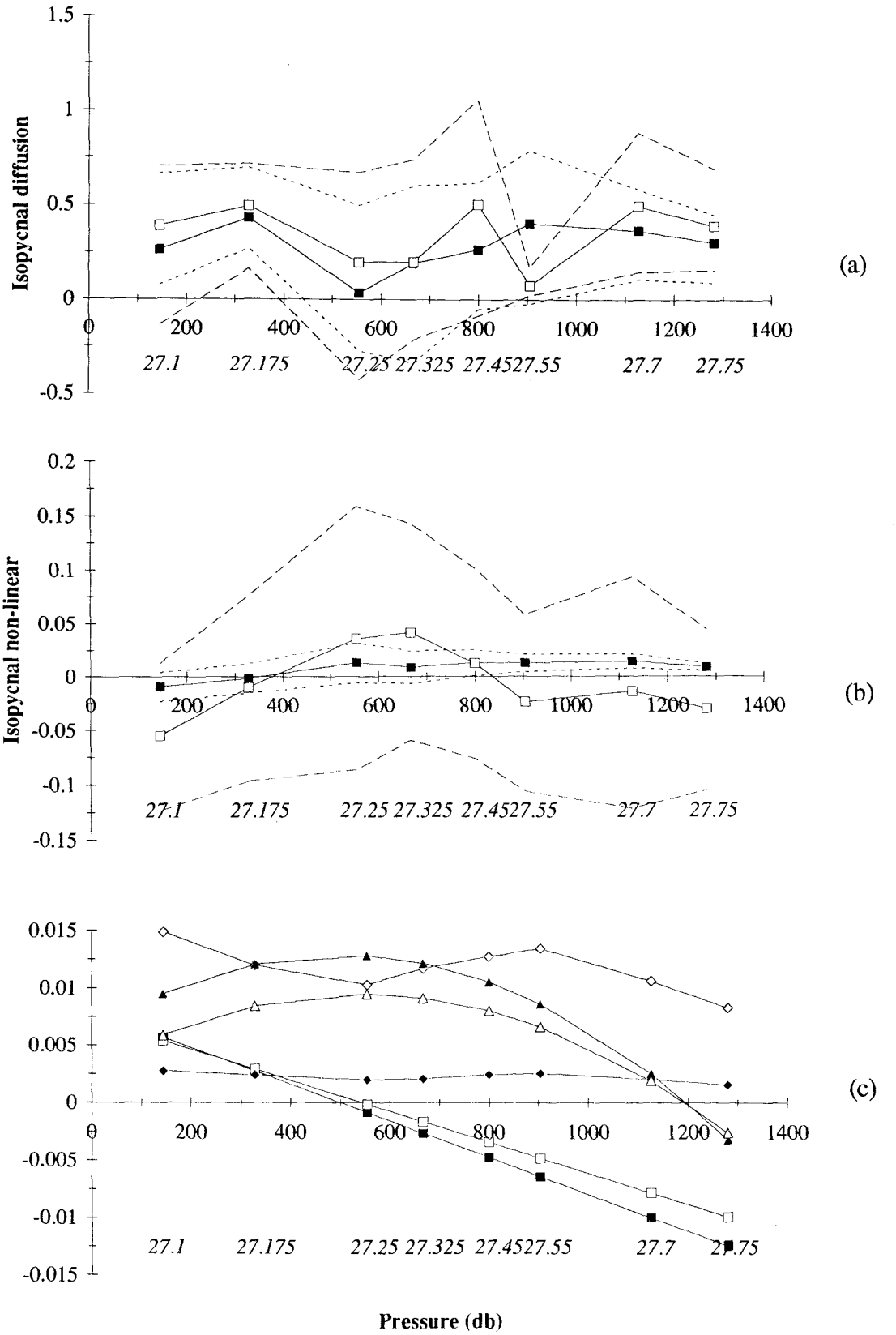

Filled symbols ⇔ CFC-113/CFC-12, Open symbols ⇔ CFC-113/CFC-11

at least for their behaviour away from the seasonally mixed ocean; the boundary condition age = 0 is not, in general appropriate as discussed in Chapter 5.

Table 6.1. Typical profiles at about 45°N 20°W based on plane fits to VIVALDI data shown in Figure 4.7 on various isopycnals.

σ_θ	Pressure	CFC-12	CFC-11	CFC-113	113/12	113/11	Age_1	Age_2
	db	pptv	pptv	pptv	#	#	years	years
27.1	145	404	255	56.6	0.139	0.220	2.0	5.5
27.175	328	366	238	46.7	0.126	0.196	4.5	8.1
27.25	554	321	204	35.8	0.109	0.176	8.5	10.0
27.325	667	260	159	26.9	0.100	0.168	9.7	10.6
27.45	799	179	112	15.8	0.084	0.140	11.7	12.3
27.55	904	143	90	11.3	0.076	0.131	12.7	12.8
27.7	1127	117	75	8.4	0.070	0.118	13.5	13.6
27.75	1281	110	70	7.3	0.065	0.112	13.8	13.9

N.B. $Age_1 \Leftrightarrow$ CFC-113/CFC-12 Age, $Age_2 \Leftrightarrow$ CFC-113/CFC-11 Age.

The simple box model of Section 6.2 suggests that in a *diffusively* dominated regime $\frac{\partial \tau}{\partial t} \neq 0$, where the flushing time of the box is of the same order as the characteristic tracer time scale. The diffusive limit to Equation 6.4.1 is

$$\frac{\partial \tau}{\partial t} \approx 1 + K_i \nabla_i^2 \tau \qquad 6.4.2.$$

This expression applies when the ventilation age clock runs too fast initially; corresponding to the rise in CFC-113 ventilation ages shown in Figure 6.1(a) from the box model calculation. During this period the diffusion acts to smooth the age field and $K_i \nabla_i^2 \tau$ is positive and of order 1. However, in a regime dominated by *advection*, one assumes $\frac{\partial \tau}{\partial t}$ to be small, at least for those regions not close to the front of advancing tracer (this follows JK's work on tritium/helium ages; Section 7.3 comments on this further

where the correlation with another time dependent ocean parameter (dissolved oxygen) is used to infer information about the CFC ventilation age), and so,

$$\underline{v}_i.\nabla_i\tau \approx 1 + K_i\nabla_i^2\tau \qquad 6.4.3.$$

This approximation is the most faithful to Equation 6.3.6 for the region of the north east Atlantic studied. Therefore the balance of the CFC-113 ventilation age evolution equation, in this part of the ocean, is between advection and the chronological term, with a significant contribution from isopycnic diffusion. Rearranging Equation 6.4.3,

$$\underline{v}_{i,\tau} \approx \frac{1 + K_i\nabla_i^2\tau}{\nabla_i\tau} = \frac{(1 + K_i\nabla_i^2\tau)\,\nabla_i\tau}{|\nabla_i\tau|^2} \qquad 6.4.4$$

where $\underline{v}_{i,\tau}$ is the isopycnic velocity *in the direction of* $\nabla_i\tau$. This is an important point, and it is discussed in detail in Section 6.6. It is worth remarking that JK does not make this clear in his analogous treatment of tritium/helium-3 ages. He asserts

$$\underline{v}_i \approx \frac{1}{\nabla_i\tau} \qquad 6.4.5$$

Table 6.2. Magnitudes and directions of $|\underline{v}_{i,\tau}|$ as determined from Equation 6.4.4, using plane fits for the τ field (Section 6.4.1), and taking the value at the centre of the survey region.

σ_θ		27.2	27.275	27.25	27.325	27.45	27.55	27.7	27.75
$\lvert\underline{v}_{i,\tau}\rvert$	cm/s	1.18	1.25	2.63	3.38	1.7	1.9	3.08	4.41
Direction	°	254	256	96	97	108	110	109	121

which is formally incorrect (here $\underline{v}i$ corresponds to JK's **V**, and in his expression $K_i\nabla_i^2\tau << 1$). Table 6.2 shows the values of $\underline{v}_{i,\tau}$ on the isopycnals used for this analysis as calculated by straightforward application of Equation 6.4.4. Section 6.5 discusses appropriate error estimates for these quantities.

6.5. Influence of Errors on the Calculation of $\underline{v}_{i,\tau}$.

Consider the effect of an error, ε, on the measurement of $\nabla_i\tau$ in calculating $\underline{v}_{i,\tau}$ by Equation 6.4.4, viz.

$$\underline{v}_{i,\tau} \approx \frac{1 + K_i\nabla_i^2\tau}{\nabla_i(\tau \pm \varepsilon)} \qquad 6.5.1.$$

Equation 6.5.1 and Figure 6.4 show that for rapid velocities ε eventually dominates the calculation, regardless of its size. This is because, under these conditions, the $\nabla_i\tau$

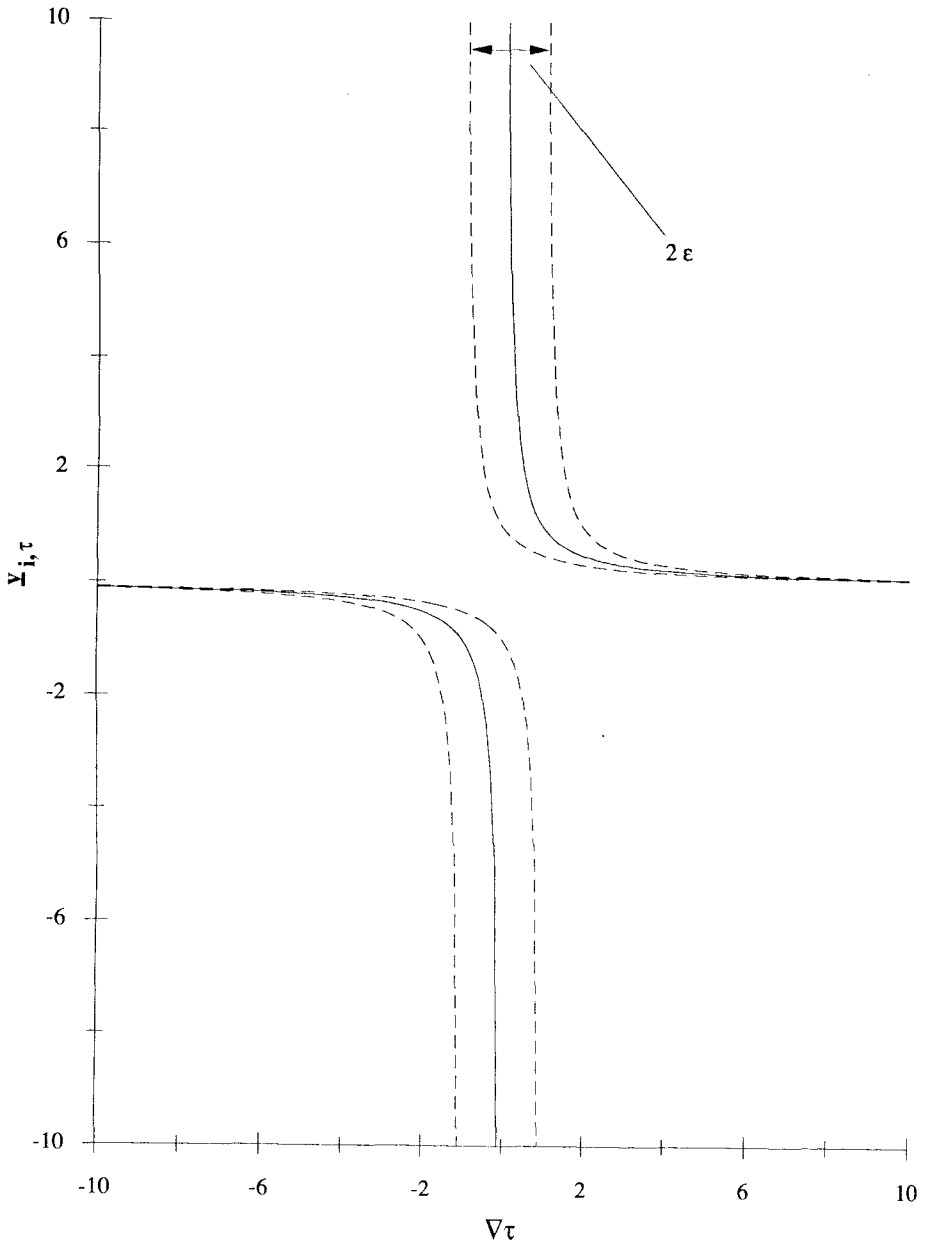

Figure 6.4. Schematic diagram of the effect of an error, ε, on the diagnosed isopycnic velocity in the direction of the ventilation age gradient, $\underline{v}_{i,\tau}$ (Equation 6.5.1). The full curve is the unperturbed velocity, and either side of it lie the velocities calculated by including the error $\pm\,\varepsilon$ in the value of $\nabla\tau$. The scales in this figure are arbitrary.

term is very small. Indeed, there comes a point when the sign of $\underline{v}_{i,\tau}$ is no longer known, since the sign of $\nabla_i\tau$ cannot be determined. The best that can be done in these circumstances is to place a lower bound on the magnitude of the velocity. Even in the advective limit, where $K_i \rightarrow 0$, the efficacy of Equation 6.4.4 is curtailed for large $\underline{v}_{i,\tau}$. The key issue here is that $1/\nabla_i\tau$ cannot be measured properly when $\nabla_i\tau$ is small. The length scale, l, over which observations must be made in order to unambiguously determine the sign of $\nabla_i\tau$ is given by,

$$l = 2\,\varepsilon\,|\underline{v}_{i,\tau}| \qquad 6.5.2$$

i.e. the length over which the τ field varies by more than 2 ε. Table 6.3 shows values of l for various characteristic velocities (assuming $|\underline{v}_{i,\tau}| \approx |\underline{v}_i|$; see Section 6.6 for a discussion of this). Values of ε are chosen to be 1.5 and 0.9 years here, corresponding to the uncertainty in τ near the surface and between 1500-2000db, from the results of Section 4.3.3. Equation 6.5.2 shows that for the uncertainty in τ during the VIVALDI cruise maximum velocities of order 0.5cm/s (near surface) and 0.8cm/s (1500-2000db) can be sensibly derived. None of the values of $\underline{v}_{i,\tau}$ in Table 6.2 can be treated as accurate, therefore, even without including errors accumulated as a result of forcing a plane fit through the τ fields.

Table 6.3. Values of length scale, l, required to determine the correct sign of $\nabla_i\tau$ for two values of ε (see text and Equation 6.5.2).

$\underline{v}_i$	(cm/s)	0.01	0.1	1	10	100
l (ε=1.5 years)	(km)	9.5	95	950	9500	95000
l (ε=0.9 years)	(km)	5.7	57	570	5700	57000

The limit of small velocity, conversely, is characterised by large $\nabla_i\tau$ and consequently $\nabla_i\phi$, and $\nabla_i r$. As one might anticipate, with large tracer gradients, diffusion becomes progressively more important until a point is reached where Equation 6.4.4 is no longer a faithful surrogate of Equation 6.3.6.

Equation 6.4.4 applies, therefore, to a range of velocities $\underline{v}_{i,\tau}$. For small speeds the expression itself is invalid; the diffusive (and ultimately the non-linear terms) tend to dominate. For high speeds the direction of the velocity becomes ill-determined as the effects of errors control the denominator of the right hand side of Equation 6.4.4. So far no mention has been made of uncertainties in $K_i\nabla_i^2\tau$; these are important, but their discussion is postponed until Section 6.7.

6.6. The Effect of Sheared Flow on $\underline{v}_{i,\tau}$.

In the derivation of Equation 6.4.4 attention is drawn to the distinction between $\underline{v}_{i,\tau}$, the velocity one can infer from fields of CFC ventilation ages, and $\underline{v}_i$ the true isopycnic velocity vector. The scalar product $\underline{v}_i.\nabla_i\tau$ in Equation 6.4.3 ensures that

$$|\underline{v}_{i,\tau}| = \frac{|\underline{v}_i|}{\cos(\alpha)} \qquad 6.6.1$$

where α is the angle between $\underline{v}_{i,\tau}$ and $\underline{v}_i$. The simple example discussed in this section attempts to make this point more succinctly.

Consider a steady fluid, free of diffusion, which moves in a purely meridional direction away from a boundary (Figure 6.5(a)). The flow is a simple Gaussian jet, with a non-zero speed far from the jet axis. The boundary represents an isopycnic outcrop where an ideal tracer age, τ, is set to zero. The fluid simply advects the age tracer into the interior, and so,

$$\tau(x,y) = \frac{y}{v(x)}, \quad \tau(x,0) = 0 \qquad 6.6.2.$$

Figure 6.5(b) shows a contour plot of τ isolines in the (x,y) plane. The key point is that the direction $\nabla\tau$ is not in the same sense as the velocity, which is entirely meridional. Rather,

$$\nabla_i\tau = \left\{\frac{-y}{v^2}\frac{dv}{dx}, \frac{1}{v}\right\} \qquad 6.6.3$$

in this example. And so,

$$\tan(\alpha) = \frac{-y}{v}\frac{dv}{dx} \qquad 6.6.4$$

which is non-zero when the flow is sheared ($\frac{dv}{dx} \neq 0$), despite the implication of Equation 6.6.3 that $\underline{v}_i.\nabla_i\tau = 1$ identically. Equation 6.6.4 reiterates the comments made above; knowledge of τ fields alone cannot reveal anything about α and hence $\underline{v}_i$. This discussion applies equally well to tritium/helium-3 ages which JK examines, although he does not mention this problem. The velocities he derives assume implicitly that $\alpha = 0$, which is only true for regions free of isopycnic shear in the mean flow. (Mean flow, in this context, refers specifically to the flow averaged over time scales of order τ.)

Furthermore, the velocity $\underline{v}_{i,\tau}$, as defined by Equation 6.4.4, is *divergent* in a sheared flow. I.e.

$$\nabla_i.\underline{v}_{i,\tau} \neq 0 \qquad 6.6.5$$

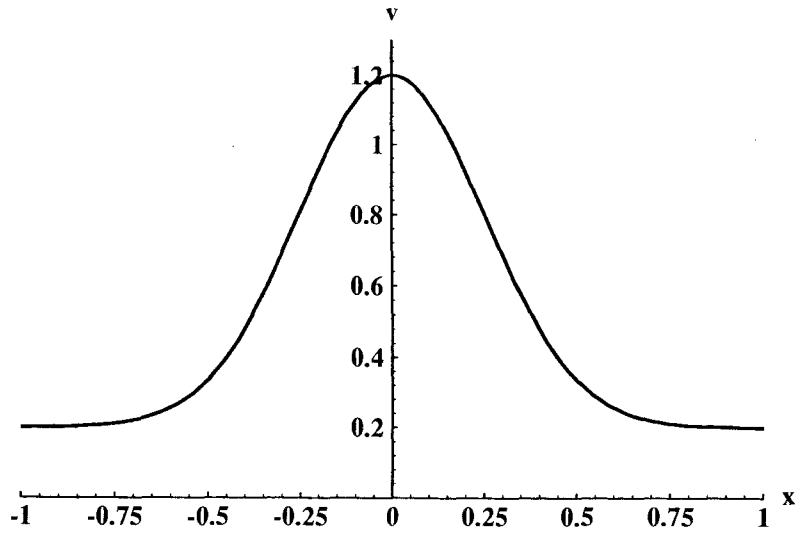

(a)

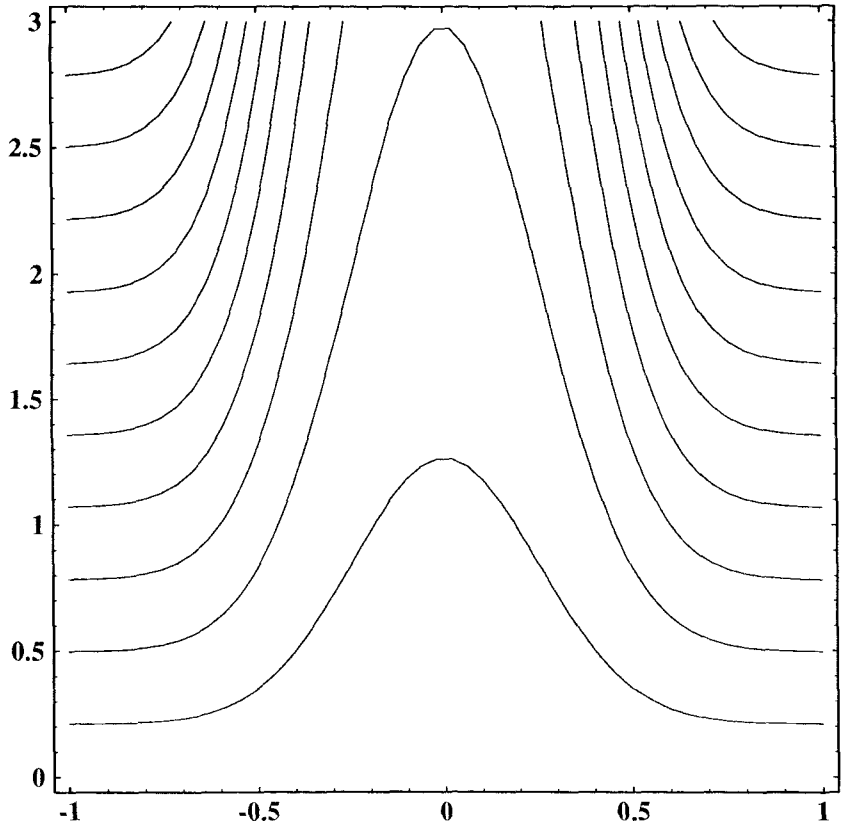

(b)

Figure 6.5. (a) Plot of meridional (northwards) velocity, v, against distance, x, in the conceptual advection model of Section 6.6. A simple Gaussian jet is postulated with a non-zero velocity at great distance from the jet axis. (b) Field of age isolines resulting from the steady jet in (a). The axis scales in (a) and (b) and the spacing of contours in (b) are arbitrary.

which is in contradiction (under these circumstances) with the premise of incompressibility. This can be demonstrated most easily by considering a uniform, meridional shear flow (to which an arbitrary shear may be approximated under suitable scalings). The true velocity field, $\underline{v}$ is thus,

$$\underline{v} = \begin{pmatrix} 0 \\ v_0 + v_x x \end{pmatrix} \qquad 6.6.6$$

where $v_x = \frac{dv}{dx}$ = constant here (Equation 6.6.6 expresses the velocity, $\underline{v}$ as a Taylor expansion with one term). Equation 6.6.2 leads to,

$$\tau(x,y) = \frac{y}{v_0 + v_x x}, \quad \tau(x,0) = 0 \qquad 6.6.7$$

whence,

$$\nabla_i \tau = \frac{1}{v_0 + v_x x} \begin{pmatrix} - \frac{v_x y}{v_0 + v_x x} \\ 1 \end{pmatrix} \qquad 6.6.8.$$

Equation 6.4.4 defines $\underline{v}_{i,\tau}$, and so,

$$\underline{v}_{i,\tau} = \frac{\nabla \tau}{|\nabla \tau|^2} = \frac{(v_0 + v_x x)^3}{v_x^2 y^2 + (v_0 + v_x x)^2} \begin{pmatrix} - \frac{v_x y}{v_0 + v_x x} \\ 1 \end{pmatrix} \qquad 6.6.9$$

when one considers the limit of $K_i \rightarrow 0$. Taking the divergence of $\underline{v}_{i,\tau}$ yields Equation 6.6.5 as required,

$$\nabla_i . \underline{v}_{i,\tau} = \frac{- 2 v_x^2 y (v_0 + v_x x)}{v_x^2 y^2 + (v_0 + v_x x)^2} \qquad 6.6.10$$

$$\nabla_i . \underline{v}_{i,\tau} \neq 0 \quad \text{provided } v_x \neq 0.$$

It is thus impossible to define a streamfunction based on integrating $\underline{v}_{i,\tau}$ when the flow is sheared.

In principle one can recast the definition of $\underline{v}_{i,\tau}$ (Equation 6.4.4) to include the angle, α, between $\nabla_i \tau$ and $\underline{v}$, and then by *asserting* that $\nabla_i . \underline{v}_{i,\tau} = 0$ derive a condition for α entirely in terms of functions of τ. This is a current topic of study; it should not influence the conclusion that deriving $\underline{v}$ from τ is difficult however, since one requires derivatives of the form $\frac{\partial |\nabla_i \tau|}{\partial x}$ and $\frac{\partial |\nabla_i \tau|}{\partial y}$ which, in practice, are hard to evaluate precisely.

6.7. Concluding Remarks.

Section 6.4 examines the full CFC ventilation age evolution equation (Equation 6.3.6) and shows that for the north east Atlantic, at scales of ~ 500km, a simple expression applies (namely Equation 6.4.3). Section 6.5 reveals that errors will always

dominate any estimate of isopycnic velocities for large speeds; in fact, the current analytical precision severely limits the magnitudes of velocities which can be faithfully resolved. Section 6.6 shows that, in a sheared flow, the direction of the flow cannot be determined from the tracer data; the velocity field derived from the tracer age distribution is divergent when the true flow is sheared. The salient point of this chapter is, therefore, that knowledge of CFC-113 ventilation age fields is generally insufficient for determination of the flow; it is difficult to invert τ for velocity.

One final remark merits consideration. The error in $\underline{v}_{i,\tau}$ given by Equation 6.4.4 is considerably less than the error in $\underline{v}_{i,P}$, where P is another steady, conservative tracer (e.g potential temperature, salinity). This is because,

$$\underline{v}_{i,P} = \frac{K_i \nabla_i^2 P}{\nabla_i P} \qquad 6.7.1$$

is a direct result of the advection/diffusion balance for P (i.e. D(P) = 0). Although one may be able to measure P much more precisely than τ, by adding the chronological term to $K_i \nabla_i^2 \tau$ the overall error in the numerator of the right hand side of Equation 6.4.4 is much reduced (and hence in $\underline{v}_{i,\tau}$ too). If, in addition, $|\nabla_i \tau . \nabla_i P| < 1$ then by use of both τ and P fields the isopycnic velocity can be resolved, i.e. $\nabla_i P$ and $\nabla_i \tau$ are in different directions, allowing $\underline{v}_i$ to be determined. In general, however, $|\nabla_i \tau . \nabla_i P| \approx 1$ for usable P because they have similar boundary conditions, set in the mixed layer (Section 7.3 examines this assertion when property P is dissolved oxygen).

CHAPTER 7

DATA INTERPRETATION AND CONCLUSIONS.

7.1. Introduction.

This chapter draws together the material introduced in the preceding three chapters. Sections 7.2 and 7.3 involve the interpretation of CFC-113 ventilation ages. There is a general discussion in the former, where the topic of interest is direct understanding of CFC-113 age fields, without recourse to other oceanographic variables. Section 7.2 shows it is hard to infer information about oceanic processes in this way. In Section 7.3 the discussion widens to address the question of simultaneous interpretation of CFC-113 age with dissolved oxygen observations to infer oxygen utilisation rates (OURs). It is possible that in combination with another parameter CFC ventilation age provides a stronger constraint on oceanographic parameters. OURs are reasonably well understood, and in Section 7.3 comparison is drawn between OURs calculated using CFC-113 ages and other accepted methods. The discrepancies between these two techniques suggest features of the CFC-113 behaviour which the simple model of Section 6.2 exhibits. The concluding remarks of this thesis are in Section 7.4, and Section 7.5 contains comments on possible avenues for future work.

7.2. Interpretation of CFC-113 Ventilation Ages.

Figure 4.11 is a map of CFC-113 ventilation age on a density surface for a σ_θ surface outcropping in the VIVALDI region. This map is initially introduced in Section 4.3.3, where a few comments on interpretation of the age distribution are made. This isopycnal is the focus for discussion in this section, and in Section 7.3 too. With the ideas of Chapters 5 and 6 in mind a less myopic interpretation of this figure can be attempted. Since the ocean is unimportant as a sink for atmospheric CFCs (Section 1.3.2), explaining fields of concentration in terms of existing oceanographic paradigms is rather unproductive. The spirit of the following discussion is to attempt to use CFC observations *a posteriori* to infer information regarding oceanic processes.

Chapter 5 shows that the CFC-113 age boundary condition for the main thermocline is not straightforwardly age = 0. The modelling results are that an initial age of 1-2 years is realistic, and this makes interpretation of absolute ages difficult. One can assume that the boundary condition is steady, but without measurements being made when the mixed layer shallows the exact circumstances pertaining will remain uncertain. These comments apply equally well to use of CFC concentration fields as tracers. The comment in Section 4.3.3 about diagnosing the outcrop of the 27.10 isopycnal, and its maximum depth of annual mixing, is, by coincidence, reasonably accurate in this case. The mixed layer model of Chapter 5 certainly cannot explain ages as old as those in

Figure 4.11 at depths so shallow; fluid older than about 1-2 years old cannot have been in the mixed layer of the winter preceding the VIVALDI survey based on the model results (Figure 5.6(b) is used to guide an interpretation).

The research reported in Chapter 6 shows that the evolution of CFC-113 age in the ocean interior of a region of the north east Atlantic (Figure 4.7) is a balance between advection, diffusion and the tendency for ventilation age to increase with time. The effect of diffusion may be considered to make the CFC 'clock' run too fast (it adds to the chronological term in Equation 6.4.3). Therefore, even if the age boundary condition for the main thermocline is known, the ventilation age is not necessarily a reliable proxy for the true fluid age. Consequently, interpretation of absolute ventilation ages is difficult. Indeed, even for regions of the ocean where the effect of diffusion is small (i.e. the advective approximation of Equation 6.3.7 applies) there is no guarantee that the upstream diffusion is small too. For example, the region downstream of the VIVALDI survey area may well be characterised by strong advection. For this part of the ocean, the CFC-113 age would then be a reliable clock, but with an offset obtained during the period spent passing through the diffusive locale. This comment is pertinent to the work of Jenkins (1987; abbreviated JK) on tritium/helium-3 ages in the β triangle area, approximately 1500km to the south west of the VIVALDI survey. He found that "the ^{3}H-^{3}He age distributions indicate that mixing is not a significant source of error for those density horizons which outcrop in the region of Ekman downwelling (i.e. $26.35 \leq \sigma_\theta \leq 27.15$)". This is true local to the β triangle, but not necessarily upstream (perhaps in the VIVALDI region where mixing is significant for CFC-113 ages). The absolute ages may well be corrupted as a result of this mechanism.

JK does not use his absolute tritium/helium-3 ages however, rather he derives isopycnic velocities based on fields of $1/\nabla\tau$. Sections 6.5 and 6.6 show this method can be influenced by errors and shear in the flow. Because the CFC-113 age evolution involves a component due to mixing, the exact magnitude of which is uncertain, no attempt is made to render velocities based on isopycnic gradients of CFC ventilation age (the values in Table 6.2 are reported for comparison with the errors discussed in Section 6.5, and should not be treated literally). The simple estimate of Section 4.3.3 cannot be treated with any real credibilty therefore; indeed the agreement with previous work noted there is not surprising; Pollard & Pu (1985) use a technique relying on interpretation of the dissolved oxygen field which is influenced by the same effects as CFC-113 age as Section 7.3 explains. In summary, direct interpretation of the τ field of Figure 4.11 is complicated by real (and potential) ambiguities. The example of OURs in Section 7.3 examines the use of CFC-113 ages considering these factors.

A major conclusion of Chapter 6 is that it is extremely difficult to invert τ distributions for the oceanic circulation. It may be possible, however, to use them to constrain models of the flow which are based on other theories. For instance one could

attempt to simultaneously satisfy a physical model and the requirements of the tracer field. Whether or not CFC ventilation ages provide a powerful check of consistency, or are redundant in comparison to other oceanographic variables is an open question. The next section examines use of CFC age fields in combination with another oceanographic observable; dissolved oxygen concentration. Although CFC-113 age is difficult to interpret in isolation, use of other variables in combination may reveal information about oceanographic features in a less ambiguous manner. Section 7.3 is an initial investigation of this possibility, where the behaviour of the particular oceanographic feature in question (oxygen utilisation rates) is reasonably well understood.

7.3. Oxygen Utilisation Rates.

Oxygen utilisation rates (OURs) are important oceanographic parameters (see for example Jenkins, 1982; Jenkins & Goldman, 1985). By simultaneous measurements of dissolved oxygen and CFC concentrations one hopes to use the transient tracer age to judge the time since seclusion of the water, and hence determine the integrated OUR. This section reports the results of initial OUR calculations, based on linear regressions between oxygen and CFC-113 age on the isopycnals used in Chapter 6. The discussion then develops in an attempt to understand the factors controlling oxygen distribution, and comments concerning the implications for CFC-113 age behaviour are made.

Figure 7.1 is a plot of CFC-113/CFC-12 age versus dissolved oxygen on the isopycnal $\sigma_\theta = 27.10$. (Griffiths *et al.* (1992) describe the VIVALDI dissolved oxygen observations used in this section.) There is very good correlation between these two variables, encouraging one to believe that the technique to render OURs is accurate. The OUR can be estimated simply as the gradient of the regression between oxygen and CFC-113 age. It is common in these calculations to make use of a variable called apparent oxygen utilisation (AOU), defined such that,

$$AOU = F_{O_2}(\theta,S) - O_2 \qquad 7.3.1$$

where $F_{O_2}(\theta,S)$ is the oxygen solubility in seawater of potential temperature θ, and salinity S (Weiss, 1970). By correlating AOU against ventilation age the variation between water masses of different θ and S can be accounted for, since the dissolved oxygen boundary condition for these water parcels is different. Equation 7.3.1 assumes equilibrium saturation for oxygen at the time of permanent entrainment, albeit an unrealistic situation judging by the results of Chapter 5 and the effect of photosynthesis in the mixed layer.

Table 7.1 and Figure 7.2 report the results of correlations between both dissolved oxygen concentration and AOU with CFC-113/CFC-12 age (plotted against σ_θ in Figure 7.2 to compare with other estimates). The dissolved oxygen calculations are retained because the correlation coefficients are higher, in general, than for the regressions with

AOU. These results are unexpected and imply that the variation of the ventilation age boundary condition is in sympathy with that of the dissolved oxygen concentration. This remark is incidental, however, since there is no significant discrepancy between either OUR profile within the errors of the regression. The OURs from the four shallowest surfaces considered (mean pressure ≤ 667db) show reasonably good consistency with the previous estimates of Doney (1991) and JK. Deeper than this however, the correlations are poorer, and the implied OURs increase. This is in contradiction with other work (Riley, 1951; Jenkins, 1977, 1980, 1982; Jenkins & Goldman, 1985) and suggests that there is a problem with CFC ventilation age dating deeper than ~ 700db.

Table 7.1. Results of correlation analysis of dissolved oxygen and AOU against CFC-113/CFC-12 ages on isopycnals. The error in the fits, the linear correlation coefficients, r, and the number of data, N, are also shown.

			Dissolved oxygen			AOU		
σ_θ	Pressure	N	OUR	Error	r	OUR	Error	r
	db	#	μMol/l.yr	μMol/l.yr	#	μMol/l.yr	μMol/l.yr	#
27.1	145	11	4.21	0.37	0.967	4.20	0.46	0.950
27.175	328	13	4.51	0.88	0.840	4.88	1.06	0.810
27.25	554	12	4.92	0.83	0.883	5.45	1.28	0.802
27.325	667	12	5.86	0.97	0.886	6.48	1.91	0.73
27.45	799	12	7.77	4.15	0.510	37.83	53.63	0.218
27.55	904	12	9.68	7.33	0.386	26.28	29.42	0.272
27.7	1127	12	16.44	4.96	0.724	6.06	1.56	0.775
27.75	1281	12	44.94	16.56	0.651	21.27	7.55	0.67

Improvement of the OUR estimates requires consideration of the individual factors governing the distribution of oxygen. In the terminology of Section 6.3,

$$\frac{\partial O_2}{\partial t} = D(O_2) - J \qquad 7.3.2$$

where O_2 is the dissolved oxygen concentration and J is the OUR. Asserting $\frac{\partial O_2}{\partial t} = 0$ and expanding with Equation 6.3.2 requires,

Figure 7.1. Plot of CFC-113/CFC-12 ventilation age (years) against dissolved oxygen content (ml/l) on the isopycnal $\sigma_\theta = 27.10$, based on the stations shown in Figure 4.7.

Figure 7.2. Plot of oxygen utilisation rates (ml/l.yr) versus density (σ_θ).

Squares	Dissolved oxygen / ventilation age correlation,
Diamonds	AOU / ventilation age correlation,
Open circles	Doney (1991), eastern North Atlantic,
Closed circles	Jenkins (1987), 27.5°N 33.5°W.

The dashed lines are the standard errors in the dissolved oxygen and AOU correlations from the linear least squares fit (see text and Table 7.1). Only those calculated OURs with regression statistics such that $r > 0.5$ are shown.

Figure 7.3. Graph showing the relative magnitudes of isopycnic diffusion ($K_i \nabla_i^2 O_2$) and diapycnic diffusion ($K_z \frac{\partial^2 O_2}{\partial z^2}$) to the isopycnic advection ($\underline{v}_i . \nabla_i O_2$) in the oxygen budget of Equation 7.3.3, plotted against pressure. In this figure $\underline{v}_i$ was assumed to be 1cm/s throughout the water column (changing this value simply scales the y-axis of the plot). The figures in italics are the density surfaces (σ_θ) used in the analysis.

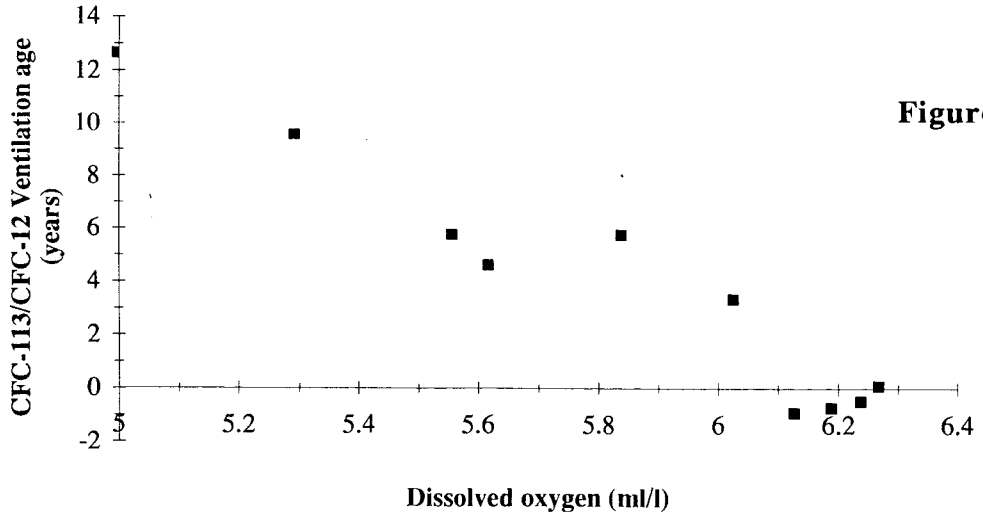

Figure 7.1.

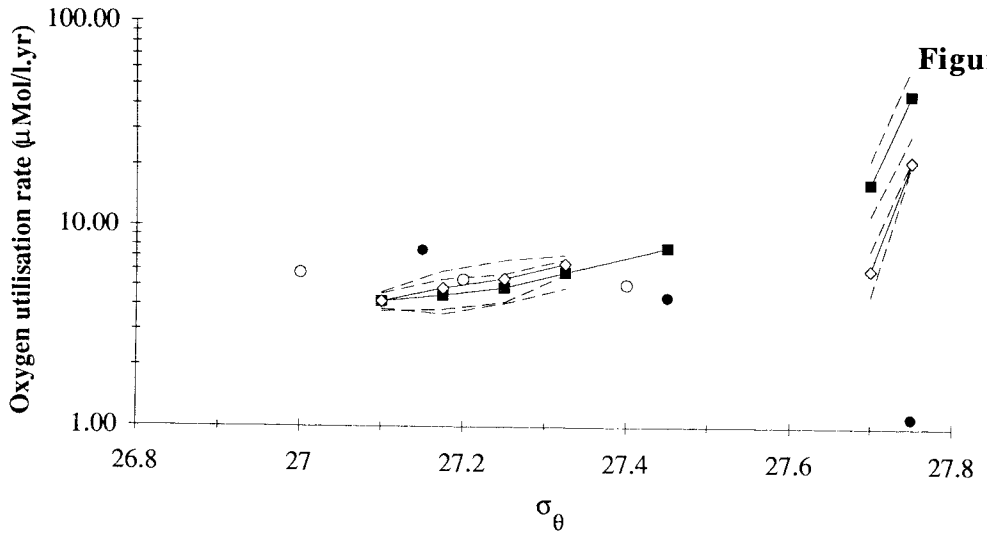

Figure 7.2.

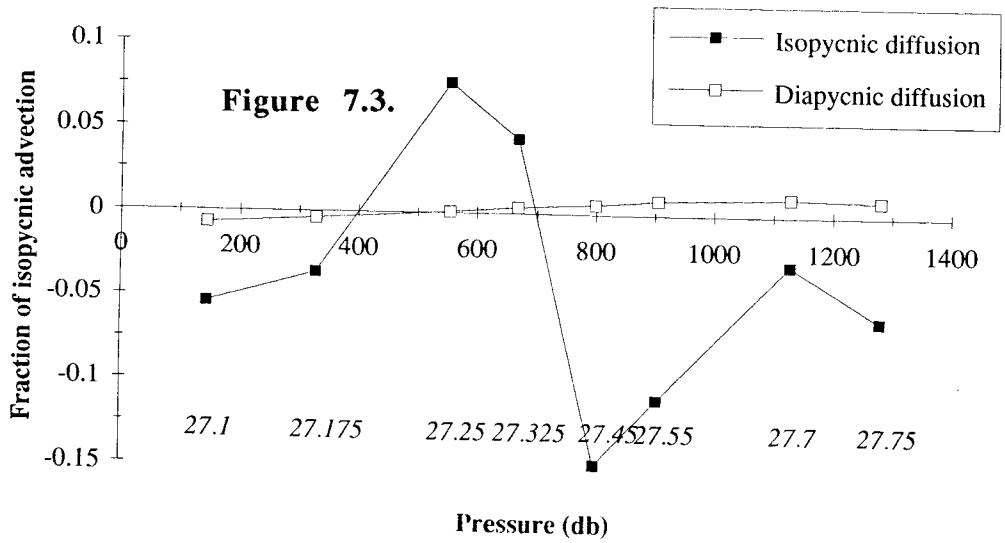

Figure 7.3.

$$K_i \nabla_i^2 O_2 + K_z \frac{\partial^2 O_2}{\partial z^2} = J + \underline{v}_i . \nabla_i O_2 \qquad 7.3.3$$

where the diapycnic advection term has been neglected following the comments in Section 6.4.3. In the advective limit (K_i, $K_z \rightarrow 0$) we have,

$$J = - \underline{v}_i . \nabla_i O_2 \qquad 7.3.4$$

and since $\underline{v}_i . \nabla_i \tau = 1$ (from Equation 6.3.7 in these circumstances),

$$J = - \frac{\underline{v}_i . \nabla_i O_2}{\underline{v}_i . \nabla_i \tau} \qquad 7.3.5.$$

The boundary condition for oxygen is similar to that of τ and one reasonably expects

$$|\nabla_i O_2 . \nabla_i \tau| \approx 1 \qquad 7.3.6$$

which implies,

$$J \approx - \left(\frac{\partial O_2}{\partial \tau} \right)_i \qquad 7.3.7$$

(subscript i refers to isopycnic derivative). The suitability of Equation 7.3.6 was investigated on the isopycnals used for the oxygen analysis. The mean of $|\nabla_i O_2 . \nabla_i \tau|$ is 0.981 (angle between gradient vectors $\Leftrightarrow$ 11°), with no single value deviating significantly from unity within standards errors.

Equation 7.3.7 is the zeroth, advective, approximation to calculating OURs using tracer ventilation ages. This analysis underpins the simple-minded approach taken at the beginning of this section and the results of this calculation are in Figure 7.2 and Table 7.1.

The next step in refinement, in order to understand the discrepancy between accepted OUR values and those calculated using Equation 7.3.7 (Figure 7.2), is to examine how suitable Equation 7.3.4 is in the real ocean as revealed by VIVALDI data. Section 6.4 reports that

$$\underline{v}_i . \nabla_i \tau \approx 1 + K_i \nabla_i^2 \tau \qquad (6.4.3)$$

is the most faithful approximation, which must be combined with the recast version of Equation 7.3.3 to estimate J. To judge truncated forms of this expression the isopycnic and diapycnic diffusion and isopycnic advection terms are computed using values for K_i and K_z as determined in Section 6.4.2. Figure 7.3 shows the magnitudes of $K_i \nabla_i^2 O_2$ / $\underline{v}_i . \nabla_i O_2$ and $K_z \frac{\partial^2 O_2}{\partial z^2}$ / $\underline{v}_i . \nabla_i O_2$ from Equation 7.3.3. There is no unambiguous choice for

$\underline{v}_i$ for this calculation and Figure 7.3 uses a constant value of 1cm/s. Choice of a larger (or smaller) $\underline{v}_i$, simply decreases (or increases) the y-axis scale. By allowing a sheared $\underline{v}_i$ with pressure, the relative importance of diffusion with depth alters. For example, $|\underline{v}_i|$ of 2cm/s near the surface and 1cm/s at 1000db doubles the relative contribution from diffusion at 1000db with respect to the surface. Whatever the choice of $\underline{v}_i(z)$, however, the diapycnic diffusion term is always small compared to the isopycnic contribution, and hereafter its effect is disregarded.

Based on these data a suitable balance for the O_2 budget is thus,

$$K_i\nabla_i^2 O_2 \approx J + \underline{v}_i.\nabla_i O_2 \qquad 7.3.8.$$

Combining with Equation 6.4.3 in the same way as above yields,

$$J \approx \frac{K_i\nabla_i^2 O_2 - \underline{v}_i.\nabla_i O_2}{\underline{v}_i.\nabla_i \tau - K_i\nabla_i^2 \tau} \qquad 7.3.9.$$

This form for J is much harder to calculate than the advective limit expressed in Equation 7.3.7. There are large uncertainties in the isopycnic diffusion terms, and $\underline{v}_i$ is undetermined (at least by the tracer fields). Nevertheless, deductions can still be made with regard to the behaviour of τ. Consider the balance of terms in Equation 7.3.9 as they vary with pressure. Figure 6.3(a) shows that $K_i\nabla_i^2\tau$ is reasonably constant with pressure, and $K_i\nabla_i^2 O_2$ has comparable values on the deepest and shallowest isopycnals with constant $\underline{v}_i$ (Figure 7.3). J, however, increases from plausible surface values to rates on the deepest two surfaces which are an order of magnitude too large, as evinced by Figure 7.2. One may argue that this is a reflection of the strong shear between the surface and ~1200db. Isopycnic diffusion could then dominate the oxygen budget and increase the numerator of Equation 7.3.9 and hence the value of J. Saunders (1982) asserts that a deep level (>3000m) of no motion exists in the north east Atlantic, and the shear is such that the velocities at 1200db are reduced by a factor of about three from the near surface values (his Figure 9). This is insufficient to explain the large increase in J at these depths.

A more convincing explanation is that the suitability of Equation 6.4.3 (reproduced above), and hence Equation 7.3.9, is doubtful. Equations 6.4.1 or 6.4.2 may be more appropriate, where the possibility of non-zero $\frac{\partial\tau}{\partial t}$ is admitted, and the advection of age may be less important. A comparison with the simple mixing model of Section 6.2 is provoked, where $\frac{\partial\tau}{\partial t} \neq 0$ and a maximum observable ventilation age exists when τ is of order the characteristic time for the transient tracer itself (certainly the case here). In these circumstances τ is far from the ideal steady clock, reliably timing the consumption of oxygen, and this can explain the discrepancy in OUR values.

Let us recap. Naïve use of dissolved oxygen and CFC-113/CFC-12 ventilation ages to determine OURs yield reasonable estimates in the upper ~ 700db of the region surveyed (centred on ~ 45°N 20°W). The error estimates for these values are of order 30-40%. On deeper isopycnals unreasonably large OURs result which are difficult to reconcile without conceding that $\frac{\partial \tau}{\partial t} \neq 0$, or there exists a restriction on the maximum possible τ. In either case the τ clock runs too slowly and is a poor indicator of the 'true' fluid age. One final comment on the direction of this argument is important. In no rigorous manner have independent OUR estimates been derived. Rather, acceptable values based on previous work have been used to deduce features of the CFC-113/CFC-12 ventilation age behaviour. To the extent that the existing paradigm of oxygen consumption is incorrect so too are these deductions.

7.4. Thesis Conclusions.

An ECD-GC analytical system and methodology has been developed which allows observations of CFC-113 dissolved in seawater with greater precision and dynamic range than has been previously possible. Dissolved CFCs 11 and 12 can also be measured, with slightly inferior accuracies and precisions when compared with other published techniques. The chromatographic column used is capable of baseline resolution of all the compounds of interest from other species which have similar retention times. To achieve this performance a competent injection is required, and the current arrangement is marginally successful; problems with methyl iodide coeluting with CFC-113 can occur. Primary standards have been prepared and calibrated which compare well with Scripps Institution of Oceanography CFC standards. Over 450 seawater samples have been analysed at sea during the VIVALDI '91 expedition to the north east Atlantic.

Use of the surface water data allows factors relating the unknown CFC-113 solubility to those of CFC-11 and CFC-12. The results of this exercise are significantly lower than the previously published estimate (Wisegarever & Gammon, 1988), possibly as a result of contamination of the CFC-113 data in the previous estimate. The CFC-11 and CFC-12 surface values have also been used in comparison with other CFC data in an attempt to reveal the influence that the seasonal ocean has on the CFC boundary condition for the main thermocline. Both concentration (important for CFCs 11 and 12) and CFC-113 ventilation age have been considered. An analytical model suggests that the increase in atmospheric concentrations can bias the CFC ventilation age boundary condition, but different exchange rates at the air/sea interface have a larger effect. A physically reasonable one dimensional numerical model of upper ocean seasonality suggests that current uncertainty in gas transfer at the air/sea interface gives rise to 0.2-0.4 year uncertainty in the ventilation age boundary condition. The maximum depth of mixing and details of the seasonal cycle are more important however; responsible for ~ 2.5 year initial ventilation ages for an 800m deep winter mixed layer. The exact boundary

condition is found to be sensitive to the subtleties of the mixed layer history for a period of about 3-4 years before permanent sequestration. The numerical model is incapable of simulating the complete range of surface conditions typically observed, probably as a result of neglecting baroclinic influences, and the temperature dependence of the gas transfer.

An analysis of advection and diffusion, relevant for the ocean away from the seasonal boundary, is developed to yield an expression for the evolution of CFC ventilation age. Use of VIVALDI '91 data on several isopycnals suggests that CFC-113 ventilation age evolution is a balance between advection and the tendency for the age to increase with time, plus a contribution from diffusion on the free horizon. The ventilation age field cannot be inverted to yield the circulation; shear in the flow causes a particular problem, even in the limit of no diffusion, and the errors in observations ultimately dominate in the case of rapid advection. This makes interpretation of CFC-113 ventilation age distributions difficult. Their use to derive oxygen utilisation rates is discussed and plausible values are obtained on isopycnals $27.1 \leq \sigma_\theta \leq 27.325$. Deeper than this a systematic problem with the technique emerges. It is likely that unsteadiness in the ventilation age, or an asymptotic saturation value causes an underestimate of the true fluid age. This is a manifestation of the source boundary condition for CFC-113 ventilation age and is also suggested by the results of a simple box-mixing model.

7.5. Future Work.

This thesis is a report of research that is work in progress and there are several possible areas that merit further investigation. Section 4.2.1 discusses minor alterations to the analysis procedure. However, there are two more important refinements. Firstly the injection method involving the packed trap should be improved. This would eliminate the problem of methyl iodide coelution so the potential of the column could be realised and resolution improved. Secondly the baseline fluctuation, which appears consistently beneath the rising edge of the CFC-113 peak, should be identified and eliminated. This would avoid the need to reprocess chromatograms and also improve reproducibility. In a broader context of data quality control and instrument appraisal, collaboration with other researchers, in the laboratory and at sea, is vital. Intercalibration cruises are ideal in this respect.

Acquisition of CFC-113 solubility data in the manner of the functions available for CFCs 11 and 12 and oxygen would greatly reduce the uncertainty in the CFC-113 ventilation age and allow a clearer picture of the ocean/atmosphere exchange to emerge. Further research regarding the seclusion and dispersion of inert transient tracers in ocean simulations is also timely. The three dimensional mixed layer / mesoscale interaction could be examined in the light of the simple one dimensional model of Chapter 5. Similarly, in a regime where the diffusion is prescribed, the interior evolution of

CFC-113 ventilation age could be studied. In particular, the effects of baroclinicity and unsteadiness could be investigated. The use of CFC fields as constraints on circulation models conceived by other methods may be a fruitful area of future study. Although transient tracer fields themselves cannot be used in formal inverse calculations which assume a steady state, the derived ventilation ages may prove to be useful however, at least for those parts of the ocean which have a well defined, steady age. Finally, it is worth remarking that the CFC replacements, which are less polluting and now in preparation, may well have a greater utility because for those species the analytical instruments and conceptual models will already be in place.

BIBLIOGRAPHY.

Armi L. and H. Stommel (1983) Four views of a portion of the North Atlantic sub-tropical gyre. *J. Phys. Oceanogr.*, **13**, 828-857.

Broecker W. S. and T-H. Peng (1982) Tracers in the Sea, Lamont-Doherty Geological Observatory Press, 690 pp.

Bullister J. L. and R. F. Weiss (1983) Anthropogenic chlorofluoromethanes in the Greenland and Norwegian Seas. *Science,* **221**, 265-268.

Bullister J. L. (1984) Atmospheric CFMs as tracers of ocean circulation and mixing : Measurement and calibration techniques and studies in the Greenland and Norwegian Seas. Ph.D. Thesis, University of California, San Diego.

Bullister J. L. and R. F. Weiss (1988) Determination of CCl_3F and CCl_2F_2 in seawater and air. *Deep-Sea Res.*, **35**, 839-853.

Chemical Manufacturers Association (1983) Production, sales and calculated release of CFC-11 and CFC-12 through 1982.

Cunningham S. C. and T. W. N. Haine (In Prep.)

Cunnold D. M., R. G. Prinn, R. A. Rasmussen , P. G. Simmonds, F. N. Alyea, C. A. Cardelino, A. J. Crawford, P. J. Fraser and R. D. Rosen (1983a) The ALE IV : Lifetime methodology and application to 3 years of $CFCl_3$ data. *J. Geophys. Res.*, **88**, 8379-8400.

Cunnold D. M., R. G. Prinn, R. A. Rasmussen, P. G. Simmonds, F. N. Alyea, C. A. Cardelino, A. J. Crawford, P. J. Fraser and R. D. Rosen (1983b) The ALE V : Results for CF_2Cl_2 based on 3 years data. *J. Geophys. Res.*, **88**, 8401-8414.

Cunnold D. M., R. G. Prinn, R. A. Rasmussen, P. G. Simmonds, F. N. Alyea, C. A. Cardelino, A. J. Crawford, P. J. Fraser and R. D. Rosen (1986) Atmospheric lifetime and annual release estimates for $CFCl_3$ and CF_2Cl_2 from 5 years of ALE data. *J. Geophys. Res.*, **91**, 10797-10817.

Czeplak G. and C. Junge (1974) Studies of interhemispheric exchange in the troposphere by a diffusion model. *Adv. Geophys.*, **18B**, 57-72.

Dickson R. R., E. M. Gmitrowicz and A. J. Watson (1990) Deep water renewal in the northern North Atlantic. *Nature*, **344**, 848-850.

Doney S. C. (1991) A study of North Atlantic ventilation using transient tracers. Ph.D. Thesis, Massachusetts Institute of Technology/Woods Hole Oceanographic Institution.

DuPont, Freon fluorocarbons. Properties and applications. "Freon" products division, chemicals & pigments department, DuPont de Nemours international S.A. CH-1211 Geneva 24, Switzerland. Bulletin B-2E.

Fiadeiro M. E. and G. Veronis (1982) On the determination of absolute velocities in the ocean. *J. Mar. Res.*, **40 (Supplement)**, 159-192.

Fine R. A., M. J. Warner and R. F. Weiss (1988) Water mass modification at Agulhas Retroflection : CFM studies. *Deep-Sea Res.*, **35**, 311-332.

Fine R. A. and R. L. Molanari (1988) A continuous deep western boundary current between Abaco (26.5°N) and Barbados (13°N). *Deep-Sea Res.*, **35**, 1441-1450.

Fuchs G., W. Roether and P. Schlosser (1987) Excess ^{3}He in the ocean surface layer. *J. Geophys. Res.*, **92**, 6559-6568.

Fukumori I., F. Martel and C. Wunsch (1991) The hydrography of the North Atlantic in the early 1980s. An atlas. *Prog. Oceanog.*, **27**, 1-110.

Gammon R. H., J. Cline and D. Wisegarver (1982) CFMs in the North-East Pacific ocean : Measured vertical distributions and application as transient tracers of upper ocean mixing. *J. Geophys. Res.*, **87**, 9441-9454.

Garrett C. (1979) Mixing in the ocean interior. *Dyn. Atmos. Oceans*, **3**, 239-265.

Gill A. (1982) Dynamics of atmospheres and oceans. Academic Press, London, 662pp.

Gordon A. L., R. F. Weiss, W. M. Smethie and M. J. Warner (1992) Thermocline and intermediate water Communication between the South Atlantic and Indian Oceans. *J. Geophys. Res.*, **97**, 7223-7240.

Griffiths G., S. A. Cunningham, M. Griffiths, R. T. Pollard *et al.* (1992) CTD oxygen, tracer and nutrient data from RRS Charles Darwin cruises 58 & 59 in the North East Atlantic as part of VIVALDI '91. Institute of Oceanographic Sciences Deacon Laboratory, 296.

Hähne A., A. Volz, D. Ehhalt, H. Cosatto, W. Roether and W. Weiss (1978) Depth profiles of CFMs in the Norwegian Sea. *Pure Appl. Geophys.*, **116**, 575-582.

Haine T. W. N., A. J. Watson and M. I. Liddicoat (Submitted, 1991) A high resolution technique to determine the concentration of chlorofluorocarbon-113 in seawater. *J. Geophys. Res.*

Hammer P., J. Hayes, W. Jenkins and R. Gagosian (1978) Exploratory analysis of F-11 in North Atlantic water columns. *Geophys. Res. Letters*, **5**, 645-648.

Harvey J. (1982) θ-S relationships and water masses in the eastern North Atlantic. *Deep-Sea Res.*, **29**, 1021-1033.

Harvey J. and M. Arhan (1988) The water masses of the central North Atlantic in 1983-1984. *J. Phys. Oceanogr.*, **18**, 1855-1875.

Hayduk W. and H. Laudie (1974) Prediction of diffusion coefficients for non-electrolytes in dilute aqueous solutions. *A. I. Ch. E. Journal*, **20**, 611-615.

Hunter-Smith R. J., P. W. Balls and P. S. Liss (1983) Henry's Law constants and the air-sea exchange of various low molecular weight halocarbon gases. *Tellus*, **35B**, 170-176.

IPCC (1990) Climate change ; the IPCC scientific assessment., Cambridge University press, 339 pp.

Isemer H. J. and L. Hasse (1985) The Bunker climate atlas of the Atlantic Ocean. 1, Observations. Springer-Verlag, Berlin.

Jenkins W. J. (1977) Tritium-helium dating in the Sargasso Sea : a measurement of oxygen utilisation rates. *Science*, **196**, 291.

Jenkins W. J. (1980) Tritium and ^{3}He in the Sargasso Sea. *J. Mar. Res.*, **38**, 533-569.

Jenkins W. J. (1982) Oxygen utilisation rates in the North Atlantic subtropical gyre and primary production in oligotrophic systems. *Nature*, **300**, 246-248.

Jenkins W. J. and J. C. Goldman (1985) Seasonal oxygen cycling and primary production in the Sargasso Sea. *J. Mar. Res.*, **43**, 465-491.

Jenkins W. J. (1987) ^{3}H and ^{3}He in the beta triangle : Observations of gyre ventilation and oxygen utilisation rates. *J. Phys. Oceanogr.*, **17**, 763-783.

Jenkins W. J. (1988) The use of anthropogenic tritium and helium-3 to study subtropical gyre ventilation and circulation. *Trans. R. Soc. Lond.*, **325**, 43-61.

Krysell M. (1988) Arctic Ocean ventilation studied with a suite of anthropogenic halocarbon tracers. *Science*, **242**, 746-749.

Kraus E. B. and J. S. Turner (1967) A one dimensional model of the seasonal thermocline. II General theory and its consequences. *Tellus*, **19**, 98-105.

Leetmaa A., P. Niiler and H. Stommel (1977) Does the Sverdrup relation account for the mid-Atlantic circulation? *J. Mar. Res.*, **35**, 1-9.

Leetmaa A. and A. F. Bunker (1978) Updated charts of the mean annual wind stress, convergence in the Ekman layers, and Sverdrup transports in the North Atlantic. *J. Mar. Res.*, **20**, 397-400.

Levitus S. (1982) Climatological atlas of the world ocean. US Dept. of Commerce, Rockville, MD NOAA professional paper No.13.

Liddicoat M. I., A. J. Watson and T. W. N. Haine (In Prep.)

Liss P. S. and L. Merlivat (1986) Air Sea gas exchange rates : introduction and synthesis. In: The role of air sea exchange in geochemical cycling. P. Buet-Menard, editor, Reidel publishing company, pp. 113-128.

Lovelock J. E. (1971) Atmospheric fluorine compounds as indicators of air movements. *Nature,* **230**, 379.

Lovelock J. E., R. J. Maggs and R. J. Wade (1973) Halogenated hydrocarbons in and over the Atlantic. *Nature,* **241**, 194-196.

Lovelock J. E. (1974) The electron capture detector : Theory and practice. *J. Chrom.*, **99**, 3-12.

Lovelock J. E. and A. J. Watson (1978) Electron capture detector. Theory and practice II. *J. Chrom.*, **158**, 123-138.

Lovelock J. E. (1991) The ECD and green politics. *LC-GC International*, **4**, 26-35.

Marshall J. C. and A. J. G. Nurser (1992) Fluid dynamics of thermocline ventilation. *J. Phys. Oceanogr.*, **22**, 583-595.

Marshall J. C., A. J. G. Nurser and R. G. Williams (1992, Submitted) Inferring the subduction rate and period over the North Atlantic. *J. Phys. Oceanogr.*

McCarthy R. L., F. A. Bower and J. P. Jesson (1977) Production and release - world production and release of CCl_3F and CCl_2F_2 (F11 and F12) through 1975. *Atmos. Environ.*, **11**, 491-497.

Molina M. J. and F. S. Rowland (1974) Stratospheric sink for CFMs : Chlorine atom-catalysed destruction of ozone. *Nature,* **249**, 810-812.

Musgrave D. (1985) A numerical study of the roles of sub-gyre scale mixing and the western boundary current on homogenisation of a passive tracer. *J. Geophys. Res.*, **90**, 7037-8952.

Musgrave D. L. (1990) Numerical studies of tritium and helium-3 in the thermocline. *J. Phys. Oceanogr.*, **20**, 344-373.

Niiler P. P. (1977) One dimensional models of the seasonal thermocline. In: The Sea, 6. , E. D. Goldberg, I. N. McCave, J. J. O'Brien and J. H. Steele, editor, Wiley-Interscience, New York, pp. 97-115.

Niiler P. P. and E. B. Kraus (1977) One dimensional models of the upper ocean. In: Modelling and prediction of the upper layers of the ocean. E. B. Kraus, editor, Pergamon Press, pp. 143-172.

Nurser A. J. G. and J. C. Marshall (1991) On the relationship between subduction rates and diabatic forcing of the mixed layer. *J. Phys. Oceanogr.*, **21**, 1793-1802.

Pack D. H., J. E. Lovelock, G. Cotton and C. Curthoys (1977) Halocarbon behaviour from a long time series. *Atmos. Environ.*, **11**, 329-344.

Pickart R. S., N. G. Hogg and W. M. Smethie (1989) Determining the strength of the Deep Western Boundary Current using the CFM ratio. *J. Phys. Oceanogr.*, **19**, 940-951.

Pollard R. T. and S. Pu (1985) Structure and circulation of the upper Atlantic ocean northeast of the Azores. *Prog. Oceanog.*, **14**, 443-462.

Pollard R. T., H. Leach, G. Griffiths *et al.* (1991) RRS Charles Darwin 58 & 59, 25 Apr-16 May ; 18 May-10 Jun 1991. VIVALDI '91. Institute of Oceanographic Sciences Deacon Laboratory, 228.

Rasmussen R. A. (1978) Interlaboratory comparison of fluorocarbon measurement. *Atmos. Environ.*, **12**, 2505-2508.

Rasmussen R. A. and M. A. K. Khalil (1981) Interlaboratory comparison of fluorocarbons -11 and -12, methylchloroform and nitrous oxide measurements. *Atmos. Environ.*, **15**, 1559-1568.

Rasmussen R. A., M. A. K. Khalil and R. W. Dalluge (1981) Atmospheric tracer gases in Antarctica. *Science*, **211**, 285-287.

Rasmussen R. A. and J. E. Lovelock (1983) The atmospheric lifetime experiment. 2 Calibration. *J. Geophys. Res.*, **88**, 8369-8378.

Rhein M. (1991) Ventilation rates of the Greenland and Norwegian Seas derived from distributions of CFMs F11 and F12. *Deep-Sea Res.*, **38**, 485-503.

Riley G. A. (1951) Oxygen, phosphate, and nitrate in the Atlantic ocean. *Bull. Bingham Oceanogr. Coll.*, **13**, 1-126.

Ríos A. F., F. F. Perez and F. Fraga (1992) Water masses in the upper and middle north Atlantic ocean east of the Azores. *Deep-Sea Res.*, **39**, 645-658.

Roether W. and G. Fuchs (1988) Water mass transport and ventilation in the North East Atlantic derived from tracer data. *Trans. R. Soc. Lond.*, **325**, 63-69.

Roether W. and R. Schlitzer (1991) Eastern Mediterranean deep water renewal on the basis of CFM and tritium data. *Dyn. Atmos. Oceans* , **15**, 333-354.

Saunders P. M. (1982) Circulation in the eastern North Atlantic. *J. Mar. Res.*, **40 (Supplement)**, 641-657.

Schlitzer R., W. Roether, H. Oster, H.-G. Junghans, M. Hausmann, H. Johannsen and A. Michelato (1991) Chlorofluoromethane and oxygen in the eastern Mediterranean. *Deep-Sea Res.*, **12**, 1531-1551.

Schmitt R. (1981) The form of the temperature salinity relationship in the Central Water : evidence for double-diffusive mixing. *J. Phys. Oceanogr.*, **11**, 1015-1026.

Schott F. and R. Zantrop (1980) On the effect of vertical mixing on the determination of absolute currents by the beta spiral method. *Deep-Sea Res.*, **17A**, 173-180.

Singh H. B., L. J. Salas, R. E. Stiles and E. Scribner (1979) Atmospheric halocarbons, hydrocarbons and sulphur hexafluoride : Global distributions, sources and sinks. *Science*, **203**, 899-903.

Singh H. B., L. J. Salas and R. E. Stiles (1983a) Selected man-made chemicals in the air and oceanic environment. *J. Geophys. Res.*, **88**, 3675-3683.

Singh H. B., L. J. Salas and R. E. Stiles (1983b) Methyl halides in and over the eastern Pacific (40°N-32°S). *J. Geophys. Res.*, **88**, 3684-3690.

Smethie W. M., D. W. Chipman, J. H. Swift and K. P. Koltermann (1988) CFMs in the Arctic Mediterranean Seas : evidence for formation of bottom water in the Eurasian Basin and deep water exchange through Fram Strait. *Deep-Sea Res.*, **35**, 347-369.

Stommel H., P. Niiler and D. Anati (1978) Dynamic topography and recirculation of the North Atlantic. *J. Mar. Res.*, **36**, 449-468.

Stramma L. (1984) Geostrophic transport in the warm water sphere of the eastern subtropical North Atlantic. *J. Mar. Res.*, **42**, 537-558.

Sy A. (1988) Investigation of large-scale patterns in the central North Atlantic Current, the Azores Current and the Mediterranean Water plume in the area of the Mid-Atlantic Ridge. *Deep-Sea Res.*, **35**, 383-413.

Tennekes H. and J. L. Lumley (1972) A first course in turbulence, MIT Press, 300 pp.

Thiele G., W. Roether, P. Schlosser and R. Kuntz (1986) Baroclinic flow and transient tracer fields in the Canary-Cape Verde Basin. *J. Phys. Oceanogr.*, **16**, 814-826.

Thiele G. and S. L. Sarmiento (1990) Tracer dating and ocean ventilation. *J. Geophys. Res.*, **95**, 9377-9391.

Trumbore S. E., S. S. Jacobs and W. M. Smethie (1991) CFC evidence for rapid ventilation of the Ross Sea. *Deep-Sea Res.*, **38**, 845-870.

Upstill-Goddard R. C., A. J. Watson, P. S. Liss and M. I. Liddicoat (1990) Gas transfer in lakes measured with SF6. *Tellus*, **42B**, 364-377.

Wallace D. W. R. and Moore R. M. (1985) Vertical profiles of CCl_3F (F-11) and CCl_2F_2 (F-12) in the central Arctic ocean basin. *J. Geophys. Res.*, **90**, 1155-1166.

Wallace D. W. R. and J. R. N. Lazier (1988) Anthropogenic CFMs in newly formed Labrador Sea Water. *Nature*, **332**, 61-63.

Wanninkof R. (1991, Submitted) Relationship between windspeed and gas exchange over the ocean. *J. Geophys. Res.*

Warner M. J. and R. F. Weiss (1985) Solubilities of CFCs 11 and 12 in water and seawater. *Deep-Sea Res.*, **32**, 1485-1497.

Warner M. J. (1988) CFMs F-11 and F-12 : Their solubilities in water and seawater and studies of their distributions in the South Atlantic and North Pacific oceans. Ph.D. Thesis, University of California, San Diego.

Weiss R. F. (1970) The solubility of nitrogen, oxygen, and argon in water and seawater. *Deep-Sea Res.*, **17**, 721-735.

Weiss W. and W. Roether (1980) The rates of tritium input to the world oceans. *Earth Planet. Sci. Lett.*, **49**, 435-446.

Weiss R. F., J. L. Bullister, R. H. Gammon and M. J. Warner (1985) Atmospheric CFMs in the deep equatorial Atlantic. *Nature*, **314**,

Weiss R. F., J. L. Bullister, M. J. Warner, F. A. Van Woy and P. K. Salameh (1990) AJAX expedition CFC measurements. SIO 90-6.

Weiss R. F., E. C. Carmack and V. M. Koropalov (1991) Deep-Water renewal and biological production in Lake Baikal. *Nature*, **349**, 665-669.

Wilke C. R. and P. Chang (1955) Correlations of diffusion coefficients in dilute solutions. *A. I. Ch. E. Journal*, **1**, 264-270.

Wisegarver D. P. and J. D. Cline (1985) Solubility of F-11 and F-12 in seawater and its relationship to surface concentrations in the North Pacific. *Deep-Sea Res.*, **32**, 97-106.

Wisegarver D. P. and R. H. Gammon (1988) A new transient tracer : Measured vertical distribution of CCl_2FCClF_2 (F-113) in the North Pacific Subarctic gyre. *Geophys. Res. Letters*, **15**, 188-191.

Woods J. D., W. Barkmann and A. Horch (1984) Solar heating of the oceans - diurnal, seasonal and meridional variation. *Q. J. Roy. Met. Soc.*, **110**, 633-656.

Woods J. D. (1985) The physics of thermocline ventilation. In: Coupled ocean-atmosphere models. J. C. J. Nihoul, editor. Elsevier, pp. 543-590.

Woods J. D. and V. Strass (1986) The response of the upper ocean to solar heating. II The wind driven current. *Q. J. Roy. Met. Soc.*, **112**, 29-42.

Woods J. D. and W. Barkmann (1986a) A Lagrangian mixed layer model of 18°C water formation. *Nature*, **319**, 574-576.

Woods J. D. and W. Barkmann (1986b) The response of the upper ocean to solar heating. I : The mixed layer. *Q. J. Roy. Met. Soc.*, **112**, 1-27.

Woods J. D. (1987 (2nd edition)) The warm water sphere of the North Atlantic. A miscellany. Institut fur Meerskunde, Kiel. 128.

Worthington L. V. (1976) On the North Atlantic circulation. Johns Hopkins Oceanographic Studies 6, 110pp.

Wright W. R. and L. V. Worthington (1970) The water masses of the North Atlantic ocean. A volumetric census of temperature and salinity. *Serial Atlas of the Marine Environment*, **19**, 8pp.

Wunsch C. (1977) The North Atlantic circulation west of 50°W determined by inverse methods. *Rev. Geophys. Space Phys.*, **16**, 583-620.